B L A

Memoria de Tesis Doctoral realizada por

Alejandro Sáez Gonzalvo

presentada ante el Departamento de Física Teórica
de la Universidad Autónoma de Madrid
para optar al Título de Doctor en Física Teórica

Supervisor: **Prof. Dr. Gregorio Herdoíza**

Instituto de Física Teórica UAM-CSIC
Departamento de Física Teórica
Facultad de Ciencias
Universidad Autónoma de Madrid

Instituto de
Física
Teórica
UAM-CSIC

UAM
Universidad Autónoma
de Madrid

2024

*Nature is the proof of dialectics, and it must be said
for modern science that it has furnished this proof with
very rich materials increasingly daily [...]*

— F. Engels, Anti-Dühring

*It is precisely the alteration of nature by men, not solely nature as such,
which is the most essential and immediate basis of human thought.*

— F. Engels, Dialectics of Nature.

ABSTRACT

Short summary of the contents in English. . . a great guide by Kent Beck how to write good abstracts can be found here:

https://plg.uwaterloo.ca/~migod/research/beckOOPSLA.html

RESUMEN

Kurze Zusammenfassung des Inhaltes in deutscher Sprache. . .

PUBLICATIONS

[1] Andrea Bussone, Alessandro Conigli, Julien Frison, Gregorio Herdoíza, Carlos Pena, David Preti, Alejandro Sáez, and Javier Ugarrio. "Hadronic physics from a Wilson fermion mixed-action approach: Charm quark mass and $D_{(s)}$ meson decay constants." In: (Sept. 2023). arXiv: 2309.14154 [hep-lat].

[2] Andrea Bussone, Alessandro Conigli, Gregorio Herdoiza, Julien Frison, Carlos Pena, David Preti, Jose Angel Romero, Alejandro Saez, and Javier Ugarrio. "Light meson physics and scale setting from a mixed action with Wilson twisted mass valence quarks." In: *PoS* LATTICE2021 (2022), p. 258. DOI: 10.22323/1.396.0258.

[3] Alessandro Conigli, Julien Frison, Gregorio Herdoíza, Carlos Pena, Alejandro Sáez, and Javier Ugarrio. "Towards precision charm physics with a mixed action." In: *PoS* LATTICE2022 (2023), p. 351. DOI: 10.22323/1.430.0351. arXiv: 2212.11045 [hep-lat].

[4] Alejandro Saez, Alessandro Conigli, Julien Frison, Gregorio Herdoíza, and Carlos Pena. "Determination of the Gradient Flow Scale t_0 from a Mixed Action with Wilson Twisted Mass Valence Quarks." In: *40th International Symposium on Lattice Field Theory*. Jan. 2024. arXiv: 2401.11546 [hep-lat].

[5] Alejandro Saez, Alessandro Conigli, Julien Frison, Gregorio Herdoiza, Carlos Pena, and Javier Ugarrio. "Scale Setting from a Mixed Action with Twisted Mass Valence Quarks." In: *PoS* LATTICE2022 (2023), p. 357. DOI: 10.22323/1.430.0357.

ACKNOWLEDGMENTS

CONTENTS

LIST OF FIGURES

LIST OF TABLES

LISTINGS

ACRONYMS

Part I

INTRODUCTION

INTRODUCTION

The Standard Model (SM) of particle physics is the theory that describes and unifies three of the four fundamental interactions in Nature: electromagnetism, the weak interaction, and the strong interaction. The theoretical framework in which the SM is formulated is that of Quantum Field Theory (QFT), and the particular theory that describes the strong interaction is Quantum Chromodynamics or QCD.

FIELDS, SPECIAL RELATIVITY AND QUANTA

The 20th century saw the two greatest developments for modern physics and our understanding of Nature: special relativity and quantum mechanics. Quantum Field Theory is the framework which unifies both theories.

The theory of special relativity reformulates Galileo's principle that the laws of physics must be left unchanged between two different inertial reference frames in such a way that the speed of light is a universal constant, consistent with the theory of electromagnetism developed by Maxwell in the 19th century. This brought incredible consequences, such as time and length dilation, according to which one observer experiences time and distances different from another depending on the speed they travel. Also the equivalence of mass and energy, as well as the formulation of 4-dimensional space-time as the manifold of the Universe, in which there is a non trivial interplay between time and space, as can be seen from the Lorentz transformations.

The principle of a constant speed of light and that nothing can travel faster than it rendered the old Newtonian view of interactions outdated. According to the latter, the force acting on a particle depends on the position of all other particles at that given time. This implies instantaneous transmission of the force from one particle to another, which is at odds with special relativity. Field Theory is the framework that allows to supersede this difficulty. It is based on the concept of fields, which are dynamical objects that fill all of space-time. Mathematically they are just functions of space and time. Treating fields as the basic degrees of freedom helps enormously in the task of formulating theories that are Lorentz invariant and thus compatible with special relativity. One example is Maxwell's theory of electromagnetism, governing the dynamics of the electric $\vec{E}(\vec{x}, t)$ and magnetic $\vec{B}(\vec{x}, t)$ fields.

On the other hand, quantum mechanics introduces the concept of probability into our description of Nature. The basic idea is that

particles are described by wave functions that represent the density probability of finding one particle at a given position in space. Position and momentum are promoted to conjugate operators rather than being degrees of freedom. These operators do not commute, resulting in Heisenberg's uncertainty principle, by which we cannot know simultaneously the position and momentum of a particle

$$\Delta x \Delta p \geq \hbar. \tag{0.1}$$

The wave function of a particle is described by Schrödinger's equation

$$i\hbar \frac{\partial \psi}{\partial t} = H\psi, \tag{0.2}$$

which is not Lorentz invariant, and thus is only useful to describe non-relativistic quantum systems. In order to bridge the gap between quantum mechanics and special relativity, one can write a version of Schrödinger's equation which respects Lorentz symmetry. One option is the Klein-Fock-Gordon equation

$$\left(\partial^2 + m^2\right)\phi = 0, \tag{0.3}$$

which describes spin-0 particles (scalars), another the Dirac equation

$$\left(i\gamma_\mu \partial_\mu - m\right)\psi = 0, \tag{0.4}$$

which describes spin-$\frac{1}{2}$ particles (e.g. an electron). These equations are Lorentz invariant and therefore they describe a relativistic quantum system. The wave functions $\phi(x), \psi(x)$ are the fields of the particles described, which take values in all of space-time. Thinking of $\psi(x)$ as the field of the electron, in analogy to $\vec{E}$ being the electric field, makes manifest that what is truly fundamental is not the electron as a particle itself, but its field. This solves another puzzle of Nature: how can two electrons separated a space-like distance (causally disconnected) look exactly the same? This is naturally explained if there is a universal field of the electron, since all electrons are simply manifestations of this field filling all of space-time. Indeed particles appear as excitations of the underlying field in Quantum Field Theory.

In order to make the transition to Quantum Field Theory, one needs to promote the classical fields to quantum operators, analogously to the case of position and momentum in quantum mechanics. This way, a quantum field is an operator valued function of space-time. Classically, eq. (0.4) has solution

$$\psi_s(x) = \frac{1}{(2\pi)^3} \int d^3p \left(u_s(p)e^{-ipx} + v_s(p)e^{ipx}\right), \tag{0.5}$$

where s is the spin state of the particle. In QFT, we promote the amplitudes $u_s(p), v_s(p)$ to quantum operators. Furthermore, the second

term in eq. (0.5) appears to have negative energy. In QFT one identifies $v_s(p)$ with the operator that creates an antiparticle with momentum p and spin s, with positive energy. These have opposite electric charge and the same mass to their corresponding particles, and are equivalent to positive energy particles propagating backwards in time, solving the problem of the negative energy modes in the classical Dirac equation.

Another advantage of QFT is that it provides with a framework in which particle number is not conserved. In the context of relativistic systems this is of relevant importance, since collisions can create and destroy particles. Furthermore, according to Heisenberg's uncertainty principle, if we place a particle in a box of size L we have an uncertainty in its momentum of

$$\Delta p \geq \hbar/L. \tag{0.6}$$

This is turn leads to an uncertainty in the energy of the particle of order $\Delta E \geq \hbar c/L$. When the energy exceeds $2mc^2$ we have enough energy to create out of the vacuum a particle-antiparticle pair. This will happen at distances of order

$$L = \lambda = \frac{\hbar}{mc}, \tag{0.7}$$

which is the Compton wavelength. At this and smaller distances (or equivalently higher energies) one expects to detect particle-antiparticle pairs swarming around the original particle, breaking down the very concept of a point-like particle. In QFT, writing interaction terms of the type

$$\psi(x)\phi(x)... \tag{0.8}$$

for some generic fields $\psi, \phi, ...$ allows for interactions in which particles and antiparticles may be destroyed or created, which can be seen easily by expanding the fields into creation and annihilation operators multiplying modes as in eq. (0.5).

GLOBAL AND GAUGE SYMMETRIES

A key ingredient to QFTs are symmetries. These are described in the mathematical language of groups, which are a collection of elements with a group operation that is associative, has an identity element and for each element there exists an inverse. Symmetries are said to be global when the group elements do not depend on space-time. These set of symmetries are of utmost importance in physics, since they provide with conservation laws through Noether's theorem. This way, by writing some theory which is invariant under Lorentz transformations one gets conservation of energy and momentum. Another example is the symmetry of the $U(1)$ group, which provides with conservation of electric charge in the context of electromagnetism. The relevant groups

in QFT are Lie groups, which are both groups and differentiable manifolds. In particular, the SM is built out of Yang-Mills theories coupled to matter. These are gauge theories whose Lie group is the special unitarity group $SU(N)$.

By letting the group elements depend on space-time coordinates one extends the symmetry of the theory to be local, what is referred to as gauge symmetry. Gauge symmetry can be seen as a redundancy of the theory, such that performing some local rotation to the fundamental fields leaves physics unchanged. Though it seems unpractical to write our theories of Nature in a redundant way, it is very useful, since these redundancies allow us to write simple Lagrangians which may have unphysical degrees of freedom that can be eliminated by use of gauge redundancy. Such is the case of the polarization of the photon. These particles are described by vector fields with four components (four degrees of freedom)

$$A_\mu(x), \quad \mu = 1, 2, 3, 4, \tag{0.9}$$

though the photon only has two physical polarizations (two degrees of freedom). Invoking gauge symmetry one can eliminate the two unphysical degrees of freedom, while writing a Lagrangian describing only the two physical polarizations of the photon would be extremely difficult.

Another beautiful property of gauge symmetries is that they allow for a geometric interpretation of interactions. For example, the interaction of a photon and a electron can be understood in terms of the parallel transport of the latter along the manifold of the $U(1)$ gauge group. The photon appears as the connection between two points in the manifold of this Lie group, and the field strength tensor as the curvature. This way, all fundamental interactions of Nature can be understood in the light of geometry, like gravity is in General Relativity.

The gauge symmetry group of the SM is

$$SU(3)_c \times SU(2)_w \times U(1)_Y, \tag{0.10}$$

with $SU(3)_c$ the gauge group of the strong interaction (whose charge is called color), $SU(2)_w$ the gauge group of the weak interaction (whose charge is weak-isospin) and $U(1)_Y$ the gauge group of hypercharge.

There are also three important discrete symmetries: charge conjugation (C), parity (P) and time reversal (T). There's a theorem that states that CPT is conserved in the SM. Antiparticles are understood as the CPT conjugate of particles.

FUNDAMENTAL PARTICLES AND THE STANDARD MODEL

Fermions (half-integer spin particles) can be right- or left-handed, corresponding to the two spin subgroups in which the Lorentz group can be decomposed

$$SO(1,3) \approx SU(2)_L \oplus SU(2)_R. \tag{0.11}$$

This way, a fermionic field ψ can be decomposed into components of these two subgroups

$$\psi = \begin{pmatrix} \psi_L \\ \psi_R \end{pmatrix}. \tag{0.12}$$

The particle content of the SM is divided into gauge bosons mediating the three fundamental interactions (gluons for the strong interaction, the photon for the electromagnetic, and the Z and W bosons for the weak interaction), and fermionic matter particles. The latter can be divided into quarks, which are charged under $SU(3)_c$, and leptons, which are not. Being fermions, they can be left- or right-handed.

In the SM, there are 6 species or flavors of left-handed leptons: electron e and electronic neutrino ν_e, muon μ and muonic neutrino ν_μ, tau τ and tauonic neutrino ν_τ. Equivalently, there are also 6 flavors of left-handed quarks: up u, down d, strange s, charm c, top t and bottom b. In turn, these 6 flavors are organized into 3 different generations, each of them a doublet under $SU(2)_w$,

$$\begin{pmatrix} e \\ \nu_e \end{pmatrix}_L , \begin{pmatrix} \mu \\ \nu_\mu \end{pmatrix}_L , \begin{pmatrix} \tau \\ \nu_\tau \end{pmatrix}_L , \tag{0.13}$$

$$\begin{pmatrix} u \\ d \end{pmatrix}_L , \begin{pmatrix} s \\ c \end{pmatrix}_L , \begin{pmatrix} t \\ b \end{pmatrix}_L . \tag{0.14}$$

On the other hand, there are the same 6 flavors of right-handed quarks, but only 3 flavors of right-handed leptons (e, μ, τ).

Finally, there is a doublet under $SU(2)_w$ of complex scalars called the Higgs doublet Φ, responsible for the Spontaneous Symmetry Breaking (SSB) of

$$SU(2)_w \times U(1)_Y \rightarrow U(1)_{em}, \tag{0.15}$$

which is responsible for the generation of mass for the fundamental particles through a non-vanishing vacuum expectation value (vev) for the Higgs field Φ.

All the particles of the SM are charged under $U(1)_Y$.

The complete Lagrangian of the SM can be written in compact form as

$$\mathcal{L} = -\frac{1}{4}F_{\mu\nu}F^{\mu\nu}$$
$$+ i\bar{\psi}\gamma_\mu D_\mu \psi + \text{h.c.}$$
$$+ \psi_i y_{ij} \psi_j \Phi + \text{h.c.}$$
$$+ |D_\mu \Phi|^2 - V(\Phi).$$

The first term contains the kinetic energy of the gauge bosons, while the second that of matter fields (leptons and quarks). The third term are the Yukawa couplings, responsible for the mass of elementary particles once the Higgs field Φ gets a non-vanishing vev, as well as for the mixing of flavor through the CKM matrix. Finally, the last term is the Lagrangian for the scalar Higgs. The pure gauge interactions depend only on three free parameters, which are the three coupling constants. Matter fields do not add any other free parameter. Adding the Higgs field however include 22 new free parameters into the theory, which govern the masses of elementary particles, flavor mixing angles and CP-violating phases.

Along the decades the SM has proven extremely successful in passing experimental tests. In 1973, neutral weak currents caused by the Z boson were discovered at CERN, which granted Glashow, Salam and Weinberg the Nobel Prize in 1979 for formulating the electroweak theory based on the gauge symmetry $SU(2)_\text{w} \times U(1)_\text{Y}$ years before. The Z and W bosons themselves were discovered experimentally in 1983. Furthermore, the ratio of their masses was found to be consistent with the SM prediction. In 1977 the bottom quark was discovered by the Fermilab E288 experiment and the top quark in 1995 by CDF and DØ at Fermilab. This granted Kobayashi and Maskawa the Nobel Prize in 2008 for introducing these quarks into the theory in order to explain CP violation in kaon decay. Finally, the only other not observed particle of the SM, the Higgs boson, was discovered in 2012 at CERN, granting Englert and Higgs the Nobel Prize in 2013.

Despite the astonishing success of the SM, we know it cannot be the whole story. To begin with, it does not explain one of the four fundamental interactions of Nature, gravity. On the other hand, there's no candidate particle in the SM for dark matter, which we know accounts for about 85% of the matter in the Universe. In addition to this, there are other theoretical puzzles, like the hierarchy problem of the Higgs mass, triviality of the Higgs coupling, the flavor puzzle or the strong CP problem, to quote a few. All this points to the fact that the SM is an effective theory that describes extremely well the Universe at the energy scales probed by modern day colliders, but that there must be some new physics lurking at high energy. Search for New Physics (NP) is the holy grail of modern day particle physics.

One way to search for NP is to perform precision tests of the SM. This involves making high precision theoretical predictions and com-

paring them to high precision experiments. This allows to disentangle subtle NP effects that may affect processes accessible to nowadays colliders. In this respect, low-energy QCD is a rich arena to look for NP effects. One good place where to look is at Flavor Changing Neutral Currents (FCNC). These are heavily suppressed by the GIM mechanism in the SM, and thus are expected to be more sensitive to NP effects. On the other hand, in recent years some anomalies have been observed in processes involving B meson decays. In all these processes, QCD plays a crucial role, and thus precise theoretical predictions in this sector of the SM are of utmost importance.

WHY LATTICE FIELD THEORY?

One difficulty arising in QFT is that when computing physical observables, like a scattering amplitude, divergences appear. These are removed from physical observables by the renormalization program. The latter consists in subtracting the divergent pieces appearing in physical quantities by redefining the parameters of the theory which are not observables. For example, one can redefine field normalizations, masses and couplings appearing in the Lagrangian in such a way that though these quantities may diverge, a physical observable like a transition amplitude remains finite. This renormalization program has been applied successfully to the three fundamental interactions described by the SM.

Renormalization introduces the concept of running of coupling constants. These are taken to run with the energy in such a way that physical observables remain finite and independent of the energy scale at which infinites are subtracted in the renormalization program. In the case of electromagnetism, the coupling (the electron electric charge) decreases at low energies. However, in the case of Yang-Mills theories like QCD the opposite is true, and the coupling becomes stronger at lower energies.

The technology usually employed to study Quantum Field Theory is perturbation theory. It consists in expanding expectation values in powers of the coupling of the theory, which must be smaller than 1 in order for the series to be convergent. Perturbation theory can thus be applied for the study of Quantum Electrodynamics at low energies, but not to the study of QCD at these energies. The only other known first-principles method to study QFTs is Lattice Field Theory. It consists in discretizing space-time into a grid or lattice, with space-time points separated by a non-zero lattice spacing a, and Wick rotating to the Euclidean. This allows to treat the theory as a statistical physics system, computing integrals and expectation values numerically. This approach enables to make reliable predictions of non-perturbative phenomena present in the SM such as low-energy

QCD, and thus is of utmost relevance for precision tests of the SM and search of NP.

Non-perturbative treatment of QCD is not only needed for the search of NP. It is also crucial to understand QCD and thus the SM itself, since most of the interesting phenomena of QCD appear due to it being strongly coupled at low energies. This is responsible for the phenomenon of confinement, by which no color charged particles are observed in Nature at low energies. Spontaneous chiral symmetry breaking is also caused by non-perturbative effects, and is responsible for the light mass of pions. It is also expected that a mass gap is dynamically generated by the theory due to its non-perturbative character. This means that the spectrum of QCD (or any other Yang-Mills theory) contains no arbitrarily light particles. This is confirmed experimentally but there is no definite theoretical proof that QCD predicts such a mass gap, though numerical simulations using Lattice Field Theory indicate the existence of it. A definite theoretical proof is one of the famous Millennium Prize Problems. Another important aspect of QCD is to understand its vacuum and the role of the θ-term and topology of the gauge group. Again, to this task is of crucial importance a non-perturbative treatment of the theory.

Non-perturbative treatment of QFT is also crucial for other theoretical reasons beyond QCD. In many popular Beyond the Standard Model (BSM) theories, non-perturbative effects play a central role: in SUSY, non-perturbative effects are invoked to break SUSY at low energies. Also, nearly conformal field theories and technicolor models (which are up-scale version of QCD) require a non-perturbative treatment. More importantly, the SM version of the Higgs potential suffers from the triviality problem. This means that the renormalized Higgs coupling vanishes after perturbative renormalization except if there is a finite energy cutoff in the theory, meaning that the SM is nothing but an Effective Field Theory (EFT) valid up to some energy cutoff. If this is the case, it is expected that the Higgs mass receives large contributions from the high-energy scales, making it naturally heavy, as opposed to what is measured at CERN. This is referred to as the hierarchy problem. Non-perturbative numerical approaches show triviality of any scalar quartic theory (which is the case of the Higgs potential in the SM). However, coupling this scalar to other particle content as in the SM could change the triviality behavior of the coupling. Again, these issues can only be tackled with using non-perturbative approaches.

A MIXED ACTION LATTICE APPROACH TO LIGHT, STRANGE AND CHARM PHYSICS

We have already motivated the need for precision calculations of SM physics involving the strong interaction in order to constrain the

search for NP in experiments. In this thesis we are interested in the definition and setting of a mixed action approach for the study of charm physics with Lattice QCD. This mixed action uses the Wilson fermion regularization for quarks in the sea, with up/down and strange quarks, and the Wilson twisted mass regularization for quarks in the valence, with up/down, strange and charm quarks. When tuning the twisted mass quarks at maximal twist, systematic effects of order $\mathcal{O}(a)$ coming from the discretization of space-time are expected to cancel, improving the scaling of physical observables towards the continuum. This is of relevance for the study of charm physics, since the discretization effects associated to the charm quark are of order $\mathcal{O}(am_c)$ and large due to the heavy mass of the charm m_c. Thus our mixed action is expected to substantially help in the extraction of precision charm observables with a controlled continuum limit.

The use of this mixed action breaks unitarity of the theory, even in the continuum, due to the use of different lattice regularizations for the sea and valence sectors. In order to correct for this effect we must match the physical quark masses in both sectors. Since the sea contains only light (up and down, which are treated as mass degenerate) and strange quarks, we need to tune the parameters of the mixed action in order to impose that the valence up/down and strange physical quark masses are the same as the ones in the sea. This involves precise calculations in the light and strange sectors of QCD, which is what we focus on in this thesis.

Furthermore, in Lattice Field Theory any physical quantity is computed in units of the lattice spacing a. Thus in order to make predictions, one needs to find the value of a in physical units to convert any prediction in the lattice to physical units. This task is called scale setting, and is one of the main focus of this thesis. As computations in Lattice Field Theory have become more and more precise in the recent years, setting the scale with a high accuracy has become one of the main tasks for the community. This is so because its determination affects any prediction of the theory, and in particular its uncertainty affects any other quantity we want to express in physical units.

The thesis is structured as follows. In Chapter 1 we introduce the QCD action in the continuum and its gauge structure. Then we review how it can be formulated in a lattice with finite lattice spacing a. We explain how expectation values are computed numerically bridging the gap between the path integral formalism and statistical mechanics. We explain how the continuum limit is taken and its relation to renormalizability in the continuum. We review the Symanzik improvement program thought to reduce the discretization systematic effects and help in the task of taking the continuum limit. We also explain the program of setting the scale. In Chapter 2 we define all the relevant physical observables that we will need in this thesis and how they are extracted in the lattice. These are meson masses, decay constants,

PCAC quark masses and the Wilson gradient flow scale t_0. We also explain how do we extract the ground state signals of these observables, isolating them from excited states, using model variation techniques. In Chapter 3 we introduce our mixed action regularization. We explain the differences between the sea and valence sectors, and perform the matching between both to impose equality of the physical quark masses in both sectors. We simultaneously tune the valence to maximal twist in order to obtain $\mathcal{O}(a)$ improvement. We also introduce the line of constant physics followed by the ensembles under study and the mass shifting procedure needed to correct for small mistunings along it. In Chapter 4 we perform the scale setting of our mixed action by computing the gradient flow scale t_0 in physical units, using as external physical input the decay constants of the pion and kaon. We explore a set of different models to make the chiral extrapolation to the physical pion mass and the continuum limit to $a \to 0$. We use model averaging techniques to compute a final average result of t_0 in physical units accounting for the systematic uncertainty coming from the model variation. Treating t_0 as an intermediate scale allows to extract the lattice spacing in fm. Finally we present our conclusions in Chapter 5.

This thesis is supplemented with a set of appendices. In Appendix A we present some conventions regarding the Gamma matrices, quark bilinears and the twisted and physical basis used in the different lattice regularizations. In Appendix B we review the gauge ensembles used in this work. In Appendix C we review some useful simulation details of Lattice Field Theories. We give details on the error propagation and treatment of (auto)correlations in Appendix D. In Appendix E we briefly discuss how the Dirac operator needed to compute n-point functions is inverted in the lattice. In Appendix F we give details on the fitting strategy we follow throughout this work. In Appendix G we give expressions for correcting finite volume effects as given by Chiral Perturbation Theory. Finally, in Appendix H we sum up all the results for t_0 in physical units in the continuum and physical pion mass for each model explored for the chiral-continuum extrapolation.

INTRODUCCIÓN

Blabla

Part II

FOUNDATIONS

QCD ON THE LATTICE

1.1 INTRODUCTION

The theory that describes the strong interaction between quarks and gluons is called Quantum Chromodynamics, or QCD.

The underlying symmetry of QCD is associated to the non-abelian $SU(N = 3)$ Lie group. The elements of this group are non-commuting, traceless unitary 3×3 matrices Ω whose determinant det $\Omega = 1$. In order to have a gauge theory we must allow these elements to depend on space-time coordinates. The map

$$\Omega(x) = e^{i\alpha^{(a)}(x)T^{(a)}}, \tag{1.1}$$

provides with a local parametrization of the group close to the identity with coordinates $\alpha^{(a)}(x)$. Summation over $a = 1, ..., N^2 - 1 = 8$ is implicit and $T^{(a)}$ are the 8 generators of the $SU(3)$ Lie group. These live in the Lie algebra $su(3)$, which is the tangent space to the group $SU(3)$ at the identity $I \in SU(3)$. They satisfy the commutation relations

$$\left[T^{(a)}, T^{(b)} \right] = i f_{abc} T^{(c)}, \tag{1.2}$$

where f_{abc} are the structure constants of the group. Unitarity of the group elements means that

$$\Omega^\dagger \Omega = 1. \tag{1.3}$$

The group elements Ω must be in some representation, which determines how they act on a vector space where the degrees of freedom of the theory live. In QCD these are quarks and gluons. The former are described by spinor fields $\psi_{\alpha,i}, \bar{\psi}_{\alpha,i}$. They carry a Dirac spinor index $\alpha = 1, 2, 3, 4$ and a flavor index $i = 1, ..., N_f$, to each flavor corresponding a different mass (in Nature $N_f = 6$). They transform under SU(3) in the fundamental representation,

$$\psi(x) \to \Omega(x)\psi(x), \quad \bar{\psi}(x) \to \bar{\psi}(x)\Omega(x)^\dagger. \tag{1.4}$$

They thus live in a 3-dimensional vector space, having an additional index $c = 1, 2, 3$, called color. Being spinor fields, their dynamics is governed by the Dirac action, which in the Euclidean reads

$$S_F = \sum_{i=1}^{N_f} \int d^4x \ \bar{\psi}^i(x) \left(\gamma_\mu \partial_\mu + m_i \right) \psi^i(x). \tag{1.5}$$

We implicitly sum over the repeated μ index, and we omitted the spinor and color indices. This action is invariant under global $SU(3)$

transformations (Ω independent of x). In order to promote this to a local or gauge symmetry, we need to substitute the derivative by a covariant one

$$\partial_\mu \psi(x) \rightarrow D_\mu(x)\psi(x) = \partial_\mu \psi(x) + iA_\mu(x)\psi(x), \tag{1.6}$$

with A_μ a new field, called the gauge field, which must transform under $SU(3)$ in the adjoint representation

$$A_\mu(x) \rightarrow \Omega(x)A_\mu(x)\Omega^\dagger(x) + i\Omega(x)\partial_\mu\Omega^\dagger(x), \tag{1.7}$$

in order to ensure gauge invariance of the Dirac action. This field A_μ lives in the $su(3)$ algebra, and thus it is a hermitian, traceless 3×3 matrix which can be decomposed as a linear combination of the algebra generators $T^{(a)}$

$$A_\mu = A_\mu^{(a)} T^{(a)}, \tag{1.8}$$

where we again implicitly sum over the repeated index a. The gauge or gluon fields must have a kinetic piece in the action for them to be dynamical. The most general term which satisfies gauge invariance is

$$\frac{1}{2g_0^2} \int d^4x \ \text{tr}(F_{\mu\nu}(x)F_{\mu\nu}(x)). \tag{1.9}$$

This is the Yang-Mills action which describes dynamical gauge fields in the absence of matter. The dimensionless parameter g_0 is the coupling constant and the energy strength tensor $F_{\mu\nu}$ is given by

$$F_{\mu\nu}(x) = \partial_\mu A_\nu(x) - \partial_\nu A_\mu(x) + i\left[A_\mu(x), A_\nu(x)\right]. \tag{1.10}$$

Again, this object lives in the $su(3)$ algebra and can be expressed as

$$F_{\mu\nu} = F_{\mu\nu}^{(a)} T^{(a)}. \tag{1.11}$$

From the transformation in eq. (1.7) we derive the transformation relations of $F_{\mu\nu}$

$$F_{\mu\nu}(x) \rightarrow \Omega(x)F_{\mu\nu}(x)\Omega^\dagger(x). \tag{1.12}$$

Finally, the QCD action in continuum space-time is given by

$$S_{\text{QCD}} = \sum_{i=1}^{N_f} \int d^4x \ \bar{\psi}^i(x) \left(\gamma_\mu D_\mu(x) + m_i\right) \psi^i(x) \tag{1.13}$$

$$+ \frac{1}{2g_0^2} \int d^4x \ \text{tr}\left(F_{\mu\nu}(x)F_{\mu\nu}(x)\right). \tag{1.14}$$

The only parameters of this action are the quark masses m_i and the dimensionless coupling constant g_0.

As mentioned in the Introduction, QCD is strongly coupled at low energies or large distances. One cannot thus rely on perturbation theory to compute physical observables, as an expansion on powers of the

coupling does not converge. The only known first-principles method other than perturbation theory to perform theoretical predictions in Quantum Field Theory is Lattice Quantum Field Theory, or Lattice QCD when applied to the study of Quantum Chromodynamics. This method is based on the discretization of space-time into a hypercubic box or lattice

$$\Lambda = \{n_0, n_1, n_2, n_3 | n_0 = 0, ..., T/a - 1; n_i = 0, ..., L/a - 1; i = 1, 2, 3\},$$
(1.15)

where a is the lattice spacing between two adjacent sites, and L, T are the spatial and temporal lattice extents (in physical units) respectively. The discretization of space-time and introduction of a finite lattice spacing a provides a natural energy cutoff for momenta $\sim a^{-1}$, removing UV divergences. On the other hand, the finite volume lattice ensures the absence of IR divergences. This means that the lattice formulation can be seen as a way to regularize any particular Quantum Field Theory. However, this also implies the presence of finite volume and discretization effects, which should be removed from the predictions. To do this, after having computed the physical observables in the lattice setup, one must perform a continuum extrapolation to obtain results at $a \to 0$ and simulate large enough volumes in order to be able to neglect the effects associated with finite volume. If the theory is renormalizable, physical quantities will remain finite in the continuum limit.

Having discretized space-time, fields are placed at the lattice sites $n \in \Lambda$. Fermions thus look like

$$\psi(n), \bar{\psi}(n), \quad n \in \Lambda.$$
(1.16)

For the gauge fields, it will be helpful to use the definition of a parallel transporter in the manifold of the Lie group $SU(N)$. An N-component unit vector v is parallel transported along a curve in this manifold parameterized by $z_\mu(t)$ from point $z_\mu(a) = x$ to $z_\mu(b) = y$ as

$$v(b) = P(y, x)v(a),$$
(1.17)

$$P(y, x) = e^{i \int_x^y A_\mu(z)dz_\mu},$$
(1.18)

with A_μ the $SU(N)$ gauge fields. This means that a fermion in the fundamental representation picks up a phase of $P(y, x)$ when going from x to y. This parallel transporter is called a gauge link and its discrete version will be the variable to be used in the lattice for the gauge fields. It is an element of the group and transforms as

$$P(x, y) \to \Omega(x)P(x, y)\Omega^\dagger(y).$$
(1.19)

Having defined the fields in the lattice, one needs to discretize the QCD action, formulating it in a finite box Λ in terms of said fields in

such a way that in the continuum limit $a \to 0$ the continuum QCD action is recovered. We discuss this in the following sections.

The Chapter is structured as follows. In Sec. 1.2 we show the Wilson formulation of the gauge action in the lattice, in terms of the link variables. In Sec. 1.3 we show different ways of discretizing the fermion action. In Sec. 1.3.1 we discuss the problem of doublers that appear with a naive fermion discretization and its relation with formulating chiral symmetry in the lattice, briefly commenting on Ginsparg-Wilson fermions. In Sec. 1.3.2 we show the solution to the doublers problem proposed by Wilson, which implies adding a term which explicitly breaks chiral symmetry. This term gives a heavy mass to the doublers that grows with the inverse of the lattice spacing a, and thus they decouple in the continuum. In Sec. 1.3.3 we discuss a modification of Wilson fermions which adds a chirally rotated mass term. This regularization poses some advantages which will be of importance for our study. In Sec. 1.4 we review some concepts of the path integral formalism and how expectation values are computed numerically in the lattice. In Sec. 1.5 we review some concepts of renormalizability and the continuum limit in the lattice. In Sec. 1.6 we discuss the Symanzik improvement program, which allows to reduce cutoff effects associated to the lattice action and fields, helping in the task of performing the continuum limit. Finally, in Sec. 1.7 the procedure to set the scale in the lattice is discussed. This is necessary in order to extract lattice predictions in physical units.

1.2   PURE GAUGE SU(3) IN THE LATTICE

In the lattice, gluon fields can be defined by the link variables $U_\mu(x) \in SU(3)$ that act as a discrete version of the gauge transporters connecting points x and $x + \hat{\mu}$, with $\hat{\mu} = \{a\hat{x}_0, a\hat{x}_1, a\hat{x}_2, a\hat{x}_3\}$

$$U_\mu(x) = \exp\left(iaA_\mu(x)\right). \tag{1.20}$$

The links transform as

$$U_\mu(x) \to \Omega(x)U_\mu(x)\Omega^\dagger(x + \hat{\mu}), \tag{1.21}$$

These fields live on the links of the lattice that connect sites x and $x + \hat{\mu}$.

A common discretization of the gluonic action is the Wilson gauge action [77], which is expressed in terms of the link variables $U_\mu(x)$

$$S_{\mathrm{G}} = \frac{1}{g_0^2} \sum_x \sum_{\mu,\nu} \mathrm{Re}\ \mathrm{tr}\left(1 - U_{\mu\nu}(x)\right), \tag{1.22}$$

where $U_{\mu\nu}(x)$ is the plaquette centered on the lattice site x

$$U_{\mu\nu}(x) = U_\mu(x)U_\nu(x + \hat{\mu})U_\mu^\dagger(x + \hat{\nu})U_\nu^\dagger(x), \tag{1.23}$$

and we have used

$$U_\mu^\dagger(x) = U_{-\mu}(x + \hat{\mu}).$$ (1.24)

Using the Baker-Campbell-Hausdorff formula iteratively

$$\exp\left(A\right)\exp\left(B\right) = \exp\left(A + B + \frac{1}{2}\left[A, B\right] + ...\right),$$ (1.25)

and using eq. (1.20) we get

$$S_\text{G} = a^4 \frac{\beta}{6} \sum_x \sum_{\mu,\nu} \text{tr}\left(F_{\mu\nu}^2(x)\right) + \mathcal{O}(a^2),$$ (1.26)

where we introduced the inverse coupling

$$\beta = \frac{6}{g_0^2}.$$ (1.27)

Taking the continuum limit $a^4 \sum_x \to \int d^4x$ we recover the continuum Yang-Mills action.

Eq. (1.26) shows that the effects related to the discretization of space-time are of order $\mathcal{O}(a^2)$ for the Wilson gauge action. The discretization of the SU(3) pure Yang-Mills action is not unique, and different choices result in different cutoff effects.

The $\mathcal{O}(a^2)$ cutoff effects present in the Wilson regularization of the gauge action can be further reduced by adding additional terms that respect the symmetries of the theory following the Symanzik improvement program. One such choice is the Lüscher-Weisz action [48], which we discuss in Sec. 1.6.

1.3   INTRODUCING FERMIONS IN THE LATTICE

After discretizing the SU(3) gauge action, we still need to find a suitable discrete version of the fermion action in eq. (1.13) to fully formulate QCD on the lattice. It will be shown that theoretical challenges arise with the naive fermion discretization and how these can be addressed with alternative formulations.

1.3.1   *Naive fermions*

To discretize the continuum fermion action in the absence of gauge fields, considering only one flavor with mass m,

$$S_\text{F} = \int d^4x \bar{\psi}(x)\left(\gamma_\mu \partial_\mu + m\right)\psi(x),$$ (1.28)

the derivative ∂_μ needs to take a discrete form, which can be done easily by

$$\partial_\mu \psi(x) \to \hat{\partial}_\mu \psi(x) = \frac{1}{2a}\left(\psi(x + \hat{\mu}) - \psi(x - \hat{\mu})\right).$$ (1.29)

To respect gauge symmetry in our action, we must promote the derivative $\hat{\partial}_\mu$ to a covariant one, as in the continuum case. To achieve this, we note that terms like

$$\bar{\psi}(x)\psi(x+\hat{\mu}), \tag{1.30}$$

which arise from $\bar{\psi}(x)\hat{\partial}_\mu\psi(x)$ are not gauge invariant

$$\bar{\psi}(x)\psi(x+\hat{\mu}) \rightarrow \bar{\psi}(x)\Omega^\dagger(x)\Omega(x+\hat{\mu})\psi(x+\hat{\mu}). \tag{1.31}$$

The solution is again to introduce the link variable or parallel transporter $U_\mu(x)$ from site x to $x+\hat{\mu}$ defined in eq. (1.20) which transforms as in eq. (1.21). This way, the discretized fermion action reads

$$S_{\mathrm{F}} = a^4 \sum_x \bar{\psi}(x) \left(\gamma_\mu \frac{U_\mu(x)\psi(x+\hat{\mu}) - U_\mu^\dagger(x-\hat{\mu})\psi(x-\hat{\mu})}{2a} + m\psi(x) \right). \tag{1.32}$$

However, this naive formulation of the fermion action exhibits the problem of doubling. This means that although we wrote our action to describe one fermion of mass m, for finite lattice spacing a additional poles with the same ground state energy will appear, spoiling the dynamics of the theory. These unwanted additional poles are known as doublers. To see how they appear, consider the massive Dirac operator $D(x,y)$ in the continuum, which can be defined such that

$$S_{\mathrm{F}} = \int d^4x d^4y \ \bar{\psi}(x)D(x,y)\psi(y). \tag{1.33}$$

In the lattice this takes the form

$$S_{\mathrm{F}} = a^4 \sum_{n,m} \bar{\psi}(n)D(n,m)\psi(m), \tag{1.34}$$

with the Dirac operator for the naive fermion formulation given by

$$D(n,m) = \gamma_\mu \frac{U_\mu(n)\delta_{n+\hat{\mu},m} - U_\mu^\dagger(n-\hat{\mu})\delta_{n-\hat{\mu},m}}{2a} + m\delta_{n,m}. \tag{1.35}$$

Restricting to the free massless fermion case $U_\mu = 1$ for illustration, upon Fourier transform we get

$$\tilde{D}(p,q) = \frac{1}{V} \sum_{n,m} e^{-ip\times na} D(n,m) e^{iq\times ma} \tag{1.36}$$

$$= \frac{1}{V} \sum_{n,m} e^{-i(p-q)na} \left(\gamma_\mu \frac{e^{iq_\mu a} - e^{-iq_\mu a}}{2a} \right) \tag{1.37}$$

$$= \delta(p-q)\tilde{D}(p), \tag{1.38}$$

with V the 4-dimensional volume of the lattice and

$$\tilde{D}(p) = \sum_\mu \frac{i}{a}\gamma_\mu \sin(p_\mu a), \tag{1.39}$$

where we made explicit again the sum over μ. The inverse of this operator can be computed as

$$\tilde{D}^{-1}(p) = \frac{ia^{-1}\sum_\mu \gamma_\mu sin(p_\mu a)}{a^{-2}\sum_\mu sin(p_\mu a)^2}. \tag{1.40}$$

We can see that in the continuum $a \to 0$ we recover the correct form of the Dirac operator

$$\tilde{D}(p)^{-1}|_{m=0} \to_{a \to 0} \frac{-i\gamma_\mu p_\mu}{p^2} \tag{1.41}$$

with one single pole at $p^2 = 0$. However, at finite lattice spacing, the denominator in eq. (1.40) vanishes not only for $p = (0, 0, 0, 0)$ but also for

$$p = (\pi/a, 0, 0, 0), \ (0, \pi/a, 0, 0), \ ..., \ (\pi/a, \pi/a, \pi/a, \pi/a). \tag{1.42}$$

These are 15 unwanted poles, the doublers, that only disappear in the continuum, once they become infinitely heavy. These doublers have the same ground energy as the true pole at $p^2 = 0$ and they affect the dynamics of the theory.

The problem of doublers is related to chiral symmetry and its implementation in the lattice. Chiral symmetry in continuum QCD can be expressed as

$$\{D, \gamma_5\} = 0, \tag{1.43}$$

with D the Dirac operator. There's a theorem by Nielsen and Ninomiya [63, 64] that states that one cannot implement chiral symmetry in the way of eq. (1.43) in the lattice without the appearance of doublers. In this lattice formulation of chiral symmetry, there must be an equal number of right movers and left movers. In particular, this means having just one pole is not possible. Ginsparg and Wilson [37] proposed a suitable version of chiral symmetry for the lattice as

$$\{D, \gamma_5\} = aD\gamma_5 D, \tag{1.44}$$

such that in the continuum eq. (1.43) is recovered. With this definition of chiral symmetry in the lattice, it is possible to construct Dirac operators that satisfy eq. (1.44) and are free of doublers.

If one is not interested in studying physics related to chiral symmetry, another choice is to build a Dirac operator that explicitly breaks chiral symmetry but removes the doublers. Wilson fermions and Wilson twisted mass fermions are examples of such a choice, which we will now study.

1.3.2 *Wilson fermions*

Wilson proposed [77] adding an extra term to the naive fermion action in eq. (1.32) to distinguish the doublers from the true pole. The Wilson fermion action reads

$$S_{\mathrm{W}} = a^4 \sum_x \bar{\psi}(x) \frac{1}{2} \left(\gamma_\mu \left(\nabla_\mu + \nabla_\mu^* \right) + 2m - a \nabla_\mu \nabla_\mu^* \right) \psi(x), \quad (1.45)$$

where we have defined the forward and backward discrete covariant derivatives as

$$\nabla_\mu \psi(x) = \frac{U_\mu(x) \psi(x + \hat{\mu}) - \psi(x)}{a}, \quad (1.46)$$

$$\nabla_\mu^* \psi(x) = \frac{\psi(x) - U_\mu^\dagger(x - \hat{\mu}) \psi(x - \hat{\mu})}{a}. \quad (1.47)$$

From the Wilson fermion action (1.45) the Wilson Dirac operator reads

$$D = D_{\mathrm{W}} + m = \frac{1}{2} \left(\gamma_\mu \left(\nabla_\mu + \nabla_\mu^* \right) - a \nabla_\mu \nabla_\mu^* \right) + m, \quad (1.48)$$

where we have introduced the massless Wilson Dirac operator D_{W}, and the action can be written as

$$S_{\mathrm{W}} = a^4 \sum_x \bar{\psi}(x) \left(D_{\mathrm{W}} + m \right) \psi(x). \quad (1.49)$$

For N_f flavors, an additional sum over a flavor index $i = 1, ..., N_f$ is required, and m is promoted to a diagonal matrix in flavor space, whose diagonal elements are m_i. The fermion mass m_i is commonly expressed in terms of the κ parameter

$$\kappa_i = \frac{1}{2am_i + 8}. \quad (1.50)$$

The momentum space massless Dirac operator reads for the free case

$$\tilde{D}_{\mathrm{W}}(p) = \frac{i}{a} \sum_\mu \gamma_\mu \sin(p_\mu a) + \frac{1}{a} \sum_\mu \left(1 - \cos(p_\mu a) \right). \quad (1.51)$$

The second summand in the r.h.s. comes from the Wilson extra term $a \nabla_\mu \nabla_\mu^*$ in the action, and it is responsible for giving an additional mass term to the doublers

$$\frac{2l}{a}, \quad (1.52)$$

where l is the number of momentum components with $p_\mu = \pi/a$ for the doubler. This additional mass distinguishes the doublers from the true pole and makes them decouple as we approach the continuum limit.

The Wilson term $a\nabla_\mu\nabla_\mu^*$ in the Wilson Dirac operator manifestly breaks chiral symmetry, even in the $m_i = 0$ limit, and this symmetry is only restored in the continuum limit. Consequently, the quark mass receives additive renormalization contributions,

$$m_i^R = Z_m\left(m_i - m_{cr}\right),\tag{1.53}$$

since it is no longer protected against these contributions by the axial symmetry.

The Wilson fermion action has $\mathcal{O}(a)$ cutoff effects, which again can be systematically reduced by using the Symanzik improvement program detailed in Sec. 1.6.

1.3.3 *Wilson twisted mass fermions*

Wilson twisted mass (tm) fermions [31–34, 70] introduce an imaginary mass term to the Wilson Dirac operator in eq. (1.48) of the form

$$i\bar{\psi}(x)\boldsymbol{\mu}\gamma_5\psi(x),\tag{1.54}$$

with $\boldsymbol{\mu}$ the twisted quark mass matrix in flavor space. More generally, the Wilson tm Dirac operator reads

$$D = D_W + \boldsymbol{m} + i\boldsymbol{\mu}\gamma_5.\tag{1.55}$$

Our case of interest for this thesis will be

$$\boldsymbol{\mu} = \operatorname{diag}\left(\mu_u, -\mu_d, -\mu_s, \mu_c\right),\tag{1.56}$$

$$\boldsymbol{m} = \operatorname{diag}\left(m_u, m_d, m_s, m_c\right).\tag{1.57}$$

By rotating the fields

$$\psi \;\to\; \psi' = e^{-i\frac{\pi}{2}\gamma_5\frac{T}{2}}\psi, \quad \bar{\psi} \;\to\; \bar{\psi}' = \bar{\psi}e^{-i\frac{\pi}{2}\gamma_5\frac{T}{2}},\tag{1.58}$$

$$T = \operatorname{diag}(\eta_u, \eta_d, \eta_s, \eta_c),\tag{1.59}$$

with $\alpha_i \equiv \frac{\pi}{2}\eta_i$ the so called twist angles, defined with the renormalized standard and twisted quark masses as

$$\cot\alpha_i = \frac{m_i^R}{\mu_i^R},\tag{1.60}$$

one retrieves the usual physical (standard) formulation with real fermionic mass

$$M_i^2 = m_i^2 + \mu_i^2,\tag{1.61}$$

and a chirally rotated Wilson term. The rotated fields $\psi', \bar{\psi}'$ define the so called physical basis, while the unrotated ones $\psi, \bar{\psi}$ define the twisted basis.

In practice we will be working with Wilson tm fermions at full twist

$$\eta_u = \eta_c = -\eta_s = -\eta_d = 1, \tag{1.62}$$

which can be obtained by setting the renormalized standard masses m_i^R to zero. The procedure to achieve this is explained in Sec. 3.5.

Considering for simplicity the light sector of mass-degenerate u and d quarks, at full twist the symmetry group $SU(2)_V \times SU(2)_A$ is broken into

$$SU(2)_V \times SU(2)_A \to [U(1)_A]_1 \times [U(1)_A]_2 \times [U(1)_V]_3, \tag{1.63}$$

with

$$[U(1)_A]_a = \begin{cases} \psi(x) \to e^{i\alpha_A^a \gamma_5 \frac{\tau^a}{2}} \psi(x) & a = 1,2 \\ \bar{\psi}(x) \to \bar{\psi}(x) e^{i\alpha_A^a \gamma_5 \frac{\tau^a}{2}} & a = 1,2 \end{cases}, \tag{1.64}$$

and

$$\partial_\mu V_\mu^{ij} = (m_i - m_j)S^{ij} + i(\eta_i \mu_i - \eta_j \mu_j)P^{ij}, \partial_\mu A_\mu^{ij} \qquad \qquad = (m_i + m_j)P^{ij} + i(\eta_i$$

Note that at zero twist angle $\eta_u = \eta_d = \eta_s = \eta_c = 0$ the twisted and physical basis are the same, and the standard WTIs are recovered. However, at full twist the renormalized standard masses m_i^R vanish, which in turn means that the current masses m_i in eqs. (**??**)-(**??**) also vanish (up to cutoff effects). Moreover, the exact flavor symmetry of massless Wilson fermions implies the existence of a point-split vector current $\tilde{V}_\mu^{ij}$ on the lattice such that the vector WTI holds exactly on the lattice. In the twisted basis, this current takes the form

$$\tilde{V}_\mu^{ij} = \frac{1}{2} \left[\bar{\psi}^i(x)(\gamma_\mu - 1)U_\mu(x)\psi^j(x + \hat{\mu}) + \bar{\psi}^i(x + \hat{\mu})(\gamma_\mu + 1)U_\mu^\dagger(x)\psi^j(x) \right]. \tag{1.66}$$

The conservation of this WTI on the lattice for $\tilde{V}_\mu^{ij}$ means that the point-split vector current renormalizes trivially with

$$Z_{\tilde{V}} = 1. \tag{1.67}$$

Looking at eq. (**??**) this means that for all flavors

$$Z_\mu = Z_P^{-1}. \tag{1.68}$$

1.4   PATH INTEGRAL REGULARIZATION

Having formulated the QCD action in the lattice, we need to see how physical quantities are computed. To do so, we review some aspects of the path integral formulation in Euclidean space-time. In

this formalism, physical quantities are expressed as expectation values of operators

$$\langle O(x_1,...,x_n)\rangle = \frac{1}{\mathcal{Z}} \int \mathcal{D}[\psi,\bar{\psi},U]O(x_1,...,x_n)e^{-S[\psi,\bar{\psi},U]}, \qquad (1.69)$$

$$\mathcal{Z} = \int \mathcal{D}[\psi,\bar{\psi},U]e^{-S[\psi,\bar{\psi},U]}. \qquad (1.70)$$

This is equivalent to expectation values in statistical mechanics with a Boltzmann factor of $e^{-S[\psi,\bar{\psi},U]}$. The action can be decomposed into its gluon and fermion components $S[\psi,\bar{\psi},U] = S_G[U] + S_F[\psi,\bar{\psi}]$, and fermion variables can be integrated out as

$$\langle O(x_1,...,x_n)\rangle = \frac{1}{\mathcal{Z}} \int \mathcal{D}[U]e^{-S_G[U]}\mathcal{Z}_F$$

$$\times \left[\frac{1}{\mathcal{Z}_F} \int \mathcal{D}[\psi,\bar{\psi}]O(x_1,...,x_n)e^{-S_F[\psi,\bar{\psi}]} \right] \qquad (1.71)$$

$$= \frac{1}{\mathcal{Z}} \int \mathcal{D}[U]e^{-S_G[U]}\mathcal{Z}_F \langle O(x_1,...,x_n)\rangle_F, \qquad (1.72)$$

with

$$\mathcal{Z}_F = \int \mathcal{D}[\psi,\bar{\psi}]e^{-S_F[\psi,\bar{\psi}]} = \Pi_{i=1}^{N_f}\det(D). \qquad (1.73)$$

This fermionic determinant can be expressed as an effective action as

$$\langle O(x_1,...,x_n)\rangle = \frac{1}{\mathcal{Z}} \int \mathcal{D}[U]e^{-S_G[U]-S_{\text{eff}}[U]} \langle O(x_1,...,x_n)\rangle_F, \quad (1.74)$$

$$\mathcal{Z} = \int \mathcal{D}[U]e^{-S_G[U]-S_{\text{eff}}[U]}, \qquad (1.75)$$

$$S_{\text{eff}}[U] = -\sum_{i=1}^{N_f} \log\det(D). \qquad (1.76)$$

In order to compute meson observables we will use meson interpolators, which are composite fermionic observables that share the same quantum numbers as the desired meson state. A generic meson interpolator has the form

$$O_A^{ij}(x) = \bar{\psi}^i(x)\Gamma_A\psi^j(x), \qquad (1.77)$$

with Γ_A a Gamma matrix. This way, a meson two-point function reads

$$\left\langle O_A^{ij}(x_1)O_B^{ji}(x_2) \right\rangle = \frac{1}{\mathcal{Z}} \int \mathcal{D}[U]e^{-S_G[U]-S_{\text{eff}}[U]}$$

$$\times \left\langle \bar{\psi}^i(x_1)\Gamma_A\psi^j(x_1)\psi^i(x_2)\Gamma_B\bar{\psi}^j(x_2) \right\rangle_F \qquad (1.78)$$

$$= -\frac{1}{\mathcal{Z}} \int \mathcal{D}[U]e^{-S_G[U]-S_{\text{eff}}[U]}$$

$$\times \text{tr}\left(\Gamma_A D_i^{-1}(x_1,x_2)\Gamma_B D_j^{-1}(x_2,x_1) \right), \qquad (1.79)$$

where the trace is over spin indices and D_i the massive Dirac operator for flavor i. In order to perform this integral numerically, using

the connection with statistical mechanics, a finite set of N_{cnfg} gauge configurations is generated with Boltzmann distribution $e^{-S_{\text{G}}[U] - S_{\text{eff}}[U]}$ following a Markov process (see Appendices C, D). Then, measurements of the quantity

$$P = -\text{tr}\left(\Gamma D_i^{-1}(x_1, x_2)\Gamma D_j^{-1}(x_2, x_1)\right), \tag{1.80}$$

are taken in each of these configurations, and the expectation value is computed as

$$\langle P \rangle = \frac{1}{N_{\text{cnfg}}}\sum_i^{N_{\text{cnfg}}} P_i + \mathcal{O}\left(\frac{1}{\sqrt{N_{\text{cnfg}}}}\right). \tag{1.81}$$

1.5 CONTINUUM LIMIT

The lattice regularization provides a natural energy cutoff a^{-1}, ensuring that any loop integral is finite in perturbation theory. In perturbative renormalization, it is necessary to take the cutoff to infinity, which in the lattice means taking the lattice spacing to $a \to 0$. If the theory is renormalizable, any physical quantity (e.g. a mass m_{phys}) in units of the lattice spacing must vanish in the continuum limit

$$m_{\text{phys}}a \to 0, \tag{1.82}$$

since this means that m_{phys} remains finite in this limit.

Physical quantities are dependent on the couplings of the theory, $m_{\text{phys}}(g_0)$, and accordingly change with them. In turn, one can study how the couplings of the theory change in the lattice as one approaches the continuum limit by decreasing a. To do so and for simplicity, we assume a single coupling g_0, and write the most general local effective action at lattice spacing a_1

$$S(a_1) = g_0(a_1)\sum_i O_i, \tag{1.83}$$

where O_i are all possible local operators respecting the lattice symmetries. When the lattice spacing is reduced to $a_2 < a_1$, all the short-range extra degrees of freedom can be integrated out and reabsorbed into a redefinition of the coupling, such that the new action has the same generic form but with different couplings

$$g_0(a_1) \to R(g_0(a_1)) = g_0(a_2). \tag{1.84}$$

R here stands for the renormalization group (RG) transformation that defines the change in the couplings when varying the lattice spacing.

Since physical quantities change with the couplings, they also do with the lattice spacing, and we want to ensure eq. (1.82) to ensure renormalizability. It can be observed then that renormalizability corresponds to fixed points g_0^* of the RG transformation

$$R(g_0^*) = g_0^*. \tag{1.85}$$

In the context of SU(N) Yang-Mills theory, perturbation theory shows that at a fixed value of the renormalized coupling g_R the bare coupling runs with the lattice spacing as

$$a\frac{\partial g_0}{\partial a} \equiv \beta(g_0) = -\beta_0 g_0^3 - \beta_1 g_0^5 + ...,$$ (1.86)

where $\beta_{0,1}$ are universal coefficients (do not depend on the renormalization scheme) and positive for $N = 3$ colors and $N_f = 6$ flavors, as in the case of QCD. This shows that $g_0 = 0$ is a fixed point of the RG transformations and thus corresponds to the continuum limit. As the fixed point is in the weak coupling regime, this perturbative argument is expected to be valid. Therefore the continuum limit corresponds to

$$g_0 \to 0,$$ (1.87)

or in terms of the inverse coupling β

$$\beta \to \infty.$$ (1.88)

In practice, one cannot numerically simulate at infinite inverse coupling β. Therefore, physical observables are computed at several finite values of β. This introduces $\mathcal{O}(a^n)$ cutoff effects in the results, with some power n. To obtain results in the continuum, one parameterizes these cutoff effects with some function of the lattice spacing and extrapolates to $a \to 0$. However, this task is far from trivial and it has been shown that spectral quantities receive logarithmic corrections in the lattice spacing [42]. To help in the continuum limit extrapolation, one can systematically reduce lattice artifacts, e.g. from $\mathcal{O}(a)$ to $\mathcal{O}(a^2)$ following the Symanzik improvement program.

1.6 SYMANZIK IMPROVEMENT PROGRAM

Symanzik improvement requires improving both the action of the theory and the lattice interpolators that enter the different correlators.

In order to improve a lattice action, one can describe the target continuum action in terms of an effective action in powers of the lattice spacing a

$$S_{\text{eff}} = \int d^4x \sum_k c_k \mathcal{L}_k(x) a^{k-4}.$$ (1.89)

Here $\mathcal{L}_0(x)$ is the discretized lattice Lagrangian unimproved, and the higher-dimension terms $\mathcal{L}_k(x)$ are all possible Lagrangians built from fermion and gluon field operators that preserve the symmetries of the regularized theory, i.e. the lattice theory, with mass dimension $4 + k$, and c_k are numerical coefficients.

In the case of Lattice QCD, we saw that in the Wilson gauge action in eq. (1.26) lattice artifacts appear at $\mathcal{O}(a^2)$, and therefore no

$\mathcal{O}(a)$ improvement is required. However, these $\mathcal{O}(a^2)$ effects can be further reduced by adding all possible dimension $4 + k = 6$ operators that preserve the underlying symmetries of the gauge action. These dimension-6 operators are all three possible ways of writing a closed path in a rectangular lattice with 6 gauge links: planar, twisted and L-shaped rectangles. The action then reads

$$S_G = \frac{\beta}{3} \sum_{\mu\nu} \left[c_0 \sum_p \mathrm{Re}\left(\mathrm{tr}\left(1 - U_{\mu\nu}(p)\right)\right) + \sum_{i=1}^{3} c_i \sum_r \mathrm{Re}\left(\mathrm{tr}\left(1 - U^{(i)}(r)\right)\right) \right],$$

(1.90)

with $U^{(i)}$ said dimension-6 operators. Tuning the coefficients c_i properly leads to $\mathcal{O}(a^2)$ improvement. In our study, the CLS ensembles we employ (see Sec. 3.2) use the so called Lüscher-Weisz gauge action [47, 48], with these coefficients computed at tree-level

$$c_0 = \frac{5}{3}, \quad c_1 = -\frac{1}{12}, \quad c_2 = c_3 = 0.$$

(1.91)

Thus, in the Lüscher-Weisz gauge action the only dimension-6 operators that survive are planar rectangles $U^{(1)}$.

We also need to improve the fermion action. Wilson fermions have $\mathcal{O}(a)$ cutoff effects. In order to improve the Wilson fermion action to $\mathcal{O}(a^2)$ we need to look for all possible operators with dimension $4 + k = 5$ that preserve the lattice symmetries. These are

$$\mathcal{L}_{k=1}^{(1)} = i\bar{\psi}(x)\sigma_{\mu\nu}\hat{F}_{\mu\nu}(x)\psi(x),$$

(1.92)

$$\mathcal{L}_{k=1}^{(2)} = m\mathrm{tr}\left(\hat{F}_{\mu\nu}(x)\hat{F}_{\mu\nu}(x)\right),$$

(1.93)

$$\mathcal{L}_{k=1}^{(3)} = m^2\bar{\psi}(x)\psi(x),$$

(1.94)

with

$$\sigma_{\mu\nu} = \frac{[\gamma_\mu, \gamma_\nu]}{2i},$$

(1.95)

$$\hat{F}_{\mu\nu}(x) = \frac{-i}{8a^2}\left(Q_{\mu\nu}(x) - Q_{\nu\mu}(x)\right),$$

(1.96)

$$Q_{\mu\nu} = U_{\mu\nu}(x) + U_{\nu,-\mu}(x) + U_{-\mu,-\nu}(x) + U_{-\nu,\mu}(x).$$

(1.97)

$\mathcal{L}_{k=1}^{(1),(2)}$ are already present (up to numerical factors) in the original Wilson fermion action and can therefore be reabsorbed in those terms. The $\mathcal{O}(a)$ improved Wilson Dirac operator appearing in the improved fermion action reads

$$D_W + m + c_{sw}a\frac{1}{2}\sum_{\mu<\nu}\sigma_{\mu\nu}\hat{F}_{\mu\nu},$$

(1.98)

with c_{sw} the Sheikholeslami-Wohlert coefficient determined non-perturbatively in [69].

Improving the lattice action ensures improvement of on-shell quantities such as meson masses. However, if one is interested in matrix elements mediated by some current $\mathcal{J}_\mu$, it is also necessary to improve the lattice interpolators that enter into the definition of those currents. In analogy with the improvement of the action, a local operator O is expressed in the Symanzik effective theory as

$$O_{\text{eff}}(x) = \sum_k a^k O_k(x). \tag{1.99}$$

Again, O_k are gauge invariant local operators with the right mass dimensions. Following this, a generic n-point function reads

$$\langle \Phi \rangle = \langle \Phi_0 \rangle - a \int d^4 y \, \langle \Phi_0 \mathcal{L}_1(y) \rangle + a \langle \Phi_1 \rangle + ..., \tag{1.100}$$

with

$$\langle \Phi_0 \rangle = \langle O_0(x_1)...O_0(x_n) \rangle, \tag{1.101}$$

$$\langle \Phi_1 \rangle = \sum_{i=1}^{n} \langle O_0(x_1)...O_1(x_i)...O_0(x_n) \rangle, \tag{1.102}$$

and vacuum expectation values taken in the continuum. The generic form of the O_k operators is a sum over all possible operators Ψ_k with the right mass dimension and that are local and gauge invariant,

$$O_k = \sum_i c_i \Psi_k, \tag{1.103}$$

with c_i some non-perturbatively determined coefficients required to suppress $\mathcal{O}(a^k)$ cutoff effects in the correlation functions. In Sec 2 we discuss the details of operator improvement for the observables of interest.

The $\mathcal{O}(a)$ improved Wilson tm fermion action is analogous to the Wilson case, with the improved Dirac operator given by

$$D_W + m + i\gamma_5 \mu + c_{\text{sw}} a \frac{1}{2} \sum_{\mu < \nu} \sigma_{\mu\nu} \hat{F}_{\mu\nu}. \tag{1.104}$$

The advantage of Wilson tm fermions is that at full twist (vanishing renormalized standard quark mass) one achieves automatic $\mathcal{O}(a)$ improvement [31, 70]. This means that physical quantities are automatically improved without the need of any improvement coefficients for lattice operators. The following argument is based on the original work [31] to which we refer for a complete proof.

At full twist, the Wilson tm Dirac operator reads

$$D_W + i\mu\gamma_5. \tag{1.105}$$

Working in the twisted basis, this action in the continuum is invariant under a discrete chiral symmetry

$$\mathcal{R}_5^{1,2} = \begin{cases} \psi(x) \to i\gamma_5 \tau^{1,2} \psi(x) \\ \bar{\psi}(x) \to \bar{\psi}(x) i\gamma_5 \tau^{1,2} \end{cases}, \tag{1.106}$$

while $\mathcal{L}_{k=1}^{(1)}$ in eq. (1.92) is not

$$\mathcal{L}_{k=1}^{(1)} \to -\mathcal{L}_{k=1}^{(1)}. \tag{1.107}$$

This is key for automatic $\mathcal{O}(a)$ improvement. For correlation functions like eq. (1.100), we have that operators may be even or odd under $\mathcal{R}_5$, $\langle \Phi_0 \rangle$ and $\langle \Phi_1 \rangle$ having opposite $\mathcal{R}_5$-chirality

$$\langle \Phi_0 \rangle \to \pm \langle \Phi_0 \rangle, \quad \langle \Phi_1 \rangle \to \mp \langle \Phi_1 \rangle. \tag{1.108}$$

This means that for even $\langle \Phi_0 \rangle$

$$\langle \Phi_0 \rangle = \langle \Phi_0 \rangle, \quad \left\langle \Phi_0 \mathcal{L}_{k=1}^{(1)} \right\rangle = -\left\langle \Phi_0 \mathcal{L}_{k=1}^{(1)} \right\rangle = 0, \tag{1.109}$$

$$\langle \Phi_1 \rangle = -\langle \Phi_1 \rangle = 0, \tag{1.110}$$

and thus even operators are automatically $\mathcal{O}(a)$ improved. On the other hand, for odd operators what we have is

$$\langle \Phi_0 \rangle = -\langle \Phi_0 \rangle = 0, \quad \left\langle \Phi_0 \mathcal{L}_{k=1}^{(1)} \right\rangle = \left\langle \Phi_0 \mathcal{L}_{k=1}^{(1)} \right\rangle, \tag{1.111}$$

$$\langle \Phi_1 \rangle = \langle \Phi_1 \rangle, \tag{1.112}$$

and thus they vanish in the continuum. Summing up, the only tuning required for Wilson tm fermions to achieve $\mathcal{O}(a)$ improvement is to set the bare quark mass m to its critical value m_{cr} in order to obtain full twist.

In our particular case, we will be working with a mixed action setup employing standard Wilson quarks in the sea and fully twisted Wilson tm quarks in the valence (see Sec 3). This means valence observables still get residual $\mathcal{O}(a)$ cutoff effects from the sea sector, and thus improvement is still needed. However, these effects are expected to be $\mathcal{O}(g_0^4)$ in perturbation theory.

Finally, we also need to improve the bare gauge coupling, which at $\mathcal{O}(a)$ reads

$$\tilde{g}_0^2 = g_0^2 \left(1 + a b_g \text{tr} \left(M_q \right) \right), \tag{1.113}$$

with b_g the improvement coefficient, whose value at one-loop is given in [54].

1.7 SCALE SETTING

In the lattice, all physical observables are computed in units of the lattice spacing a. Thus, in order to make any prediction, it is necessary to determine a in physical units. This task is called scale setting. It involves the precise determination of a reference observable, called the scale, in physical units, to which any other observable is compared to in order to extract the value of the latter in physical units. As an

example, we could use the proton mass m_{proton} as a reference scale, and calculate the ratio of it to a given mass m_i

$$R_i = \frac{m_i}{m_{\text{proton}}}. \tag{1.114}$$

After computing the continuum limit of R_i, we can extract the physical mass m_i as

$$m_i^{\text{ph}} = R_i(a = 0) \times m_{\text{proton}}^{\text{exp}}. \tag{1.115}$$

Here, the proton mass is used as a reference scale, and comparing any lattice observable to it allows to extract the latter in physical units, once the continuum limit is performed. This procedure is equivalent to finding the value of the lattice spacing in physical units, since it can be extracted as

$$a = \frac{(a m_{\text{proton}})^{latt}}{m_{\text{proton}}^{\text{exp}}}. \tag{1.116}$$

From eq. (1.115) it is clear that when aiming for precise lattice calculations of any physical observable like m_i, a reliable and precise scale setting is of the utmost importance. In this example this means being able to determine m_{proton} with high accuracy in the lattice in order to compute the ratios R_i, controlling the continuum limit of R_i and having a high precision in $m_{\text{proton}}^{\text{exp}}$.

In this context, baryon masses like the proton or the Ω baryon mass are popular choices to set the scale [5]. The former is determined with high accuracy experimentally [79] but suffers from the signal-to-noise problem [46, 49] in the lattice determination. This problem is also present in the Ω baryon mass, but the statistical precision is better there [5]. Furthermore, the Ω baryon mass has a weak dependence on the light quark masses and a strong one in the strange quark mass. This makes it an interesting scale for trajectories with constant strange quark mass. Another choice is using meson masses. The pion and kaon meson masses are used to define the line of constant physics along which the continuum limit is taken, and therefore are not available to set the scale. In the past, the ρ meson mass was used to set the scale of quenched simulations [10, 43, 57], but is not suited for dynamical quarks simulations. The Υ meson mass is also used [29, 39] thanks to its precise experimental determination. However large discretization effects due to the b quark are expected.

Instead of using a phenomenological scale like the ones listed above, another choice is to use intermediate scales, like the gradient flow scale t_0 [50, 55] this thesis is based on and that we introduce in Sec. 2.6. This quantity is a popular choice [5, 7, 13, 41, 45, 73] since it can be computed to a very high precision in the lattice, though it cannot be measured experimentally. To obtain its physical value, one constructs a dimensionless quantity $(\sqrt{t_0}\Lambda)^{latt}$ with some phenomenological

quantity Λ in the lattice. After performing the continuum limit, the physical value of t_0 can be extracted as

$$\sqrt{t_0^{\text{ph}}} = \frac{\left(\sqrt{t_0}\Lambda\right)^{\text{latt}}\Big|_{a=0}}{\Lambda^{\text{exp}}}. \tag{1.117}$$

In addition to the continuum limit, in the lattice often unphysical quark masses are simulated, since they are computationally cheaper. This means one needs to perform chiral extrapolations/interpolations of lattice observables to reach physical quark masses. Both chiral and continuum limits are discussed in Sec. 4 for the scale setting we perform in this thesis.

Once the physical value of t_0 is found, it can be used as an intermediate scale against which any other quantity Λ' in the lattice can be compared in order to extract the latter in physical units. For this purpose, one performs a continuum extrapolation of $\sqrt{t_0}\Lambda'$ and obtains the physical value of Λ' as

$$\Lambda'^{\text{ph}} = \frac{\left(\sqrt{t_0}\Lambda'\right)^{\text{latt}}\Big|_{a=0}}{\sqrt{t_0^{\text{ph}}}}. \tag{1.118}$$

This quantity is already a prediction of the lattice.

A popular choice [11–13, 73] for Λ in eq. (1.117) and the one used in this work is to use the pion and kaon decay constants. These exhibit large plateaux in the lattice, indicating that excited states contributions decay fast and therefore they can be determined to a high precision in the lattice. On the other hand, their experimental values are extracted from the weak process $\pi/K \to l\nu$, which leads to the measurement of $V_{ud(us)}f_{\pi(K)}$, with $V_{ud,us}$ CKM matrix elements. This leads to an increase in the uncertainty of the experimental values of $f_{\pi,K}$ coming from the determination of said CKM matrix elements [4].

Finally, other popular intermediate scales to t_0 are ω_0 [7, 11, 45] which is closely related to t_0, and the force scale r_0 [8, 60, 71] which is derived from the static quark-antiquark potential extracted from the evaluation of Wilson loops. This potential shows early plateaux [72] which again indicates that excited states contributions are small.

ON THE EXTRACTION OF PHYSICAL OBSERVABLES

2.1 INTRODUCTION

In this Chapter we discuss the technical details on the extraction of physical observables from the lattice. In Sec. 2.2 we define the two-point functions required for extracting the physical observables needed in the analysis of the scale setting and the light and strange quark masses. In Sec. 2.3 we discuss how to extract meson masses while Sec. 2.4 covers the extraction of decay constants, their improvement and renormalization. In Sec. 2.5 we define the PCAC quark masses which will be used to tune Wilson tm quarks at full twist. In Sec. 2.6 we discuss the gradient flow scale t_0 which we will use as the reference scale for the scale setting. Finally, in Sec. 2.7 we discuss the model averaging technology which we employ in order to find the ground state signals from all these lattice observables.

2.2 CORRELATION FUNCTIONS

For the extraction of the physical observables of interest for this work we need two-point functions involving the pseudoscalar and axial currents, defined as

$$P^{ij}(x) = \bar{\psi}^i(x)\gamma_5\psi^j(x), \tag{2.1}$$

$$A^{ij}_\mu(x) = \bar{\psi}^i(x)\gamma_\mu\gamma_5\psi^j(x), \tag{2.2}$$

where i, j are flavor indices. The Wilson term in the Wilson and Wilson tm fermion action breaks chiral symmetry explicitly. As a result, the Noether currents of the theory are no longer protected against renormalization. This means that both the pseudoscalar and axial currents get renormalized as

$$P^{ij,\mathrm{R}} = Z_P(g_0^2, a\mu)\left(1 + a\tilde{b}_P m_{ij} + a\bar{b}_P \mathrm{tr}\left(M_q\right)\right)P^{ij}, \tag{2.3}$$

$$A^{ij,\mathrm{R}}_\mu = Z_A(g_0^2)\left(1 + a\tilde{b}_A m_{ij} + a\bar{b}_A \mathrm{tr}\left(M_q\right)\right)A^{ij}_\mu, \tag{2.4}$$

where the b-counterterms are improvement coefficients for the renormalization constants. The renormalization constants are shown in Table 2.1, while the improvement coefficients are in Table 2.2. For our purposes, we will only need the differences $\tilde{b}_A - \tilde{b}_P$, $\bar{b}_A - \bar{b}_P$ and $\tilde{b}_A$, the latter given in perturbation theory by [74]

$$\tilde{b}_A = 1 + 0.0472 g_0^2 + \mathcal{O}(g_0^4). \tag{2.5}$$

β	Z_A	Z_P
3.40	0.75642(72)	0.35121(56)
3.46	0.76169(93)	0.34941(44)
3.55	0.76979(43)	0.34767(55)
3.70	0.78378(47)	0.34732(63)
3.85	0.79667(47)	0.35014(73)

Table 2.1: Renormalization constants Z_A and Z_P for different values of β. Z_A, which does not depend on the energy scale but only on the bare coupling g_0^2, is calculated non-perturbatively in [25] using the chirally rotated Schrödinger functional. Z_P is calculated non-perturbatively at the scale $\mu_{\text{had}} = 233(8)$ MeV in [18].

β	$\tilde{b}_A - \tilde{b}_P$	$\bar{b}_A - \bar{b}_P$	$\tilde{b}_A$
3.40	-0.324(17)	$\mathcal{O}(g_0^4)$	1.2684
3.46	-0.265(14)	$\mathcal{O}(g_0^4)$	1.2638
3.55	-0.196(14)	$\mathcal{O}(g_0^4)$	1.2571
3.70	-0.119(14)	$\mathcal{O}(g_0^4)$	1.2467
3.85	-0.073(12)	$\mathcal{O}(g_0^4)$	1.2371

Table 2.2: Summary of improvement coefficients at CLS β values. $\tilde{b}_A - \tilde{b}_P$ is taken from LCP-1 results in [28], while $\bar{b}_A - \bar{b}_P$ are computed in perturbation theory. $\tilde{b}_A$ is computed perturbatively in [74] and given by eq. (2.5)

To achieve $\mathcal{O}(a)$ improvement in the Wilson regularization, we need to improve the axial current as part of the Symanzik improvement program as follows

$$A_\mu^{ij}(x) \rightarrow A_\mu^{ij}(x) + ac_A \tilde{\partial}_{x_0} P^{ij}(x), \tag{2.6}$$

where we defined the symmetric discrete time derivative

$$\tilde{\partial}_{x_0} = \frac{\hat{\partial}_{x_0} - \hat{\partial}_{x_0}^*}{2}, \tag{2.7}$$

$$\hat{\partial}_x f(x) = \frac{f(x+a) - f(x)}{a}, \tag{2.8}$$

$$\hat{\partial}_x^* f(x) = \frac{f(x) - f(x-a)}{a}. \tag{2.9}$$

The improvement coefficient c_A is given non-perturbatively by [16]

$$c_A(g_0^2) = -0.006033 g_0^2 \left[1 + \exp\left(9.2056 - \frac{13.9847}{g_0^2} \right) \right]. \tag{2.10}$$

The two-point functions that we will focus on, projected to zero-momentum are given by

$$C_P^{ij}(x_0, y_0) = \frac{a^6}{L^3} \sum_{\vec{x}, \vec{y}} \left\langle P^{ij}(x) P^{ji}(y) \right\rangle, \tag{2.11}$$

$$C_A^{ij}(x_0, y_0) = \frac{a^6}{L^3} \sum_{\vec{x}, \vec{y}} \left\langle A_0^{ij}(x) P^{ji}(y) \right\rangle. \tag{2.12}$$

The measurements of the two-point functions (see Appendix E) are taken at fixed source times $y_0 = a, T - a$ and evaluated at all sink times x_0. Whenever we omit the source position y_0 in the following means that the average

$$C_X(x_0) = \frac{C_X(x_0, y_0 = a) \pm C_X(T - x_0, y_0 = T - a)}{2}, \tag{2.13}$$

is taken to increase statistics, with the $+$ sign for the $X = P$ case and $-$ sign for the $X = A$ case.

The spectral decomposition of the two-point functions C_X allows to extract relevant hadronic observables such as the meson masses and decay constants. In what follows we restrict to the case of the pion, but the same applies to any other flavor content. Using the Transfer Matrix formalism and imposing as boundary conditions that the initial and final states are given by

$$|\phi(0, \vec{x})\rangle = |\phi_i\rangle, \quad |\phi(T, \vec{x})\rangle = |\phi_f\rangle, \tag{2.14}$$

we can express a generic two-point function by

$$\langle O(x)O(y) \rangle = \mathcal{Z}^{-1} \left\langle \phi_f \right| e^{-(T-x_0)\hat{H}} \hat{O}(\vec{x}) e^{-(x_0-y_0)\hat{H}} \hat{O}(\vec{y}) e^{-y_0\hat{H}} |\phi_i\rangle, \tag{2.15}$$

$$\mathcal{Z} = \left\langle \phi_f \right| e^{-T\hat{H}} |\phi_i\rangle. \tag{2.16}$$

Inserting a complete set of states $|\vec{p}, n\rangle$

$$1 = \frac{1}{2E_n(\vec{p})L^3} \sum_{\vec{p}, n} |\vec{p}, n\rangle \langle \vec{p}, n|, \tag{2.17}$$

this becomes

$$\langle O(x)O(y) \rangle = \mathcal{Z}^{-1} \frac{1}{L^9} \sum_{n,m,l} \sum_{\vec{p}, \vec{q}, \vec{s}} \frac{1}{2^3 E_n(\vec{p}) E_m(\vec{q}) E_l(\vec{s})}$$
$$\times \left\langle \phi_f | \vec{q}, m \right\rangle e^{-(T-x_0)E_m(\vec{q})}$$
$$\times \left\langle \vec{q}, m | \hat{O}(\vec{x}) | \vec{p}, n \right\rangle e^{-(x_0-y_0)E_n(\vec{p})}$$
$$\times \left\langle \vec{p}, n | \hat{O}(\vec{y}) | \vec{s}, l \right\rangle e^{-y_0 E_s(\vec{l})} \left\langle \vec{s}, l | \phi_i \right\rangle. \tag{2.18}$$

The partition function reads

$$\mathcal{Z} = \left\langle \phi_f \right| e^{-T\hat{H}} |\phi_i\rangle = \frac{1}{L^3} \sum_{\vec{p}, n} \frac{1}{2E_n(\vec{p})} \left\langle \phi_f | \vec{p}, n \right\rangle e^{-TE_n(\vec{p})} \left\langle \vec{p}, n | \phi_i \right\rangle \tag{2.19}$$

$$\rightarrow \left\langle \phi_f | 0 \right\rangle e^{-TE_0} \left\langle 0 | \phi_i \right\rangle, \tag{2.20}$$

with

$$|0\rangle \langle 0| \equiv \frac{1}{2E_0 L^3} \left|\vec{0},0\right\rangle \left\langle \vec{0},0\right|. \tag{2.21}$$

We have assumed that the boundary states $\left|\phi_{i,f}\right\rangle$ share the same quantum numbers of the vacuum state $|0\rangle$. This is true when using open boundary conditions (OBC) in time, which will be the case for most of the ensembles under study (see Table B.1).

From the spectral decomposition of the two-point function, the exponentials with arguments $T - x_0$ and y_0 are contributions from the boundary states. We will label the quantum states as $\left|\vec{0}, \alpha, n\right\rangle$, with n labeling the energy level and α the other quantum numbers, and using the fact that we are projecting to zero momentum $\vec{p} = \vec{0}$ we employ the shorthand notation

$$|\alpha, n\rangle \langle \alpha, n| \equiv \frac{1}{2E_n^\alpha L^3} \left|\vec{0}, \alpha, n\right\rangle \left\langle \vec{0}, \alpha, n\right|. \tag{2.22}$$

With all this, the two-point function can be written then as

$$\begin{aligned}
\langle O(x)O(y)\rangle &= \sum_{\alpha,\beta,\gamma} \sum_{n,m,l} \frac{\langle \Omega|\beta,m\rangle}{\langle \Omega|0,0\rangle} e^{-(T-x_0)E_m^\beta} \\
&\quad \times \langle \beta,m| \hat{O}(\vec{x}) |\alpha,n\rangle e^{-(x_0-y_0)E_n^\alpha} \\
&\quad \times \langle \alpha,n| \hat{O}(\vec{y}) |\gamma,l\rangle e^{-y_0 E_s^\gamma} \frac{\langle \gamma,l|\Omega\rangle}{\langle 0,0|\Omega\rangle},
\end{aligned} \tag{2.23}$$

where we absorbed the e^{-TE_0} term coming from the partition function into the energy levels

$$E_n^\alpha \rightarrow E_n^\alpha - E_0, \tag{2.24}$$

such that $E_0^0 = 0$.

For sufficiently large source-sink separation $x_0 - y_0 \rightarrow \infty$, only the pion state $|\pi,0\rangle$ propagates between $O(x)$ and $O(y)$. On the other hand, we made the assumption that the boundary states only overlap with the vacuum, so we are left with

$$\begin{aligned}
\langle O(x)O(y)\rangle &= \sum_{m,l} \frac{\langle \Omega|0,m\rangle}{\langle \Omega|0,0\rangle} e^{-(T-x_0)E_m^0} \langle 0,m| \hat{O}(\vec{x}) |\pi,0\rangle \\
&\quad \times e^{-(x_0-y_0)m_\pi} \langle \pi,0| \hat{O}(\vec{y}) |0,l\rangle e^{-y_0 E_l^0} \frac{\langle 0,l|\Omega\rangle}{\langle 0,0|\Omega\rangle}. \tag{2.25}
\end{aligned}$$

Finally, far away from the boundaries $T - x_0, y_0 \rightarrow \infty$ the first relevant contribution from the boundaries is the one with energy E_1^0

$$\begin{aligned}
\langle O(x)O(y)\rangle &= \langle 0,0| \hat{O}(\vec{x}) |\pi,0\rangle e^{-(x_0-y_0)m_\pi} \langle \pi,0| \hat{O}(\vec{y}) |0,0\rangle \\
&\quad \times \left[1 + \eta_x e^{-(T-x_0)E_1^0} + \eta_y e^{-y_0 E_1^0} + ...\right], \tag{2.26}
\end{aligned}$$

with

$$\eta_x = \frac{\langle \Omega | 0, 1 \rangle \langle 0, 1 | O(x) | \pi, 0 \rangle}{\langle \Omega | 0, 0 \rangle \langle 0, 0 | O(x) | \pi, 0 \rangle}, \tag{2.27}$$

$$\eta_y = \frac{\langle \Omega | 0, 1 \rangle \langle \pi, 0 | O(y) | 0, 1 \rangle}{\langle \Omega | 0, 0 \rangle \langle \pi, 0 | O(y) | 0, 0 \rangle}. \tag{2.28}$$

So far we have assumed OBC in time. In the case with periodic boundary conditions (PBC), the pseudoscalar and axial correlators are periodic in time and identical (up to a relative minus sign for the axial) in x_0 and $T - x_0$. Considering only the ground state contribution we can write them as

$$C_X(x_0, y_0) = a_X \left(e^{-m_\pi(x_0 - y_0)} \pm e^{-m_\pi(T - x_0 + y_0)} \right), \tag{2.29}$$

where the $+$ sign corresponds to the pseudoscalar correlator $X = P$ and the $-$ sign for the axial $X = A$, $a_P = |\langle 0, 0 | P^{ud} | \pi, 0 \rangle|^2$ and $a_A = \langle 0, 0 | A_0^{ud} | \pi, 0 \rangle \langle 0, 0 | P^{ud} | \pi, 0 \rangle$.

2.3 MESON MASSES

Meson masses can be extracted from the pseudoscalar two-point function $C_P(x_0)$ in eq. (2.11) with the effective mass, defined as

$$a m_{\text{eff}}(x_0) = \log \left(\frac{C_P(x_0)}{C_P(x_0 + a)} \right). \tag{2.30}$$

For sufficiently large source-sink separation $x_0 \gg 1$ this effective mass $m_{\text{eff}}(x_0)$ tends to a plateau as can be seen from the spectral decomposition of the two-point function eq. (2.26).

In the case of PBC, to extract the pion mass one can alternatively build the quantity

$$\frac{C_P(x_0)}{C_P(x_0 + a)} = \frac{\cosh(a m_\pi(x_0/a - y_0/a - T/2a))}{\cosh(a m_\pi(x_0/a - y_0/a + a - T/2a))}, \tag{2.31}$$

and fit $a m_\pi$.

The pion mass for a given ensemble is shown in Fig. 2.1.

2.4 DECAY CONSTANTS

Meson decay constants are given by the vacuum-to-meson matrix elements. The matrix element we are interested in is the vacuum-to-pion mediated by the axial current

$$\langle 0, 0 | A_0^{ud} | \pi, 0 \rangle = f_\pi \sqrt{\frac{m_\pi}{2L^3}}, \tag{2.32}$$

where f_π is the bare pion decay constant. To extract this matrix element, we must remove the matrix element $\langle 0,0| P^{ud} |\pi,0\rangle$ from the axial two-point function $C_A(x_0)$ in eq. (2.11). To achieve this, we compute the ratio

$$R(x_0) = \sqrt{\frac{|C_A(x_0, y_0 = a)C_A(x_0, y_0 = T - a)|}{C_P(x_0 = T - a, y_0 = a)}}, \tag{2.33}$$

from which we extract then the decay constant as

$$f_\pi(x_0) = \sqrt{\frac{2}{L^3 m_\pi}} R(x_0). \tag{2.34}$$

In the PBC case, in order to isolate the matrix element $\langle 0,0| A_0^{ud} |\pi,0\rangle$ we fit the axial and pseudoscalar correlators in eq. (2.29) to extract the fit parameters $a_{P,A}$. This allows to compute the decay constant as

$$f_\pi = \frac{2}{L^3 m_\pi} \frac{a_A}{\sqrt{a_P}}. \tag{2.35}$$

In said fit, m_π is not a fit parameter but an external input after having determined it using eq. (2.31).

Following eq. (2.3), the pion decay constant in the Wilson regularization renormalizes as

$$f_\pi = Z_A(g_0^2) \left[1 + a\bar{b}_A \mathrm{tr}\left(M_q\right) + a\tilde{b}_A m_{ud}\right] f_\pi. \tag{2.36}$$

We assumed improvement of the axial current according to eq. (2.6).

In the Wilson tm regularization at full twist, the chiral rotation in eq. (1.58) rotates the axial to the vector current when going from the physical to the twisted basis

$$A_\mu^{ij} \to iV_\mu^{ij}, \tag{2.37}$$

which means that one can compute the decay constant from the vector current in the twisted basis following

$$\langle 0,0| V_0^{ud} |\pi,0\rangle = -if_\pi \sqrt{\frac{m_\pi}{2L^3}}. \tag{2.38}$$

The advantage of this is that the vector current is protected against renormalization (see eq. (1.67)) and thus so is f_π when extracted in this way. Furthermore, in the twisted basis we can use the PCVC Ward identity

$$\left\langle \left(\partial_0^* V_0^{ij}(x)\right) O^{ji}(y)\right\rangle = i\left(\eta_i \mu_i - \eta_j \mu_j\right)\left\langle P^{ij}(x)O^{ji}(y)\right\rangle, \tag{2.39}$$

where O is any interpolator chosen such that $\left\langle P^{ij}(x)O^{ji}(y)\right\rangle$ does not vanish and η_i are given by the maximal twist condition in eq. (1.62), in order to write the decay constant as

$$f_\pi = \sqrt{\frac{2L^3}{m_\pi^3}}\left(|\mu_u| + |\mu_d|\right)\left|\langle 0,0| P^{ud} |\pi,0\rangle\right|. \tag{2.40}$$

Different choices of the interpolator O will lead to different values of the decay constants due to cutoff effects. We choose to use the pseudoscalar density P^{ij} since it enhances the signal. To extract the matrix element $\langle 0,0|\, P^{ud}\, |\pi, 0\rangle$, analogously to the Wilson case we can estimate it by the plateau value of the ratio

$$R(x_0) = \sqrt{\frac{C_P(x_0, y_0 = a)C_P(x_0, y_0 = T - a)}{C_P(x_0 = T - a, y_0 = a)}}.$$ (2.41)

For PBC, using again the PCVC relation, the decay constant reads

$$f_\pi = \sqrt{\frac{2L^3}{m_\pi^3}}\sqrt{a_P}.$$ (2.42)

Since working at full twist, no improvement is needed in the computation of eqs. (2.40)-(2.42)

The ratios defined in this section for the extraction of decay constants are shown for the case of one particular ensemble in Fig. 2.3.

2.5 QUARK MASSES

For the quark masses we use the Partially Conserved Axial Current (PCAC) Ward-Takahashi identity

$$\left\langle \left(\partial_\mu A_\mu^{ij}(x)\right) O^{ji}(y) \right\rangle = 2m_{ij} \left\langle P^{ij}(x)O^{ji}(y) \right\rangle,$$ (2.43)

where O is any interpolator chosen such that $\left\langle P^{ij}(x)O^{ji}(y) \right\rangle$ does not vanish, and m_{ij} is the so called PCAC quark mass, where the flavor indices indicate combinations of the individual quark masses

$$m_{ij} = \frac{m_i + m_j}{2}.$$ (2.44)

The subtracted quark mass $m_i - m_{cr}$ must agree, up to cutoff effects, with the corresponding PCAC quark mass for flavor i after renormalization, so by using the latter we do not need to know a priori the additive mass renormalization. As in the decay constants case, we take $O^{ij} = P^{ij}$ since we find the signal to be enhanced. Thus, the PCAC quark masses read

$$m_{ij}(x_0) = \frac{\tilde{\partial}_{x_0} C_A^{ij}(x_0)}{2C_P(x_0)}.$$ (2.45)

As seen above, the axial current needs to be improved, and the numerator becomes

$$\tilde{\partial}_{x_0} C_A^{ij}(x_0) + ac_A\hat{\partial}_{x_0}\hat{\partial}_{x_0}^* C_P^{ij}(x_0)$$ (2.46)

with the discrete second derivative given by

$$\hat{\partial}_x\hat{\partial}_x^* f(x) = \frac{f(x + a) + f(x - a) - 2f(x)}{a^2} + \mathcal{O}(a^2).$$ (2.47)

Finally, from eq. (2.3) we see that the PCAC quark mass renormalizes as

$$m_{ij}^{\mathrm{R}} = \left[1 + a \left(\bar{b}_A - \bar{b}_P \right) \mathrm{tr} \left(M_q \right) + a \left(\tilde{b}_A - \tilde{b}_P \right) m_{ij} \right] m_{ij}. \tag{2.48}$$

Again, improvement is not needed when working with Wilson tm fermions at full twist.

In the Wilson regularization, physical quark masses are determined from the PCAC masses, while in the Wilson tm regularization at full twist, the latter vanish and the former are given by the renormalized twisted masses in eq. (??).

In Fig. 2.2 we show the dependence of the PCAC quark mass for one given ensemble.

2.6   GRADIENT FLOW

For the scale setting, we will use the gradient flow scale t_0 as an intermediate scale. Gradient flow is defined by the partial differential equation [50, 55]

$$\frac{dB_\mu(x,t)}{dt} = D_\nu G_{\mu\nu}(x,t), \quad B_\mu(x,t=0) = A_\mu(x), \tag{2.49}$$

with A_μ the usual algebra-valued gauge fields. In this equation t is a new fictitious dimension called flow time. The associated field strength tensor $G_{\mu\nu}$ is defined by

$$G_{\mu\nu}(x,t) = \partial_\mu B_\nu(x,t) - \partial_\nu B_\mu(x,t) + i \left[B_\mu(x,t), B_\nu(x,t) \right], \tag{2.50}$$

with the covariant derivative acting on it in the adjoint representation

$$D_\nu G_{\mu\nu} = \partial_\nu G_{\mu\nu} + i \left[B_\mu, G_{\mu\nu} \right]. \tag{2.51}$$

The flow equation can be rewritten as

$$\frac{dB_\mu(x,t)}{dt} = \frac{\delta S_{\mathrm{YM}}[B]}{\delta B_\mu(x,t)}, \quad B_\mu(x,t=0) = A_\mu(x), \tag{2.52}$$

with S_{YM} the continuum Yang-Mills action in eq. (1.9) in terms of the flow fields B_μ. From this we can see that the effect of integrating this equation of motion is to flow the gauge fields towards the local minima of the Yang-Mills action. By solving the flow equation to leading order in the bare coupling g_0

$$B_\mu(x,t) = \frac{g_0}{4\pi t^2} \int d^4 y \, e^{-(x-y)^2/4t} A_\mu(y). \tag{2.53}$$

From this we see that the flow field B_μ is smoothed over space-time with smearing radius $r_{\mathrm{smear}} = 2\sigma = \sqrt{8t}$, σ being the variance of the distribution in eq. (2.53), $\sigma^2 = 2t$.

In the lattice, eq. (2.49) can be expressed as

$$a^2 \frac{dV_\mu(x,t)}{dt} = -g_0^2 \frac{\delta S_G[V]}{\delta V_\mu(x,t)} V_\mu(x,t), \tag{2.54}$$

$$V_\mu(x, t = 0) = U_\mu(x), \tag{2.55}$$

with U_μ the gauge links in eq. (1.20) and S_G the Wilson gauge action in eq. (1.22).

After integrating the flow equation eq. (2.49), the action density at flow time t can be defined as

$$E(x,t) = \frac{1}{2} \text{tr} \left(G_{\mu\nu}(x,t) G_{\mu\nu}(x,t) \right). \tag{2.56}$$

In the lattice, this can be computed by

$$E(x,t) = \sum_{\mu,\nu} \text{Re tr} \left(1 - V_{\mu\nu}(x,t) \right), \tag{2.57}$$

which is just eq. (1.22) but with the plaquette $U_{\mu\nu}(x)$ of gauge links $U_\mu(x)$ replaced by the plaquette $V_{\mu\nu}(x,t)$ of flow fields $V_\mu(x,t)$. After averaging over the 4-dimensional volume

$$E(t) = \langle E(x,t) \rangle_x, \tag{2.58}$$

we are left with an average energy density that depends only on the flow time. This average is computed using the model averaging technique detailed in Sec. 2.7. The quantity $t^2 E(t)$ can be precisely calculated in the lattice, making it a suitable choice for setting the scale (see Sec. 4). To this end, the scale t_0 is defined as the flow time which satisfies

$$t^2 E(t)|_{t=t_0} \equiv 0.3. \tag{2.59}$$

It will be this gradient flow scale t_0 which we will use as an intermediate scale to convert lattice results to physical units. Fig. 2.4 shows the extraction of t_0/a^2 for one particular ensemble.

2.7 GROUND STATE SIGNALS AND MODEL AVERAGE

So far, we have expressed all physical observables under study as functions of the euclidean time x_0. As discussed in Sec. 2.2, these quantities are affected by boundary effects and excited states. In order to extract the ground state contribution of each observable, it is necessary to go to large source-sink separations and ensure sufficient distance from the boundaries. However, it is not clear how to decide when these conditions are met. In the lattice community there are different approaches to address this issue. Our choice is to employ model averaging techniques as proposed in [35, 61, 62].

The idea is to investigate multiple fit functions and/or several fit ranges and assign an Information Criterion IC to each choice, which allows to compute a weight

$$W_i \propto \exp\left(-\frac{1}{2}\text{IC}_i\right),$$

(2.60)

for each choice i of the "model", which refers to a specific fit function and fit range. Then one can compute a weighted average for a fit parameter p that is common to all models as

$$\langle p \rangle_{\text{MA}} = \sum_i p_i W_i,$$

(2.61)

(where p_i is the fit parameter result for model i) and add a systematic uncertainty related to the model variation as

$$\sigma_{\text{syst}}^2[p] = \langle p^2 \rangle_{\text{MA}} - \langle p \rangle_{\text{MA}}^2.$$

(2.62)

For fitting we use a least-squares method that seeks to minimize a χ^2 function by finding the extremal values of the fit parameters (for details see Appendix F). As proposed in [35] we use the Takeuchi's Information Criterion (TIC)

$$\text{TIC} = \chi^2 - 2\langle \chi^2 \rangle,$$

(2.63)

where $\langle \chi^2 \rangle$ is a measure of the expected value of the χ^2, for a precise definition see [14]. This IC is well-behaved for cases where fully correlated fits cannot be performed (see Appendix F for details), which is our case when fitting observables along the euclidean time direction. For a fully correlated fit, $\langle \chi^2 \rangle = \text{dof}$, and thus the TIC reduces to the proposal in [62]

$$\text{TIC} = \chi^2 - 2n_{\text{param}} - 2n_{\text{cut}},$$

(2.64)

with n_{param} the number of parameters of the fit and n_{cut} the number of points left out of the fit. We see that this Information Criterion penalizes models with large number of parameters and big cuts in data, provided the minimization of the χ^2 succeeds.

In practice, for the extraction of the ground state signals of lattice observables, the data is fitted to a constant plus two exponential signals for the OBC ensembles

$$f(x_0) = A + Be^{-Cx_0} + De^{-E(T-x_0)},$$

(2.65)

or for PBC ensembles

$$f(x_0) = A + Be^{-Cx_0} + Be^{-C(T-x_0)},$$

(2.66)

and we investigate the effects of varying the fit range. The result for the fit parameter A corresponds to the ground state signal. An illustration

of the method for the extraction of the ground state signal in the pion effective mass in Fig. 2.1 is shown in Fig. 2.5, where we selected only a subset of the fit ranges explored for visualization purposes.

This model averaging technique will also be used for the chiral and continuum extrapolations needed to set the scale, but there we will also consider the variation of the fit functions and not only cutting data (variation of the fit range), see Secs. 4 and **??**.
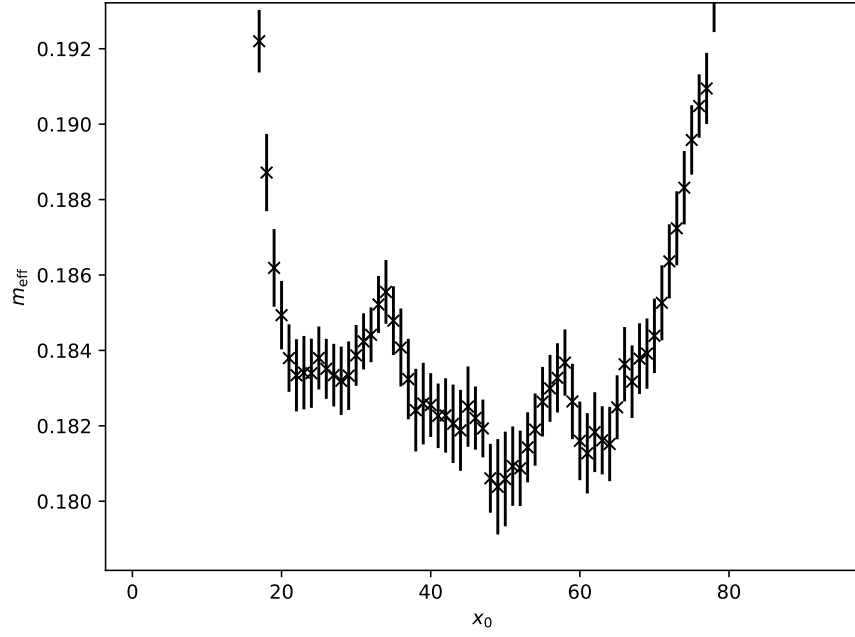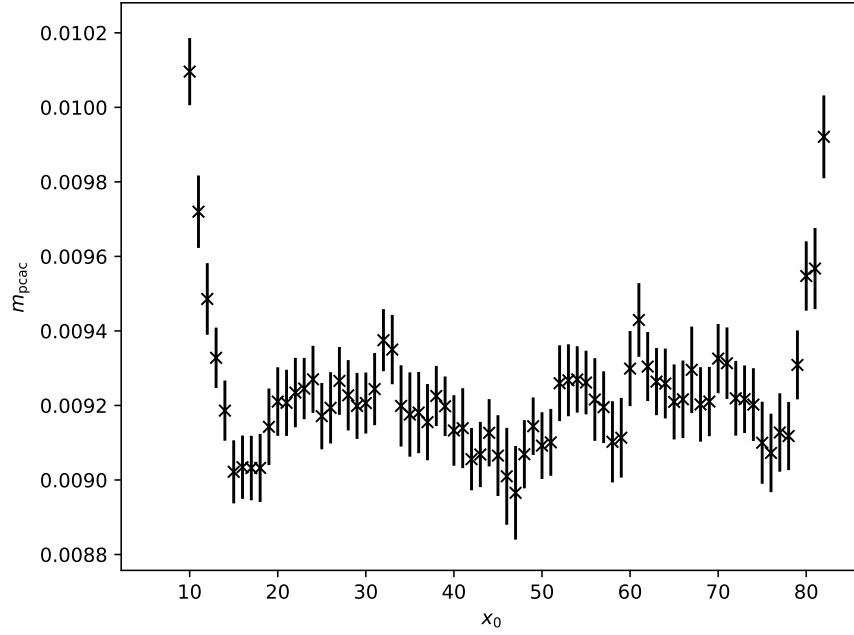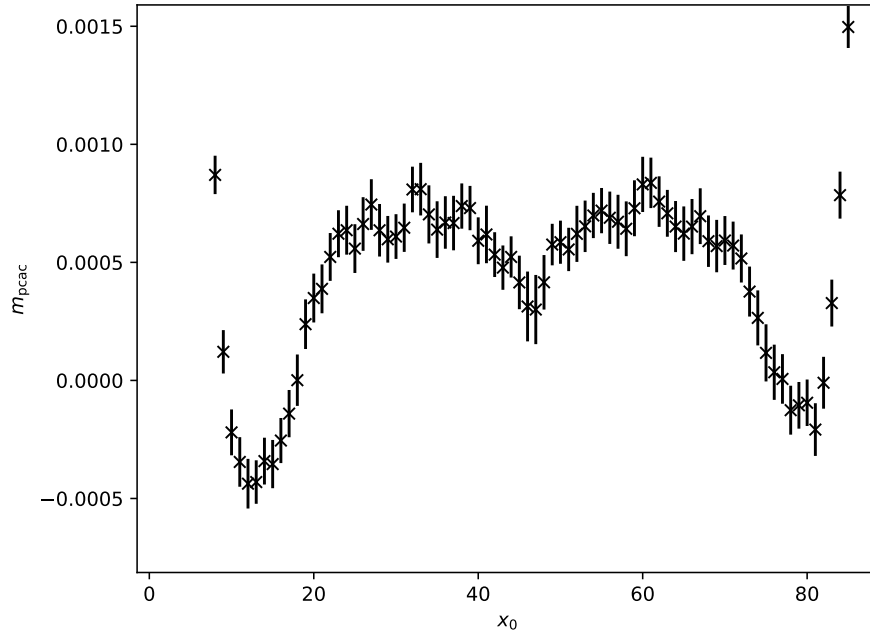
(a)
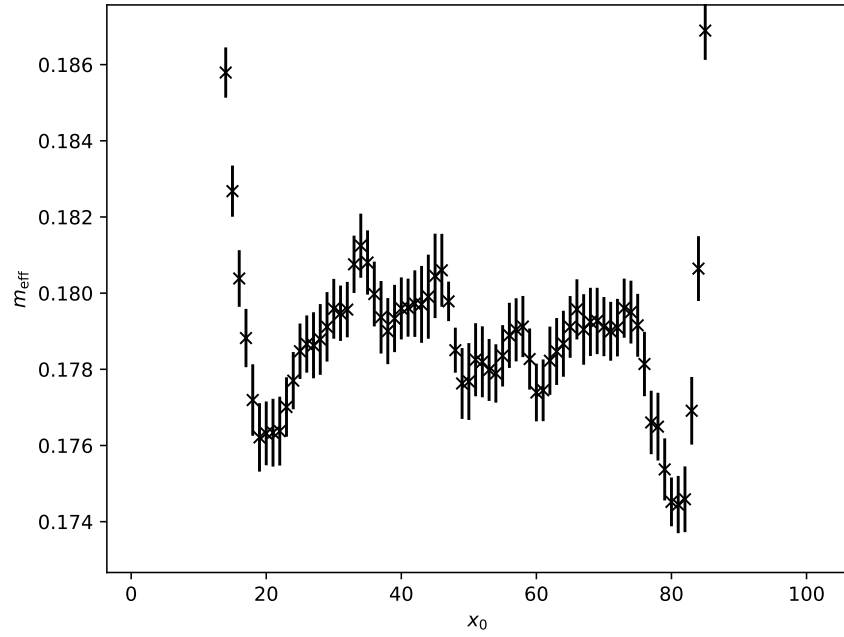
(b)

Figure 2.1: (a): pion effective mass m_{eff} in eq. (2.30) for ensemble H101 in the Wilson regularization. (b): the same but for the mixed action regularization for one point in our valence parameters grid, see Sec. 3.
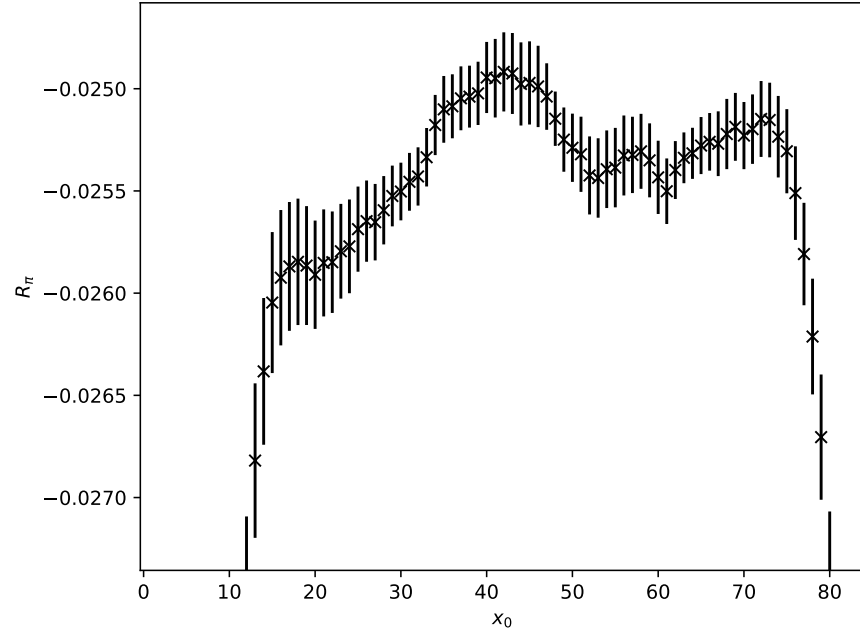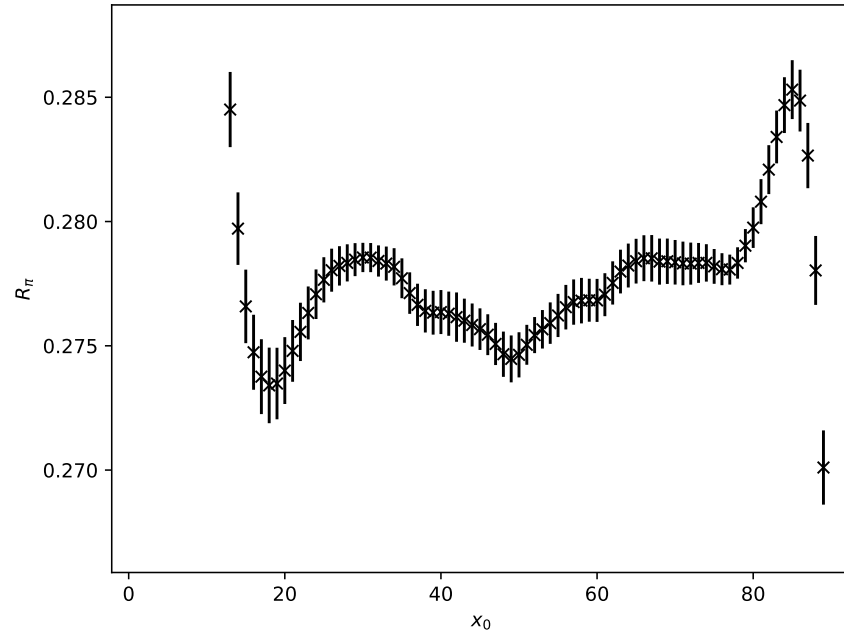
(a)

(b)

Figure 2.2: (a): up-down PCAC quark mass in eq. (2.43) for ensemble H101 in the Wilson regularization. (b): the same but for the mixed action regularization for one point in our valence parameters grid, see Sec. 3.
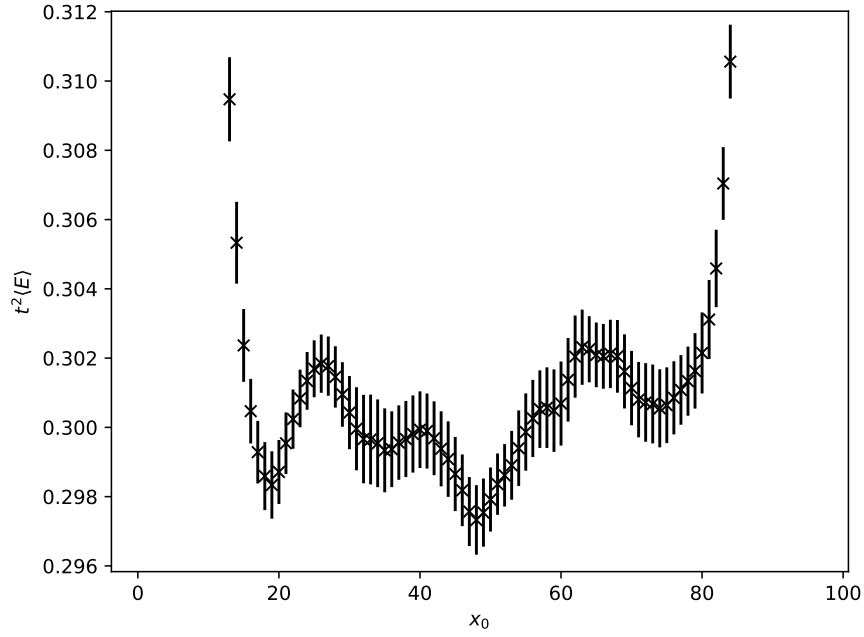
(a)

(b)

Figure 2.3: (a): vacuum-to-pion axial matrix element R_π from eq. (2.33) for ensemble H101 in the Wilson regularization. (b): the same but for the mixed action regularization for one point in our valence parameters grid, see Sec. 3.
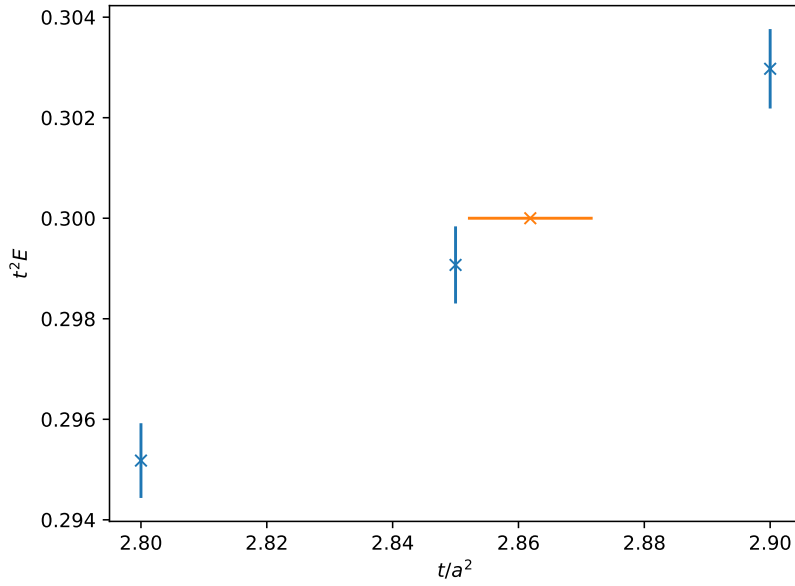
(a)

(b)

Figure 2.4: (a): $t^2E(x,t)$ for one value of the flow time t/a^2 near t_0/a^2 as a function of the euclidean time x_0/a. The energy density $E(x,t)$ is defined in eq. (2.57). (b): euclidean-time averaged values of $t^2E(t)$ for several flow times t/a^2 (blue points) near t_0/a^2 (defined in eq. (2.59)) and the interpolated result for t_0/a^2 (orange point).
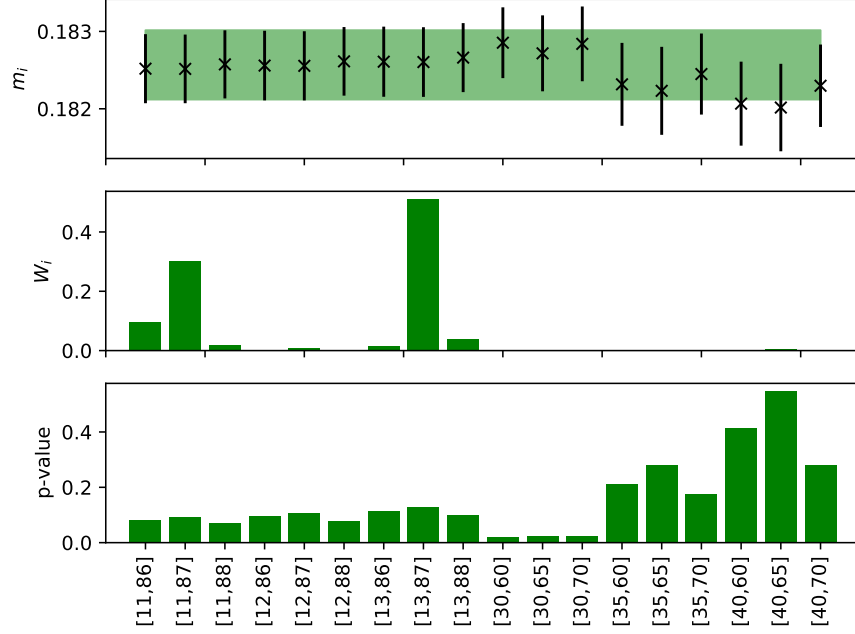
Figure 2.5: Model variation for the extraction of the ground state signal in the pion effective mass of ensemble H101 in the Wilson regularization, shown in Fig. 2.1. From top to bottom we show the ground state signal result from a fit to eq. (2.65) for each fit interval choice, the weight associated to each choice according to eq. (2.60), and the goodness of fit measured through the p-values defined in [14]. We see that the highest weights are associated to a compromise between good fits (in terms of p-values) and fits with large number of points. The right-most models in the plot are heavily penalized even though they have the best p-values, since they cut a large number of points and models with not so severe cuts get also good p-values. The band in the top figure indicates the final weighted average result with the systematic uncertainty in eq. (2.62) included.

Part III

PRECISION PHYSICS FROM A LATTICE QCD
MIXED ACTION

MIXED ACTION SETUP

3.1 MOTIVATION

Our lattice setup is based on a mixed action with Wilson $\mathcal{O}(a)$ improved quarks (see Sec. 1.3.2) in the sea and full twist Wilson tm quarks (see Sec. 1.3.3) in the valence, the goal of which is to control cutoff effects associated with the heavy mass of the charm quark. These effects are of order $\mathcal{O}(am_c)$ with m_c the mass of the charm quark. Exploiting automatic $\mathcal{O}(a)$ improvement of maximal twist Wilson tm fermions is expected to help control the continuum limit and mitigate cutoff effects without the need to introduce any improvement coefficient in the charm sector. Furthermore, the mixed action is yet another valid lattice regularization which provides an independent way of measuring physical observables in the lattice. In this respect, it will allow us to quote independent precision results for the gradient flow scale t_0 (see Sec. 4), the charm quark mass [17] and the $D_{(s)}$ mesons decay constants [17].

For the definition of the mixed action approach, we recall eq. (1.78)

$$\left\langle O^{ij}(x_1)O^{ji}(x_2) \right\rangle = -\frac{1}{\mathcal{Z}} \int \mathcal{D}[U]e^{-S_G[U]-S_{\text{eff}}[U]} \times \tag{3.1}$$

$$\text{tr}\left(\Gamma D_i^{-1}(x_1,x_2)\Gamma D_j^{-1}(x_2,x_1)\right), \tag{3.2}$$

$$S_{\text{eff}}[U] = -\sum_i^{N_f} \log \det(D_i). \tag{3.3}$$

We see that the Dirac operator D appears first in the Boltzmann factor $e^{-S_G[U]-S_{\text{eff}}[U]}$ (which is referred to as the sea sector) with which the set of gauge ensembles is generated (see Appendix C), and then in the fermionic observable whose expectation value we are interested in (which is referred to as the valence sector), thus appearing in two separate stages of the analysis: one the generation of gauge ensembles, the other the inversion of the Dirac operator on said gauge configurations (see Appendix E). This in principle allows for the use of different regularizations of the Dirac operator in these two steps or sectors of the theory. This mixed action approach violates unitarity even once the continuum limit is taken unless the physical quark masses in both sea and valence coincide. This means that our setup will require a tuning procedure in which the values of the Wilson tm parameters are chosen in order to reproduce the same physical quark masses in the valence as in the sea sectors. This process is called matching of the mixed action.

The flavor content of our setup is as follows. On the one hand, the sea sector has $N_f = 2 + 1$ flavors, i.e. two mass-degenerate light quarks (corresponding to the u and d flavors) with mass m_l and one strange quark with mass m_s. On the other hand, the valence sector consists of $N_f = 2 + 1 + 1$ flavors, adding a charm quark. Since we have $N_f = 2 + 1$ in the sea and $N_f = 2 + 1 + 1$ in the valence, the flavors we need to match are the light and strange, treating the charm quark in the valence as a partially quenched flavor.

In order to perform the matching of the theory, we need to know beforehand what values the physical quark masses take in the sea sector. This means that we need lattice measurements in the fully Wilson unitary setup (using the Wilson regularization in the sea and valence) in addition to the mixed action regularization. We therefore have two sets of data for lattice observables: those coming from the Wilson unitary setup, which we refer to as sea or Wilson results, and those coming from the mixed action itself. Using the two sets of data helps increasing the statistics of the scale setting analysis, as we will see in Sec. 4. In addition to the matching of the sea and valence sectors, we also need to tune the valence action parameters to enforce full twist and automatic $\mathcal{O}(a)$ improvement.

The Chapter is structured as follows. In Sec. 3.2 we discuss the sea sector details: ensembles under study, lattice actions and boundary conditions. In Sec. 3.3 we discuss the valence sector, which employs Wilson tm quarks. In Sec. 3.4 we discuss the line of constant physics along which the ensembles under study were generated. They follow a chiral trajectory that suffers small mistunings and that must be corrected in order to go through the physical point. We discuss the details of a mass shifting procedure to account for these effects. Finally, in Sec. 3.5 we deal with the challenges of working with a mixed action and the need to match both sea and valence sectors in order to recover unitarity in the continuum. We also explain the procedure to tune Wilson tm valence quarks to full twist.

3.2 SEA SECTOR

The gauge ensembles that we employ are CLS ensembles [15, 59] with $N_f = 2 + 1$ non-perturbatively $\mathcal{O}(a)$ improved Wilson fermions (see eq. (1.98)). They use the Lüscher-Weisz gauge action [47], which has reduced $\mathcal{O}(a^2)$ effects and is defined in eqs. (1.90-1.91).

For most of the ensembles, open boundary conditions (OBC) in time are used for the gauge fields, since it has been shown that with periodic boundary conditions (PBC) autocorrelations increase as one approaches the continuum limit, a problem known as critical slowing down. This is related to the existence of topological disconnected sectors in gauge field space, which avoids the algorithm to sample correctly different topological sectors. In contrast to this, OBC let the

topological charge flow through the boundaries and topology freezing is thus avoided. All ensembles use PBC over the spatial volume.

The ensembles we consider have 5 different values of the lattice spacing, and for each of them there is one ensemble at the symmetric point, which is defined as $m_l = m_s$, or equivalently by the κ parameter (see eq. (1.50)) as $\kappa_l = \kappa_s$. All the ensembles, the complete list of which is shown in Table B.1, follow the chiral trajectory defined in eq. (3.7).

3.3 VALENCE SECTOR

In the valence sector, we employ a $N_f = 2 + 1 + 1$ fully-twisted Wilson tm fermion action (see Sec. 1.3.3), whose Dirac operator reads

$$D_{\mathrm{W}} + \boldsymbol{m}^{(\mathrm{v})} + i\boldsymbol{\mu}^{(\mathrm{v})}\gamma_5, \tag{3.4}$$

with

$$\boldsymbol{\mu}^{(\mathrm{v})} = \mathrm{diag}(\mu_l, -\mu_l, -\mu_s, \mu_c)^{(\mathrm{v})}, \quad \boldsymbol{m}^{(\mathrm{v})} = \mathrm{diag}(m_l, m_l, m_s, m_c)^{(\mathrm{v})}. \tag{3.5}$$

In particular, we use the same standard quark mass for all flavors $m_l^{(\mathrm{v})} = m_s^{(\mathrm{v})} = m_c^{(\mathrm{v})} \equiv m^{(\mathrm{v})}$.

As discussed in Sec. 1.3.3, to impose full twist means that the twist angles α_i fulfill

$$\cot \alpha_i = \frac{m_i^{\mathrm{R}}}{\mu_i^{\mathrm{R}}} = 0. \tag{3.6}$$

To do so, it is enough to impose that the PCAC quark masses in eq. (2.43) vanish. When this is the case, automatic $\mathcal{O}(a)$ improvement of valence observables is obtained, up to cutoff effects coming from the sea sector due to the mixed action. However, these effects are expected to be $\mathcal{O}(g_0^4)$ in perturbation theory.

In order to find the valence parameters by which sea and valence physical quark masses are matched, in addition to fulfilling the maximal twist condition, we employ a grid of valence parameters values $(\kappa, \mu_l, \mu_s)^{(\mathrm{v})}$ around an estimate of the target point in order to perform small interpolations that allow us to find the said target point $(\kappa, \mu_l, \mu_s)^{(\mathrm{v})^*}$.

3.4 CHIRAL TRAJECTORY

The set of CLS ensembles that we use are generated along the trajectory in the quark mass plane defined by a constant trace of the bare sea "(s)" quark mass matrix

$$\mathrm{tr}\left(M_q^{(\mathrm{s})}\right) = 2m_l^{(\mathrm{s})} + m_s^{(\mathrm{s})} = \mathrm{cnst}. \tag{3.7}$$

This trajectory ensures that at fixed lattice spacing the improved bare coupling

$$\tilde{g}_0^2 = g_0^2 \left(1 + a b_g \text{tr} \left(M_q^{(s)} \right) \right), \tag{3.8}$$

is kept constant as we vary the sea quark masses to approach the physical point. Note that for the Wilson unitary setup, sea and valence quark masses are the same, but not for the mixed action setup. To ensure that this trajectory goes through the physical point, we define the dimensionless quantities

$$\phi_2 = 8 t_0 m_\pi^2, \tag{3.9}$$

$$\phi_4 = 8 t_0 \left(m_K^2 + \frac{1}{2} m_\pi^2 \right), \tag{3.10}$$

which to LO ChPT are proportional to the renormalized quark masses

$$\phi_2 \propto m_l^R, \tag{3.11}$$

$$\phi_4 \propto 2 m_l^R + m_s^R = \text{tr} \left(M_q^R \right). \tag{3.12}$$

The trace of the renormalized quark mass matrix $\text{tr} \left(M_q^R \right)$ is in turn proportional to the bare quark mass matrix up to $\mathcal{O}(a)$ cutoff effects

$$\text{tr} \left(M_q^R \right) = Z_m r_m \left[\left(1 + a \bar{d}_m \text{tr} \left(M_q \right) \right) \text{tr} \left(M_q \right) + a d_m \text{tr} \left(M_q^2 \right) \right]. \tag{3.13}$$

Thus, setting the sea value of ϕ_4 to its physical value for all ensembles ensure that eq. (3.7) holds and goes through the physical point, up to small mistunings due to higher terms in the chiral expansion and to cutoff effects.

To correct for these mistunings, we perform small mass shifts [13] in the bare sea quark masses by Taylor expanding lattice observables as

$$O \left(m_l^{(s)\prime}, m_s^{(s)\prime} \right) = O \left(m_l^{(s)}, m_s^{(s)} \right) + \sum_q \left(m_q^{(s)\prime} - m_q^{(s)} \right) \frac{dO}{dm_q^{(s)}}, \tag{3.14}$$

with the total derivative given by

$$\frac{dO}{dm_q^{(s)}} = \sum_i \frac{\partial O}{\partial \langle P_i \rangle} \left[\left\langle \frac{\partial P_i}{\partial m_q^{(s)}} \right\rangle - \left\langle P_i \frac{\partial S}{\partial m_q^{(s)}} \right\rangle + \langle P_i \rangle \left\langle \frac{\partial S}{\partial m_q^{(s)}} \right\rangle \right]. \tag{3.15}$$

Here O is an arbitrary lattice observable and $\{P_i\}_{i=1,2,\dots}$ is the set of primary observables on which it depends, in our case the corresponding two-point functions. The first term in the r.h.s. of this equation corresponds to the valence contribution to the derivative, while the other terms correspond to the sea contributions. Note that for the Wilson unitary setup, all terms contribute, while for the mixed action setup, since the two-point functions $\{P_i\}$ do not depend explicitly on $m_q^{(s)}$, the first term in the r.h.s. of eq. (3.15) vanishes.

In particular the sum over q in eq. (3.14) can be done in any direction of the quark mass plane, and we choose to mass shift only the strange quark. For practical purposes, since we want to mass shift all relevant observables for each ensemble to satisfy that the sea value of ϕ_4 is equal to its physical value, $\phi_4^{(s)} = \phi_4^{\text{ph}} = \text{const.}$, we rewrite the Taylor expansion as

$$O\left(\phi_4^{(s)'} = \phi_4^{\text{ph}}\right) = O\left(\phi_4^{(s)}\right) + \left(\phi_4^{\text{ph}} - \phi_4^{(s)}\right)\frac{dO}{d\phi_4^{(s)}}, \qquad (3.16)$$

with

$$\frac{dO}{d\phi_4^{(s)}} = \frac{dO/dm_s^{(s)}}{d\phi_4^{(s)}/dm_s^{(s)}}. \qquad (3.17)$$

Note that by sea value $\phi_4^{(s)}$ we refer to ϕ_4 computed in the Wilson unitary setup, and its derivative has both sea and valence contributions, while $dO/dm_s^{(s)}$ has valence and sea contributions when the observable O is computed in the Wilson unitary setup, and only sea contributions when O is computed in the mixed action regularization. In the Wilson unitary setup, imposing $\phi_4^{(s)} = \phi_4^{\text{ph}} = \text{const.}$ means that so does the valence value of ϕ_4, while for the mixed action regularization this is not true. In this case in addition to fixing $\phi_4^{(s)} = \phi_4^{\text{ph}} = \text{const.}$ with the mass shifting procedure we need later to impose $\phi_4^{(v)} = \phi_4^{(s)}$, which is done through the matching between sea and valence sectors (see Sec. 3.5).

The observables we will be interested for the scale setting (see Sec. 4) are $\sqrt{t_0}f_\pi$, $\sqrt{t_0}f_K$ and $\sqrt{t_0}f_{\pi K}$, the latter defined in eq. (4.1). We also include the derivatives of $\sqrt{t_0}m_{12}^R$, $\sqrt{t_0}m_{13}^R$. All these quantities are physical and so are their derivatives w.r.t. ϕ_4. Thus, one can measure these derivatives for each ensemble and then fit them as a function of ϕ_2 and the lattice spacing. This allows to evaluate the result of these fits at the values of ϕ_2 and t_0/a^2 corresponding to each ensemble and perform the mass shift with that result instead of using the individual measurements of each ensemble. This has the advantage of improving the precision for observables whose mass derivatives are noisy or missing, which is particularly relevant for the finest lattice spacing and the most chiral ensembles under study.

For fitting the derivatives we use

$$F = A + B\phi_2 + D\frac{a^2}{t_0}, \qquad (3.18)$$

for all choices of O except for the PCAC quark masses, for which we use

$$F = A + B\phi_2 + C\phi_2^2 + (D + E\phi_2)\frac{a^2}{t_0}, \qquad (3.19)$$

for empirical reasons.

In the case of ϕ_2 in the Wilson regularization, we exclude the symmetric point ensembles from the fit of its mass derivative, since $\phi_2^{\text{sym}} = \frac{2}{3}\phi_4$ by construction. Thus, for these ensembles we will use this relation directly to mass shift ϕ_2.

Results for the fit parameters are presented in Table 3.1, while plots are shown in Figs. 3.1-3.2.

We have assumed knowledge of the physical value of ϕ_4 to which we mass shift all ensembles. However, in order to determine it we need the physical value of the intermediate scale t_0, which is the target of the analysis. Thus, we start the process with an educated guess of t_0^{ph}, which provides with an initial guess for ϕ_4^{ph}. Once the scale setting has been done and a new determination of t_0^{ph} is obtained, the analysis is iterated, updating the value of ϕ_4^{ph} to which the ensembles are shifted, until convergence is observed in this observable. The initial guess used for $t_0^{\text{ph, guess}}$ is just a number with no error. After several iterative steps of the analysis, we obtain the new estimate

$$t_0^{\text{ph, guess}} = 0.1445(6), \tag{3.20}$$

where the uncertainty keeps all the correlations with the lattice data entering the analysis. Eq. (3.20) determines the value of ϕ_4^{ph} to which we perform the mass shifts in the subsequent sections, the input values for physical m_π and m_K given in eq. (4.3).

| O	A	B	C	D	E
$\sqrt{t_0}f_{\pi K}^{W}$	0.017(8)	-0.007(10)	-	0.024(26)	-
$\sqrt{t_0}f_{\pi}^{W}$	0.006(8)	0.008(9)	-	0.020(26)	-
$\sqrt{t_0}f_{K}^{W}$	0.024(10)	-0.016(11)	-	0.022(27)	-
$\sqrt{t_0}m_{12}^{W,\,R}$	0.006(4)	-0.033(13)	0.090(12)	0.046(17)	-0.074(27)
$\sqrt{t_0}m_{13}^{W,\,R}$	0.050(6)	0.030(17)	-0.066(18)	-0.069(33)	0.070(45)
ϕ_2^{W}	0.004(36)	0.131(92)	-	0.874(129)	-
t_0	-0.437(84)	0.214(101)	-	-0.264(274)	-
$\sqrt{t_0}f_{\pi K}^{tm}$	-0.009(7)	0.011(8)	-	-0.014(18)	-
$\sqrt{t_0}f_{\pi}^{tm}$	-0.007(6)	0.013(8)	-	-0.028(18)	-
$\sqrt{t_0}f_{K}^{tm}$	-0.009(8)	0.010(10)	-	-0.006(18)	-
$\sqrt{t_0}m_{12}^{tm,\,R}$	-0.004(3)	0.035(10)	-0.041(9)	0.020(16)	0.026(24)
ϕ_2^{tm}	0.031(17)	-0.032(23)	-	-0.102(73)	-
ϕ_4^{tm}	0.006(37)	0.050(47)	-	-0.298(126)	-
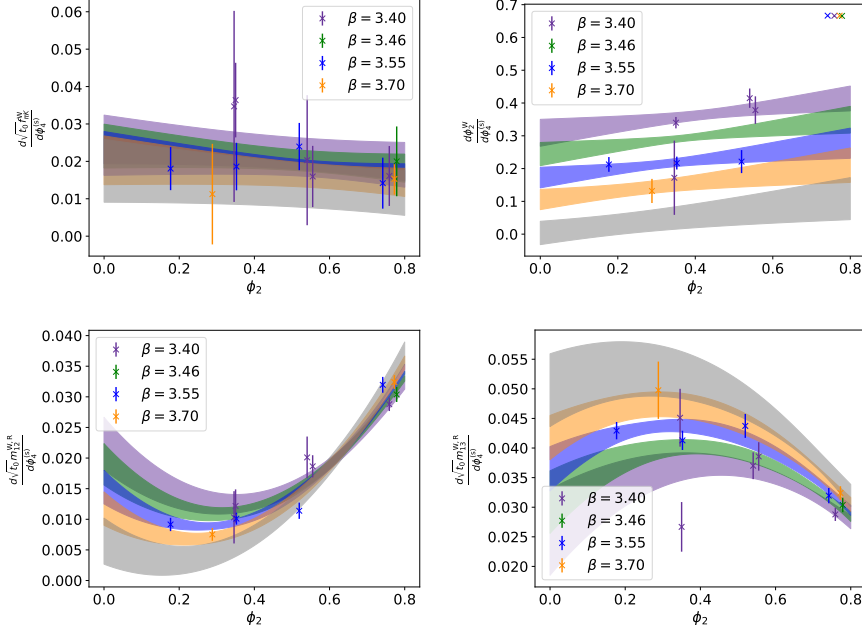
Figure 3.1: Derivatives $dO/d\phi_4^{(s)}$ for the Wilson unitary setup for $O = \sqrt{t_0}f_{\pi K}$, ϕ_2, $\sqrt{t_0}m_{12}^R$, $\sqrt{t_0}m_{13}^R$. For the fit eqs. (3.18)-(3.19) were used. Results for the fit parameters are presented in Table 3.1.

Table 3.1: Results for the fit parameters in eqs. (3.18)-(3.19) for the lattice observables that will be used in the analysis. The superscript "W" refers to the observable being computed in the Wilson unitary setup, while "tm" refers to the mixed action setup.

3.5 MATCHING AND TUNING AT FULL TWIST

As explained in Sec. 3.3, when working with a mixed action, after performing the mass shifts in Sec. 3.4, we need to match the physical quark masses of the sea and valence sectors. To do this, we use a grid of valence parameter values to find the target point with small interpolations. In order to know the values of the relevant observables in the sea, we need measurements in the fully Wilson unitary setup (with Wilson fermions in both sea and valence). These will be referred to as Wilson or sea data or results, while the mixed action measurements, once the matching is done, will be referred to as Wtm or mixed action data or results.

In practice, to compute the physical quark masses we need the relevant improvement coefficients. In order not to rely on these for the matching procedure, instead of matching the physical quark masses
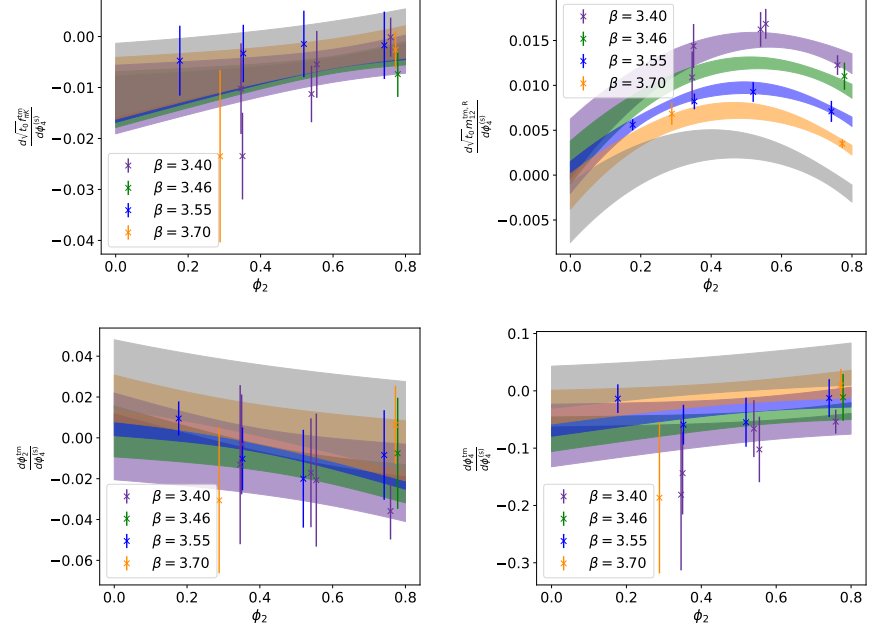
Figure 3.2: Derivatives $dO/d\phi_4^{(s)}$ for the mixed action setup for $O = \sqrt{t_0}f_{\pi K}$, ϕ_2, ϕ_4, $\sqrt{t_0}m_{12}^R$. For the fit eqs. (3.18)-(3.19) were used. Results for the fit parameters are presented in Table 3.1.

we choose to use the pion and kaon masses in units of the gradient flow scale t_0

$$\phi_2^{(s)} = \phi_2^{(v)}, \tag{3.21}$$

$$\phi_4^{(s)} = \phi_4^{(v)}. \tag{3.22}$$

since these quantities are proportional to the physical quark masses to LO ChPT (see eq. (3.9)).

In addition to this, we need to tune the Wilson tm action to full twist, which means setting the valence PCAC quark mass to zero

$$m_{ud}^{(v)} = m_{ll'}^{(v)} \equiv m_{12}^{(v)} = 0. \tag{3.23}$$

In principle, we should also set the strange PCAC quark mass to zero. However, since the $\kappa^{(v)}$ parameter we use is flavor degenerate, this condition is automatically satisfied (up to cutoff effects) once eq. (3.23) is imposed.

To impose eqs. (3.21)-(3.23), we perform interpolations of the valence observables $m_{12}^{(v)}, \phi_2^{(v)}, \phi_4^{(v)}$ in the $(\kappa, \mu_l, \mu_s)^{(v)}$ hyperplane, using as fit functions the following expressions motivated by ChPT

$$m_{12}^{(v)} = p_1 \left(\frac{1}{\kappa^{(v)}} - \frac{1}{\kappa^{(v)*}} \right) + p_2 \left(\mu_l^{(v)} - \mu_l^{(v)*} \right), \tag{3.24}$$

$$\phi_2^{(v)} = \frac{p_3}{\mu_l^{(v)}} \left(\frac{1}{\kappa^{(v)}} - \frac{1}{\kappa^{(v)*}} \right)^2 + p_4 \left(\mu_l^{(v)} - \mu_l^{(v)*} \right) + \phi_2^{(s)}, \tag{3.25}$$

$$\phi_2^{(v)} = \frac{p_5}{\mu_l^{(v)}} \left(\frac{1}{\kappa^{(v)}} - \frac{1}{\kappa^{(v)*}} \right)^2 + \frac{p_6}{\mu_s^{(v)}} \left(\frac{1}{\kappa^{(v)}} - \frac{1}{\kappa^{(v)*}} \right)^2 \tag{3.26}$$

$$+ p_7 \left(\mu_l^{(v)} - \mu_l^{(v)*} \right) + p_8 \left(\mu_s^{(v)} - \mu_s^{(v)*} \right) + \phi_4^{(s)}. \tag{3.27}$$

This way, the target point values $(\kappa, \mu_l, \mu_s)^{(v)*}$ are found as fit parameters. The interpolation is shown in Fig. 3.3. A simultaneous fit of these three quantities is performed.

The mixed action results for the quark masses are given exactly by the target twist mass parameters $\mu_{l,s}^{(v)*}$, while the extraction of the pion and kaon decay constants in the mixed action setup requires an additional interpolation along the valence grid to the target point. The fit functions for this interpolation are

$$f_\pi^{(v)} = q_1 \left(\frac{1}{\kappa^{(v)}} - \frac{1}{\kappa^{(v)*}} \right)^2 + q_2 \left(\frac{1}{\kappa^{(v)}} - \frac{1}{\kappa^{(v)*}} \right) + q_3 \mu_l^{(v)}, \tag{3.28}$$

$$f_K^{(v)} = r_1 \left(\frac{1}{\kappa^{(v)}} - \frac{1}{\kappa^{(v)*}} \right)^2 + r_2 \left(\frac{1}{\kappa^{(v)}} - \frac{1}{\kappa^{(v)*}} \right) + r_3 \mu_l^{(v)} + r_4 \mu_s^{(v)}. \tag{3.29}$$

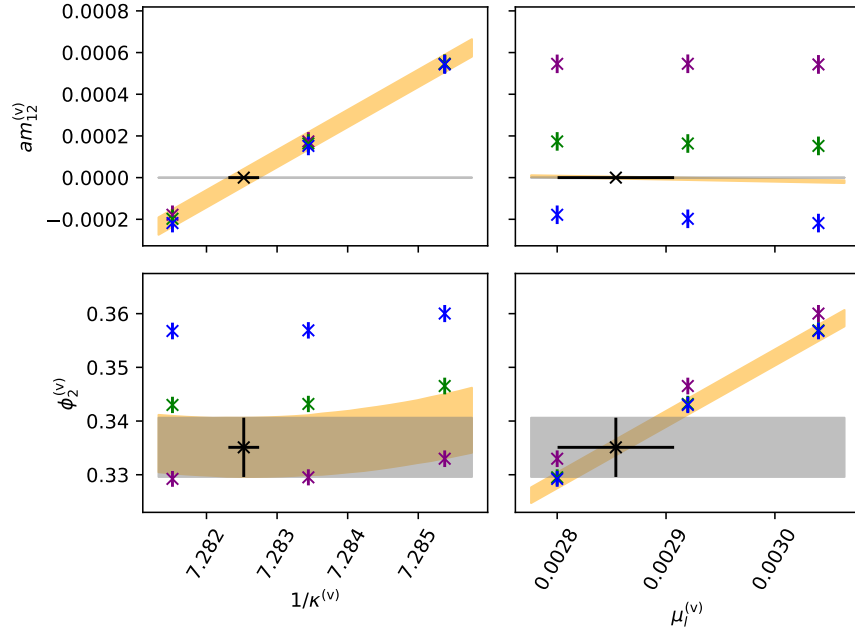The interpolation for the decay constants combination $f_{\pi K}$ defined in eq. (4.1) is shown in Fig. 3.4.

Figure 3.3: Plot of the matching of sea (gray band) and valence values of
ϕ_2 and tune to full twist $am_{12}^{(v)} = 0$ along the grid of valence
parameters values. Each point represents a different measurement
of a lattice observables in the valence along the grid, and the
orange band represents the interpolation. The black point is the
target result $(\kappa, \mu_l, \mu_s)^{(v)*}$. Here we only show the matching of $\phi_2^{(v)}$
and $am_{12}^{(v)}$, though the matching of $\phi_4^{(v)}$ is done simultaneously.
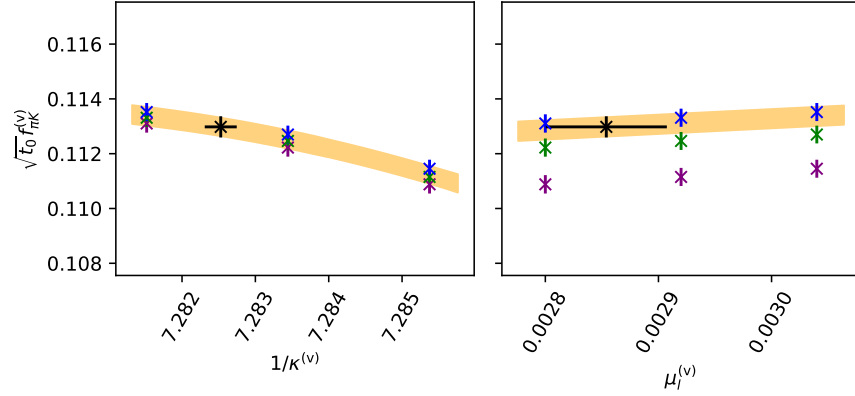Ensemble is H105.

Figure 3.4: Interpolation of $\sqrt{t_0}f_{\pi K}$ (see eq. (4.1)) along the valence grid to
the target point $(\kappa, \mu_l, \mu_s)^{(v)*}$. The points with different colors rep-
resent measurements at different values of the valence parameters.
Ensemble is H105.

4

SCALE SETTING

4.1 MOTIVATION

The scale setting involves the precise determination of one reference observable, the scale, in physical units, to which any other observable is compared in order to extract the value of the latter in physical units.

We decide to use the gradient flow scale t_0 introduced in Sec. 2.6 as an intermediate reference scale since it can be computed in the lattice with high precision. Following the discussion in Sec. 1.7, we choose for the phenomenological input the decay constants of the pion and kaon

$$\Lambda \equiv f_{\pi K} = \frac{2}{3} \left(f_K + \frac{1}{2} f_\pi \right). \tag{4.1}$$

After measuring $\sqrt{t_0} f_{\pi K}$ for each ensemble, one must perform a chiral-continuum limit in order to extract its value at physical quark masses and in the continuum. To define the physical point we use the pion and kaon physical masses, or equivalently the dimensionless quantities ϕ_2 and ϕ_4. For the determination of the physical value of these quantities we need again the physical value of t_0, which is the target of the analysis. As in Sec. 3, we start with an initial guess in eq. (3.20) and iterate the analysis until convergence is observed. Thus, with each iterative step both the values of ϕ_2 to which we perform the chiral extrapolation and the value of ϕ_4 to which we shifted our observables are updated.

Since all lattice observables and the action that we use are $\mathcal{O}(a)$ improved, we expect lattice artifacts to start at $\mathcal{O}(a^2)$.

In order to perform the chiral-continuum limit, we explore different ways of parameterizing the dependence on ϕ_2 (ϕ_4 is constant thanks to the mass shifting procedure of Sec. 3.4) and on the lattice spacing a, and employ the same techniques of model averaging discussed in Sec. 2.7.

After performing the chiral-continuum limit, using as external physical input the values of the pion and kaon decay constants we can determine the value of the scale t_0 as

$$\sqrt{t_0^{\text{ph}}} = \frac{\left(\sqrt{t_0} f_{\pi K} \right)^{\text{latt}} (\phi_2^{\text{ph}}, a = 0)}{f_{\pi K}^{\text{exp}}}. \tag{4.2}$$

In particular, we are studying ensembles which employ $N_f = 2 + 1$ fermions, and thus assume isospin symmetry for the up and down flavors. This means that the physical input for the masses and decay

constants we need is not that of Nature, but that of isosymmetric QCD (isoQCD). These values are given by the Flavor Lattice Average Group (FLAG) in [4]

$$m_\pi^{\text{isoQCD}} = 134.9768(5) \text{ MeV}, \quad m_K^{\text{isoQCD}} = 497.611(13) \text{ MeV},$$

$$(4.3)$$

$$f_\pi^{\text{isoQCD}} = 130.56(2)_{\text{exp}}(13)_{\text{QED}}(2)_{|V_{ud}|} \text{ MeV}, \tag{4.4}$$

$$f_K^{\text{isoQCD}} = 157.2(2)_{\text{exp}}(2)_{\text{QED}}(4)_{|V_{us}|} \text{ MeV}. \tag{4.5}$$

As we see, the kaon decay constant receives a large contribution to its uncertainty from the determination of the $|V_{us}|$ CKM matrix element. Also, QED corrections are stronger in the kaon than in the pion. All these subtleties motivate a scale setting that uses only the pion decay constant as physical input. For this reason we also study this possibility when doing the model variation for the chiral-continuum extrapolation.

4.2   RESULTS: THE PHYSICAL POINT

The choice of the decay constants to set the scale, and in particular of the combination in eq. (4.1) is due to its chiral behavior, since at fixed value of ϕ_4 (as in our case thanks to the mass shifting procedure, see Sec. 3.4) to NLO SU(3) ChPT it only depends on ϕ_2 through chiral logarithms. To this order we have, using $m_u = m_d \equiv m_l$ [3, 6]

$$t_0 = t_{0,\text{ch}} \left(1 + k_1 \frac{2m_K^2 + m_\pi^2}{(4\pi f)^2} \right), \tag{4.6}$$

$$m_\pi^2 = 2B_0 m_l, \tag{4.7}$$

$$m_K^2 = B_0(m_l + m_s), \tag{4.8}$$

$$m_\eta^2 = \frac{4}{3} m_K^2 - \frac{1}{3} m_\pi^2, \tag{4.9}$$

$$f_\pi = f \left[1 + \frac{16 B_0 L_5}{f^2} m_l + \frac{16 B_0 L_4}{f^2} (2m_l + m_s) - 2L(m_\pi^2) \right. \tag{4.10}$$

$$\left. - L(m_K^2) \right], \tag{4.11}$$

$$f_K = f \left[1 + \frac{8 B_0 L_5}{f^2} (m_l + m_s) + \frac{16 B_0 L_4}{f^2} (2m_l + m_s) \right. \tag{4.12}$$

$$\left. - \frac{3}{4} L(m_\pi^2) - \frac{3}{2} L(m_K^2) - \frac{3}{4} L(m_\eta^2) \right], \tag{4.13}$$

where $L(x)$ are chiral logarithms, defined as

$$L(x) = \frac{x}{(4\pi f)^2} \log \frac{x}{(4\pi f)^2}, \tag{4.14}$$

and $f, t_{0,\text{ch}}, k_1, B_0, L_i$ are low energy constants (LECs). The combination $\sqrt{8t_0} f_{\pi K}$ reads

$$F^{\text{cont}}_{\chi,\pi K}(\phi_2) \equiv \left(\sqrt{8t_0} f_{\pi K}\right)^{\text{cont}} = \tag{4.15}$$

$$= \frac{A}{4\pi}\left[1 - \frac{7}{6}\tilde{L}\left(\frac{\phi_2}{A^2}\right) - \frac{4}{3}\tilde{L}\left(\frac{\phi_4 - \frac{1}{2}\phi_2}{A^2}\right)\right. \tag{4.16}$$

$$\left. -\frac{1}{2}\tilde{L}\left(\frac{\frac{4}{3}\phi_4 - \phi_2}{A^2}\right) + \frac{B}{A^2}\phi_4\right], \tag{4.17}$$

with modified chiral logarithms given by

$$\tilde{L}(x) = x\log(x), \tag{4.18}$$

and where we absorbed the LECs into the definition of the parameters A, B as

$$A = 4\pi\sqrt{8t_{0,\text{ch}}}f, \tag{4.19}$$

$$B = \frac{(16\pi)^2}{3}(L_5 + 3L_4) + k_1. \tag{4.20}$$

We use the expression in eq. (4.15) to perform the chiral-continuum extrapolation of $\sqrt{8t_0}f_{\pi K}$. We will use the label $[SU(3)\chi PT]$ for this continuum dependence.

Another possibility for the physical point extrapolation is to use Taylor expansions in ϕ_2 around the symmetric point. We can either go to second or fourth order in the Taylor expansion

$$F^{\text{cont}}_{\text{Tay},\pi K}(\phi_2) \equiv \sqrt{8t_0}f^{\text{cont}}_{\pi K} = A + B\left(\phi_2 - \phi_2^{\text{sym}}\right)^2, \tag{4.21}$$

or

$$F^{\text{cont}}_{\text{Tay},\pi K}(\phi_2) = A + B\left(\phi_2 - \phi_2^{\text{sym}}\right)^2 + C\left(\phi_2 - \phi_2^{\text{sym}}\right)^4, \tag{4.22}$$

labeling these models as $[Tay]$ and $[Tay4]$. Due to symmetry reasons, there are no terms with odd powers of $\phi_2 - \phi_2^{\text{sym}}$ [9].

In order to use $\sqrt{t_0}f_\pi$ and not $\sqrt{t_0}f_{\pi K}$ to set the scale we can use SU(2) ChPT to perform the physical point extrapolation. To NLO ChPT [2, 73]

$$F^{\text{cont}}_{\chi,\pi}(\phi_2) \equiv \sqrt{8t_0}f^{\text{cont}}_\pi = A\phi_2 + B\left(1 - 2\tilde{L}\left(\frac{\phi_2}{B^2}\right)\right), \tag{4.23}$$

$$F^{\text{cont}}_{\chi,K}(\phi_2) \equiv \sqrt{8t_0}f^{\text{cont}}_K = C\phi_2 + D\left(1 - \frac{3}{4}\tilde{L}\left(\frac{\phi_2}{B^2}\right)\right), \tag{4.24}$$

in which case we fit both $\sqrt{t_0}f_\pi$ and $\sqrt{t_0}f_K$ since they share a fit parameter, in order to help control the extrapolation in $\sqrt{t_0}f_\pi$. In the end, however, we set the scale only with external physical input for f_π.

In addition to the extrapolation in the pion mass, we need to supplement these fit functions with cutoff effects in order to describe our lattice data. For this we will explore three possibilities

$$F^{\text{latt}}(\phi_2) = F^{\text{cont}}(\phi_2) + W\frac{a^2}{8t_0}, \tag{4.25}$$

$$F^{\text{latt}}(\phi_2) = F^{\text{cont}}(\phi_2) + W\frac{a^2}{8t_0}\alpha_S(a)^\Gamma, \tag{4.26}$$

$$F^{\text{latt}}(\phi_2) = F^{\text{cont}}(\phi_2) + (W + Z\phi_2)\frac{a^2}{8t_0}. \tag{4.27}$$

We assign the labels $[a^2]$, $[a^2\alpha_S^\Gamma]$ and $[a^2 + a^2\phi_2]$ to characterize the lattice artifacts of these models. The second choice is motivated by [42] where logarithmic corrections in the lattice spacing a where found to affect the continuum limit. In particular, a whole set of powers Γ_i are found to contribute. However, due to the limited number of ensembles studied, sensitivity in this dependence is poor and we can only include one of these powers. We tested the impact of which value of Γ_i to use and no change in the result for t_0^{ph} was found for these models. Furthermore, all choices had the same value for the TIC in eq. (2.63). For these reasons we choose to include in the final model average only the choice $(\Gamma_i)_{\text{min}} = -0.111$. For an estimation of $\alpha_S(a)$ we use

$$\alpha_S(a) \propto -\frac{1}{\log(a\Lambda_{\overline{\text{MS}}})}, \quad \Lambda_{\overline{\text{MS}}}^{(3)} = 339(12) \text{ MeV [4]}. \tag{4.28}$$

The systematic uncertainty in the extraction of $\sqrt{t_0^{\text{ph}}}$ is assessed by the model variation using the TIC introduced in Sec. 2.7. We vary over the different ways of performing the chiral-continuum limits introduced above, as well as over the possibility of performing data cuts. In particular, we consider the following cuts (in addition to the "no cut" choice)

$$\beta > 3.40, \quad \beta > 3.46, \quad \phi_2 < 0.6, \tag{4.29}$$

$$\phi_2 < 0.4, \quad \beta > 3.40 \text{ \& } \phi_2 < 0.6, \tag{4.30}$$

$$m_\pi L > 4.1. \tag{4.31}$$

Finally, to perform all of these fits, we have two data sets: the Wilson unitary setup and the mixed action. Both must share the same continuum limit, but different cutoff effects. We can thus perform the continuum-chiral extrapolations for the Wilson data, for the mixed action, or for a combined data set, parameterizing the data with the same continuum limit behavior $F^{\text{cont}}(\phi_2)$ but different cutoff effects (different W, Z fit parameters for Wilson and mixed action data). This third choice allows to further constrain the continuum extrapolation and keep it well under control, while increasing the statistics and

getting better precision for $\sqrt{t_0^{\text{ph}}}$. As a universality check, we performed the continuum limit only of symmetric point ensembles of both the Wilson and mixed action data, without imposing a common value in the continuum. Since all these points have the same ϕ_2 they follow a line of constant physics as we approach the continuum. This extrapolation is shown in Fig. 4.1 and indeed it shows that both data sets agree perfectly well in the continuum, with the mixed action data having much milder cutoff effects.

Once the various models to extrapolate to the continuum and physical point have been explored, we use the model averaging technique in Sec. 2.7 to assign a weight to each model

$$W \propto \exp\left(-\frac{1}{2}\left(\chi^2 - 2\langle\chi^2\rangle\right)\right), \tag{4.32}$$

that allows us to compute a weighted average for $\sqrt{t_0^{\text{ph}}}$, as well as the associated systematic uncertainty

$$\left\langle\sqrt{t_0^{\text{ph}}}\right\rangle = \sum_i \sqrt{t_0^{\text{ph},(i)}} W^{(i)}, \tag{4.33}$$

$$\sigma_{\text{syst}}^2 = \left\langle\sqrt{t_0^{2,\text{ph}}}\right\rangle - \left\langle\sqrt{t_0^{\text{ph}}}\right\rangle^2. \tag{4.34}$$

In Figs. 4.3-4.5 we show the model average results for the Wilson unitary setup, for the mixed action and for the combined analysis. In Appendix H we show the numerical results of $\sqrt{t_0^{\text{ph}}}$ for each model considered, together with their weights and p-values, for the Wilson, mixed action and combined analysis. In Fig. 4.2 we show the pion mass dependence of the continuum-chiral extrapolation for one of the best models explored in terms of the TIC for the combined data sets, together with the lattice spacing dependence for the same model, projecting all points to the physical pion mass ϕ_2^{ph} using the fit result for the continuum piece $F^{\text{cont}}(\phi_2)$.

The final results for $\sqrt{t_0^{\text{ph}}}$ in physical units as computed from the model average for the different data sets, using $f_{\pi K}^{\text{isoQCD}}$ as physical input, are

$$\sqrt{t_0^{\text{ph}}} = 0.1436(7)_{\text{stat}}(3)_{\text{syst}} \text{ fm, Wilson } [f_{\pi K}], \tag{4.35}$$

$$\sqrt{t_0^{\text{ph}}} = 0.1441(9)_{\text{stat}}(6)_{\text{syst}} \text{ fm, Mixed action } [f_{\pi K}], \tag{4.36}$$

$$\sqrt{t_0^{\text{ph}}} = 0.1440(6)_{\text{stat}}(4)_{\text{syst}} \text{ fm, Combined } [f_{\pi K}]. \tag{4.37}$$

As mentioned above, relying on external physical input of f_K to set the scale is problematic due to uncertainties in the definition of f_K^{isoQCD} related to QED corrections. Furthermore, the very experimental measurement of f_K relies on information on the CKM matrix element V_{us},
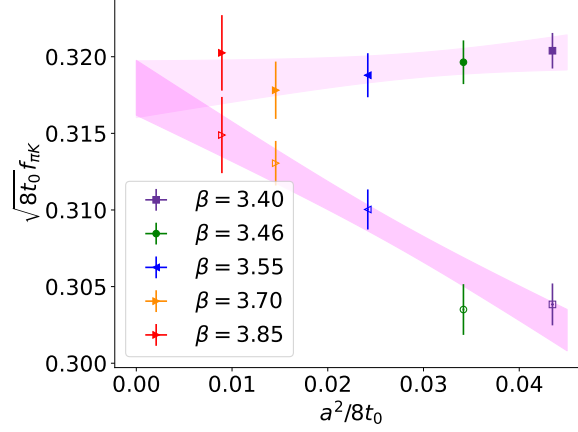
Figure 4.1: Continuum limit of symmetric point ensembles for the Wilson unitary results or sea data set (empty points) and for the mixed action results (filled points). A common continuum limit is not imposed. Cutoff effects are parameterized as pure $\mathcal{O}(a^2)$ artifacts.

and as such f_K has a big uncertainty associated to this. This makes of particular importance to set the scale using only external physical input of f_π. To this end, we explore chiral fits to eqs. (4.23)-(4.24), in addition to the different possibilities for the continuum limit and cuts in data introduced above. Though we fit both $\sqrt{t_0}f_\pi$ and $\sqrt{t_0}f_K$ simultaneously since they share a fit parameter in the chiral dependence, we extract t_0^{ph} as

$$\sqrt{t_0^{\text{ph}}} = \frac{\left(\sqrt{t_0}f_\pi\right)^{\text{latt}}\left(\phi_2^{\text{ph}}, a = 0\right)}{f_\pi^{\text{isoQCD}}}. \tag{4.38}$$

After model averaging we find the results

$$\sqrt{t_0^{\text{ph}}} = 0.1426(8)_{\text{stat}}(2)_{\text{syst}} \text{ fm, Wilson } [f_\pi], \tag{4.39}$$

$$\sqrt{t_0^{\text{ph}}} = 0.1454(9)_{\text{stat}}(8)_{\text{syst}} \text{ fm, Mixed action } [f_\pi], \tag{4.40}$$

$$\sqrt{t_0^{\text{ph}}} = 0.1438(6)_{\text{stat}}(11)_{\text{syst}} \text{ fm, Combined } [f_\pi]. \tag{4.41}$$

We show the model average results in Figs. 4.7-4.9, and the numerical values can be found in Appendix H. Finally, in Fig. 4.6 we show the particular case of one of the models entering the model average.

4.3   RESULTS: THE SYMMETRIC POINT

The symmetric point is defined as the point in the quark mass plane such that
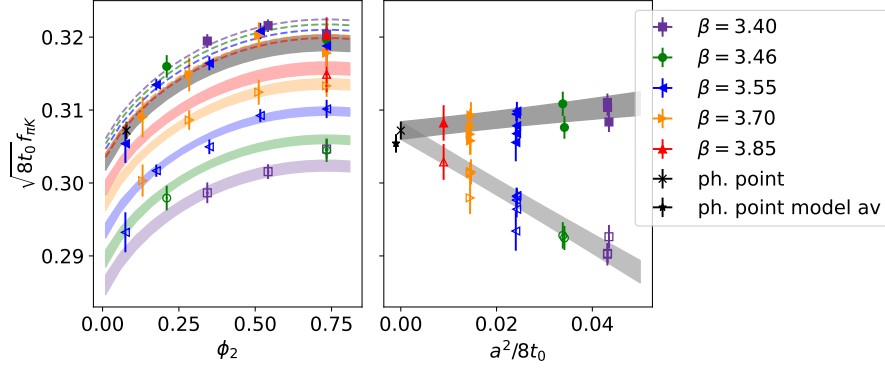
$$m_{ud} \equiv m_l = m_s. \tag{4.42}$$

Figure 4.2: *Left*: Pion mass dependence of $\sqrt{8t_0}f_{\pi K}$ for the SU(3) ChPT model with pure $\mathcal{O}(a^2)$ cutoff effects and no cut in data: $[SU(3)\chi PT][a^2][-]$. We show the result of the combined fit of both Wilson (empty) and mixed action (filled) results. The colored bands represent the pion mass dependence for each lattice spacing for the Wilson results, while the dashed lines represent the dependence for the mixed action results. In the latter case we only plot the central value of the corresponding bands for visualization purposes. *Right*: the same model, with points projected to the physical pion mass ϕ_2^{ph} using the fit result for the continuum mass dependence $F(\phi_2)^{\mathrm{cont}}$. In this plot we show the lattice spacing dependence of our ensembles. We show two physical point results: the rightmost in the plot corresponds to the result coming from the fit model itself, while the leftmost is the result obtained from the model average.
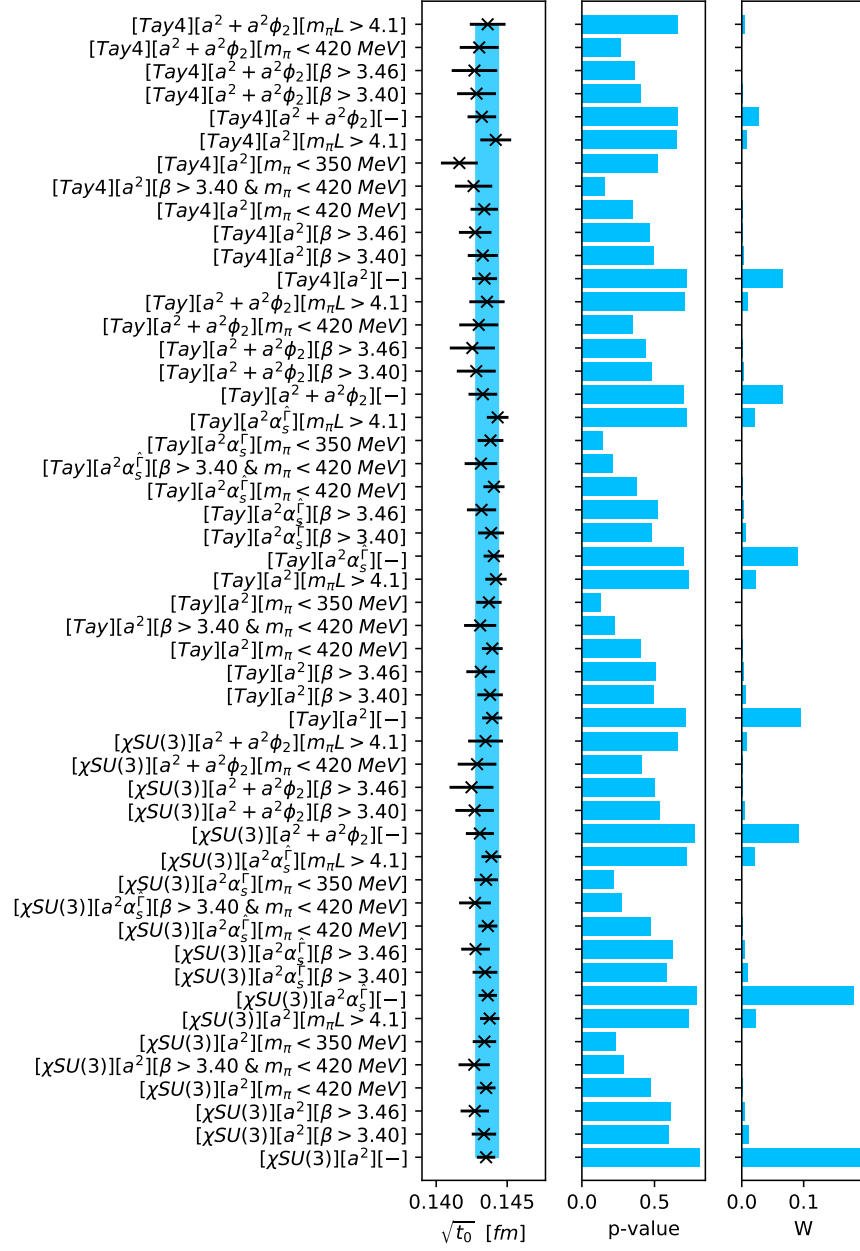
Figure 4.3: Model average results for the determination of $\sqrt{t_0}$ at the physical point using the Wilson results and $f_{\pi K}$ as physical input. In the leftmost figure we show the results coming from each fit model together with the final averaged result with the systematic uncertainty coming from the model variation added (blue band). In the middle plot we show the quality of fits as measured by the p-value [14]. In the rightmost figure we show the assigned weight to each model according to eq. (4.32). We provide a Table connecting each label to the corresponding fit models in Appendix H.
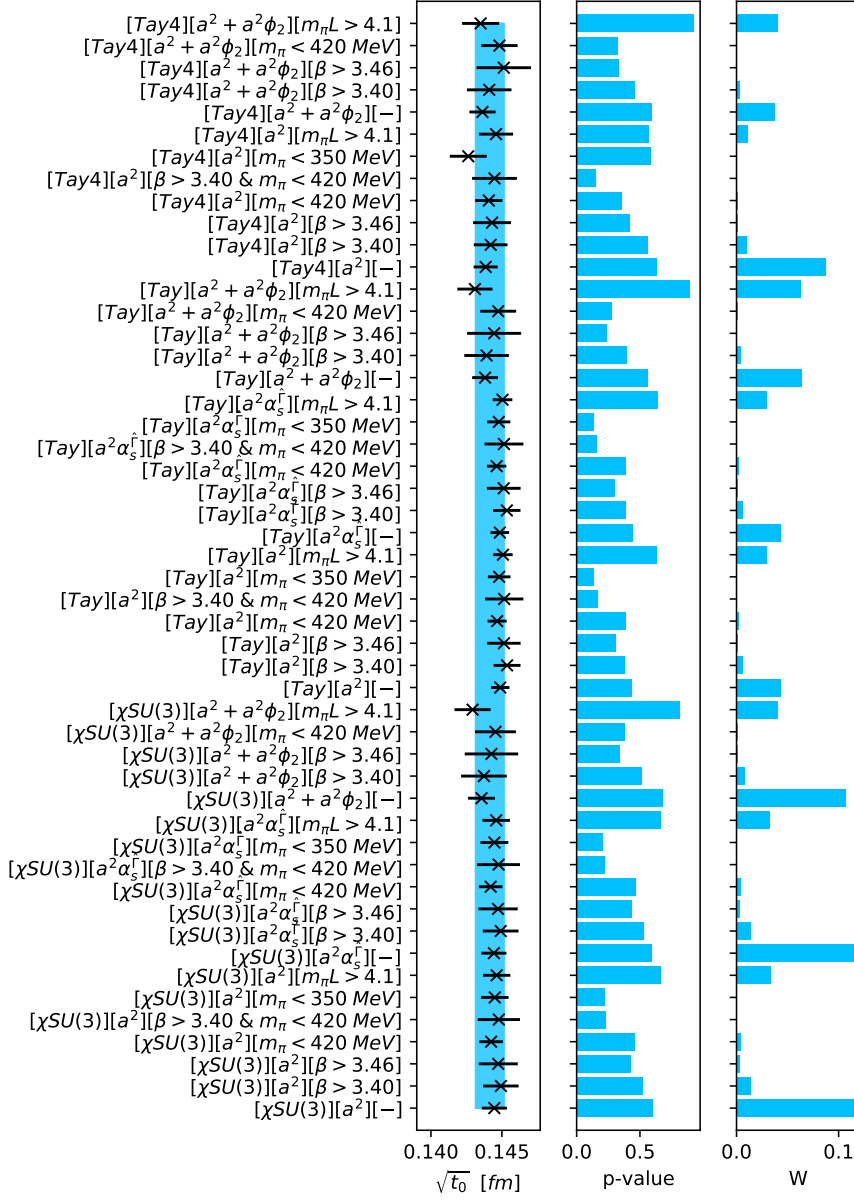
Figure 4.4: Model average results for the determination of $\sqrt{t_0}$ at the physical point using the mixed action results and $f_{\pi K}$ as physical input. In the leftmost figure we show the results coming from each fit model together with the final averaged result with the systematic uncertainty coming from the model variation added (blue band). In the middle plot we show the quality of fits as measured by the p-value [14]. In the rightmost figure we show the assigned weight to each model according to eq. (4.32). We provide a Table connecting each label to the corresponding fit models in Appendix H.
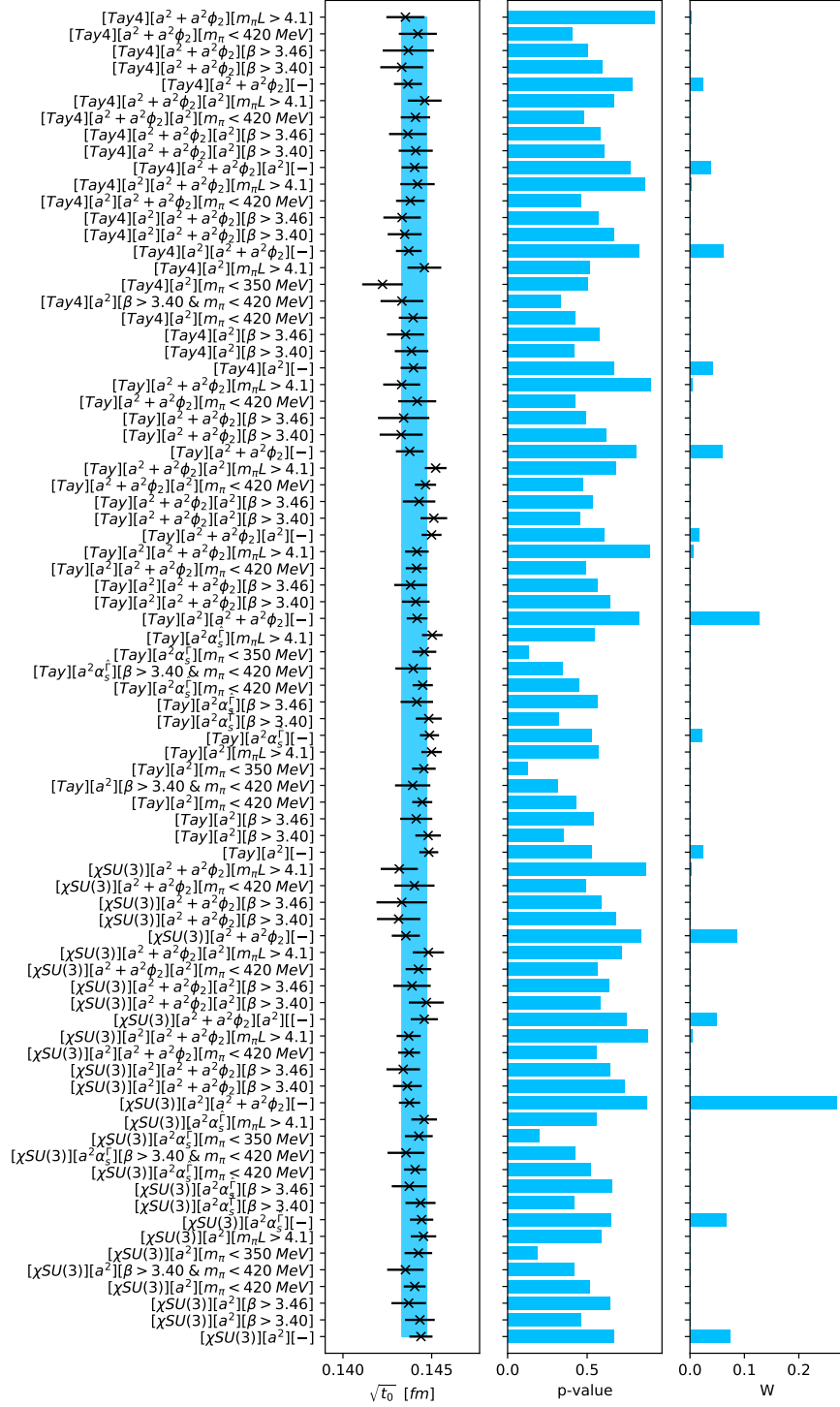
Figure 4.5: Model average results for the determination of $\sqrt{t_0}$ at the physical point using the combined analysis of both Wilson and mixed action results and $f_{\pi K}$ as physical input. In the leftmost figure we show the results coming from each fit model together with the final averaged result with the systematic uncertainty coming from the model variation added (blue band). In the middle plot we show the quality of fits as measured by the p-value [14]. In the rightmost figure we show the assigned weight to each model according to eq. (4.32). We provide a Table connecting each label to the corresponding fit models in Appendix H.
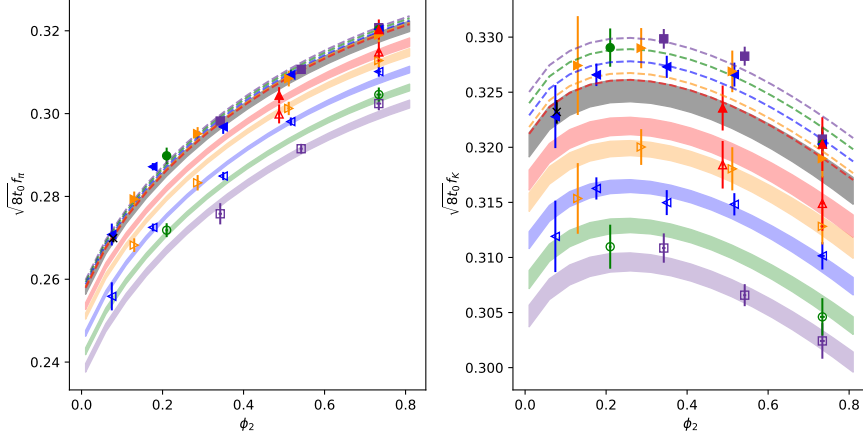
Figure 4.6: *Left*: Pion mass dependence of $\sqrt{8t_0}f_\pi$ for the SU(2) ChPT model with pure $\mathcal{O}(a^2)$ cutoff effects and no cut in data: $[SU(2)\chi PT][a^2][-]$. We show the result of the combined fit of both Wilson (empty) and mixed action (filled) results. The colored bands represent the pion mass dependence for each lattice spacing for the Wilson results, while the dashed lines represent the dependence for the mixed action results. In the latter case we only plot the central value of the corresponding bands for visualization purposes. *Right*: the same but for the dependence of $\sqrt{8t_0}f_K$. The color and symbol code is the same as in Fig. 4.2.

In terms of our usual quantities ϕ_2, ϕ_4 this means

$$\phi_2 = \frac{2}{3}\phi_4, \tag{4.43}$$

where ϕ_4 again is given by its physical value after the iterative procedure to find t_0^{ph} and after mass shifting (see Sec. 3.4). In order to extract $t_0^{\text{sym}} = t_0(\phi_2^{\text{sym}}, \phi_4^{\text{ph}})$, following [73] we build the ratio

$$\frac{\sqrt{t_0/a^2}}{\sqrt{t_0^{\text{sym}}/a^2}}, \tag{4.44}$$

where $\sqrt{t_0/a^2}$ is the measurement of the gradient flow scale in each ensemble and $\sqrt{t_0^{\text{sym}}/a^2}$ is said quantity for the symmetric point at the corresponding value of the inverse coupling β. We now fit this ratio to

$$F(\phi_2) = \sqrt{1 + p(\phi_2 - \phi_2^{\text{sym}})}. \tag{4.45}$$

The result of this fit is shown in Fig. 4.10. Once the data is fitted, we extract t_0^{sym} in physical units as

$$\sqrt{t_0^{\text{sym}}} = \frac{\sqrt{t_0^{\text{ph}}}}{F(\phi_2^{\text{ph}})}. \tag{4.46}$$
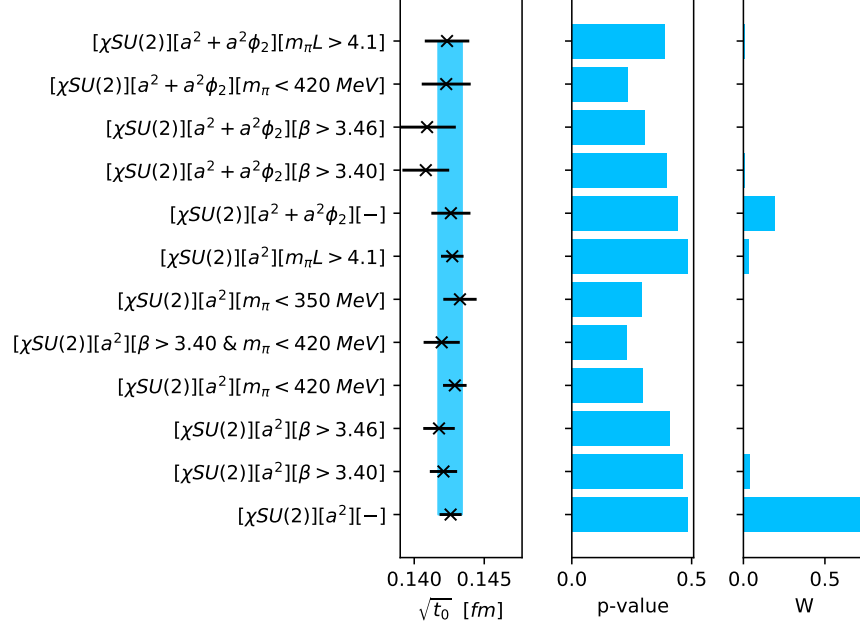
Figure 4.7: Model average results for the determination of $\sqrt{t_0}$ at the physical point using the Wilson results and f_π as physical input. In the leftmost figure we show the results coming from each fit model together with the final averaged result with the systematic uncertainty coming from the model variation added (blue band). In the middle plot we show the quality of fits as measured by the p-value [14]. In the rightmost figure we show the assigned weight to each model according to eq. (4.32). We provide a Table connecting each label to the corresponding fit models in Appendix H.

Figure 4.8: Model average results for the determination of $\sqrt{t_0}$ at the physical point using the mixed action results and f_π as physical input. In the leftmost figure we show the results coming from each fit model together with the final averaged result with the systematic uncertainty coming from the model variation added (blue band). In the middle plot we show the quality of fits as measured by the p-value [14]. In the rightmost figure we show the assigned weight to each model according to eq. (4.32). We provide a Table connecting each label to the corresponding fit models in Appendix H.
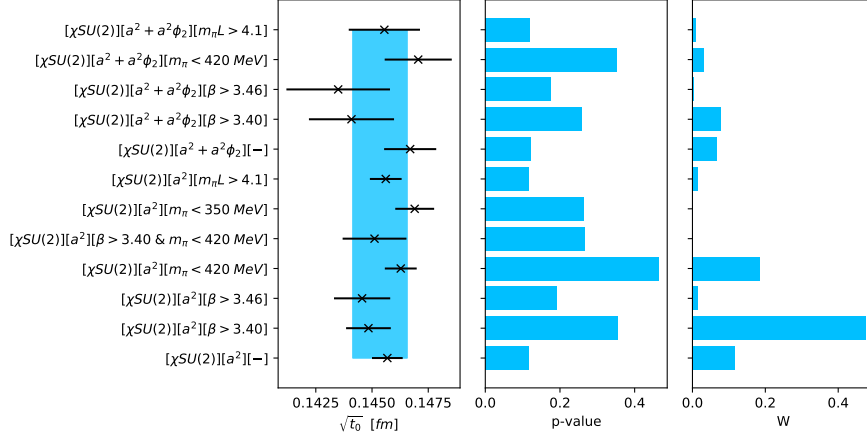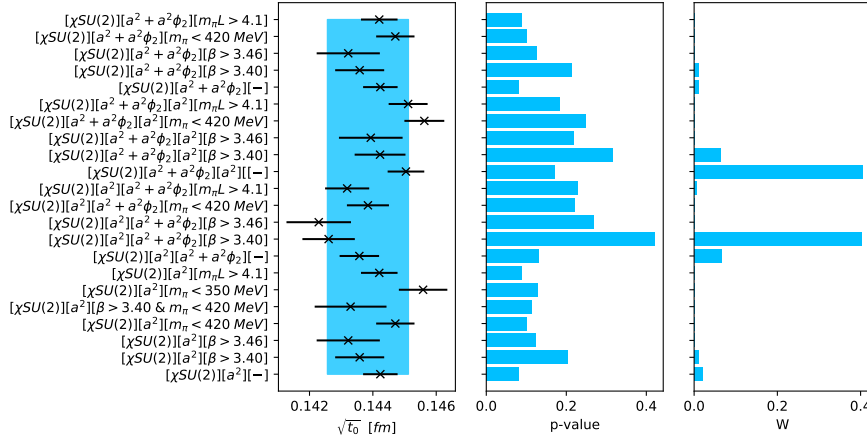

Figure 4.9: Model average results for the determination of $\sqrt{t_0}$ at the physical point using the combined analysis of both Wilson and mixed action results and f_π as physical input. In the leftmost figure we show the results coming from each fit model together with the final averaged result with the systematic uncertainty coming from the model variation added (blue band). In the middle plot we show the quality of fits as measured by the p-value [14]. In the rightmost figure we show the assigned weight to each model according to eq. (4.32). We provide a Table connecting each label to the corresponding fit models in Appendix H.
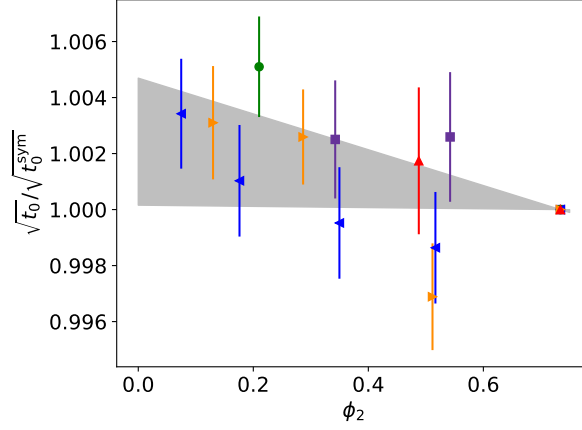
Figure 4.10: Fit to eq. (4.45) in order to extract t_0 at the symmetric point. The color and symbol code is the same as in Fig. 4.2.

For t_0^{ph} and ϕ_2^{ph} we can use our determination for the Wilson, mixed action or combined data sets. The result for the scale at the symmetric point is, depending on this choice

$$\sqrt{t_0^{\mathrm{sym}}} = 0.1433(8)_{\mathrm{stat}}(3)_{\mathrm{syst}} \text{ fm, Wilson,} \tag{4.47}$$

$$\sqrt{t_0^{\mathrm{sym}}} = 0.1438(8)_{\mathrm{stat}}(6)_{\mathrm{syst}} \text{ fm, Mixed action,} \tag{4.48}$$

$$\sqrt{t_0^{\mathrm{sym}}} = 0.1437(6)_{\mathrm{stat}}(4)_{\mathrm{syst}} \text{ fm, Combined.} \tag{4.49}$$

4.4   RESULTS: LATTICE SPACING

Just as in the previous section, we can use the fit to $\dfrac{\sqrt{t_0/a^2}}{\sqrt{t_0^{\mathrm{sym}}/a^2}}$ to compute

$$\left(\sqrt{\frac{t_0}{a^2}}\right)^{\mathrm{ph}} = \sqrt{\frac{t_0^{\mathrm{sym}}}{a^2}} F(\phi_2^{\mathrm{ph}}). \tag{4.50}$$

Then, the lattice spacing is extracted as

$$a = \frac{\sqrt{t_0^{\mathrm{ph}}}}{\left(\sqrt{\frac{t_0}{a^2}}\right)^{\mathrm{ph}}}. \tag{4.51}$$

Again, for ϕ_2^{ph} we can use either our determination of t_0^{ph} for the Wilson, mixed action or combined data sets. Results for the lattice spacing are shown in Table 4.1.

β	a [fm] Wilson	a [fm] mixed action	a [fm] combined

3.40	$0.0844(5)_{\text{stat}}(2)_{\text{syst}}$	$0.0848(5)_{\text{stat}}(4)_{\text{syst}}$	$0.0847(4)_{\text{stat}}(2)_{\text{syst}}$
3.46	$0.0749(4)_{\text{stat}}(2)_{\text{syst}}$	$0.0752(4)_{\text{stat}}(3)_{\text{syst}}$	$0.0751(3)_{\text{stat}}(2)_{\text{syst}}$
3.55	$0.0630(3)_{\text{stat}}(2)_{\text{syst}}$	$0.0632(3)_{\text{stat}}(3)_{\text{syst}}$	$0.0632(3)_{\text{stat}}(2)_{\text{syst}}$
3.70	$0.0489(3)_{\text{stat}}(1)_{\text{syst}}$	$0.0490(3)_{\text{stat}}(2)_{\text{syst}}$	$0.0490(2)_{\text{stat}}(1)_{\text{syst}}$
3.85	$0.0383(2)_{\text{stat}}(1)_{\text{syst}}$	$0.0385(2)_{\text{stat}}(2)_{\text{syst}}$	$0.0384(2)_{\text{stat}}(1)_{\text{syst}}$

Table 4.1: Values of the lattice spacing a in physical units extracted from the determination of the gradient flow scale t_0 with the Wilson, mixed action and combined analysis. The lattice spacing is extracted from measures of both t_0 at the physical and symmetric points using eq. (4.51).

4.5 RESULTS: t_0^*

Another point in the (ϕ_2, ϕ_4) plane of interest is the reference point in [13]

$$\phi_4 = 1.11, \quad \phi_2 = \frac{2}{3}\phi_4 \equiv \phi_2^{\text{sym}}. \tag{4.52}$$

The scale t_0 evaluated at this point is referred to as t_0^*

$$t_0^* = t_0 \left(\phi_2^{\text{sym}}, \phi_4 = 1.11\right), \tag{4.53}$$

and its ratio to $\sqrt{t_0^{\text{ph}}}$ plays a crucial role in the computation of the strong coupling in [24]. To compute t_0^*, we need to repeat the analysis above, this time mass shifting our ensembles to the value $\phi_4 = 1.11$ without errors and compute the gradient flow scale at the symmetric point as explained in the Sec. 4.4.

The values we find for $\sqrt{t_0^*}$ in physical units for the Wilson, mixed action and combined cases are

$$\sqrt{t_0^*} = 0.1436(7)_{\text{stat}}(4)_{\text{syst}} \text{ fm, Wilson,} \tag{4.54}$$

$$\sqrt{t_0^*} = 0.1441(7)_{\text{stat}}(5)_{\text{syst}} \text{ fm, Mixed action,} \tag{4.55}$$

$$\sqrt{t_0^*} = 0.1438(6)_{\text{stat}}(3)_{\text{syst}} \text{ fm, Combined.} \tag{4.56}$$

Part IV

CONCLUSIONS

CONCLUSIONS AND OUTLOOK

5

Blabla, semileptonics

CONCLUSIONES Y PERSPECTIVAS

Blabla, semileptónicas

Part V

APPENDIX

A

CONVENTIONS

In this appendix we set some useful notation used throughout this work. We begin with the Dirac or Gamma matrices γ_μ, which are 4×4 complex matrices defined by the anticommutator relation

$$\{\gamma_\mu, \gamma_\nu\} = 2g_{\mu\nu}1_{4\times4}, \tag{A.1}$$

with $g_{\mu\nu}$ the metric tensor of 4-dimensional space-time. We will work in the Euclidean and flat space, so

$$g_{\mu\nu} = \mathrm{diag}(+1, +1, +1, +1). \tag{A.2}$$

Some useful properties of the Gamma matrices are

- Hermiticity: $\gamma_\mu^\dagger = \gamma_\mu$.

- They are traceless: $\mathrm{tr}(\gamma_\mu) = 0$.

- Involutory: $\gamma_\mu^{-1} = \gamma_\mu$.

A fifth Gamma matrix can be defined as

$$\gamma_5 = \gamma_0\gamma_1\gamma_2\gamma_3, \tag{A.3}$$

which fulfills the same properties as above, and anticommutes with all other Gamma matrices

$$\{\gamma_5, \gamma_\mu\} = 0. \tag{A.4}$$

These matrices control the flavor content of hadrons, and as such appear in the definition of the lattice hadron interpolators. The relevant quark bilinears needed for this work are

- Scalar density: $S^{ij} = \bar{\psi}^i\psi^j$.

- Pseudoscalar density: $P^{ij} = \bar{\psi}^i\gamma_5\psi^j$.

- Axial current: $A_\mu^{ij} = \bar{\psi}^i\gamma_\mu\gamma_5\psi^j$.

- Vector current: $V_\mu^{ij} = \bar{\psi}^i\gamma_\mu\psi^j$.

These bilinears are defined in the physical basis $\{\psi, \bar{\psi}\}$. By the change of variables

$$\psi \to e^{i\frac{\pi}{2}\gamma_5 T/2}\psi, \quad \bar{\psi} \to \bar{\psi}e^{i\frac{\pi}{2}\gamma_5 T/2}, \tag{A.5}$$

we define the twisted basis, with T a diagonal matrix in flavor space. With this change of variables and at full twist with $N_f = 2 + 1 + 1$

$$T = \mathrm{diag}(+1, -1, -1, +1), \tag{A.6}$$

the bilinears are rotated as

$$S^{ij} \to S^{ij}, \tag{A.7}$$

$$P^{ij} \to P^{ij}, \tag{A.8}$$

$$A^{ij}_\mu \to iV^{ij}_\mu, \tag{A.9}$$

$$V^{ij}_\mu \to -iA^{ij}_\mu, \tag{A.10}$$

for $(i,j) = (u,d), (u,s), (c,d), (c,s)$, and

$$S^{ij} \to -iP^{ij}, \tag{A.11}$$

$$P^{ij} \to iS^{ij}, \tag{A.12}$$

$$A^{ij}_\mu \to A^{ij}_\mu, \tag{A.13}$$

$$V^{ij}_\mu \to V^{ij}_\mu, \tag{A.14}$$

for $(i,j) = (u,u), (u,c), (d,d), (d,s), (s,s), (c,c)$.

LATTICE ENSEMBLES

id	β	m_π [MeV]	m_K [MeV]	T/a	L/a	$m_\pi L$	cnfg	BC
H101	3.40	421	421	96	32	5.8	1001,1009	OBC
H102r001	3.40	355	442	96	32	4.9	997	OBC
H102r002	3.40	360	445	96	32	5.0	1008	OBC
H105	3.40	284	471	96	32	3.9	947,1042	OBC
H105r005	3.40	286	467	96	32	3.9	837	OBC
H400	3.46	426	426	96	32	5.2	505,540	OBC
D450	3.46	222	480	128	64	5.4	1000	PBC
N202	3.55	416	416	128	48	6.4	899	OBC
N203	3.55	348	446	128	48	5.4	756,787	OBC
N200	3.55	287	468	128	48	4.4	856,856	OBC
D200	3.55	203	486	128	64	4.2	2001	OBC
E250	3.55	130	497	192	96	4.0	1009	PBC
N300r002	3.70	424	424	128	48	5.1	1521	OBC
N302	3.70	348	453	128	48	4.2	2201	OBC
J303	3.70	259	480	192	64	4.1	1073	OBC
E300	3.70	176	496	192	96	4.2	1139	OBC
J500	3.85	417	417	192	64	5.2	789,655,431	OBC
J501	3.85	340	453	192	64	4.3	1635,1142,1150	OBC

Table B.1: List of CLS ensembles [15, 59] under study. They use the Lüscher-Weisz gauge action defined in eq. (1.91) and non-perturbatively $\mathcal{O}(a)$ improved $N_f = 2 + 1$ Wilson fermions (see eq. (1.98)). All ensembles use open boundary conditions (OBC) in time except for E250 and D450 (periodic), and periodic boundary conditions for all spatial directions.

C

SIMULATION DETAILS

In this Appendix we discuss the details of the generation of gauge field configurations with dynamical quarks for the study of Lattice QCD.

All ensembles studied in this thesis were generated using the openQCD software, and hence the details we review here are those of the algorithms implemented for this software [49, 53].

Typically simulations of lattice QCD with dynamical quarks require a large amount of computer resources due to the large number of degrees of freedom, the need for big volumes and small lattice spacings. The constant efforts by the community paved the way for simulations with up to four dynamical quarks.

As outlined in Sec. 1.4, the expectation value of a composite operator O can be computed in the lattice as

$$\langle O \rangle = \frac{1}{\mathcal{Z}} \int \mathcal{D}[U] e^{-S_{\mathrm{G}}[U] - S_{\mathrm{eff}}[U]} O[U] \approx \frac{1}{N_{\mathrm{cnfg}}} \sum_{i=1}^{N_{\mathrm{cnfg}}} O[U_i] + \mathcal{O}\left(\frac{1}{\sqrt{N_{\mathrm{cnfg}}}} \right),$$

$$(\mathrm{C.1})$$

where the gauge fields U_i are sampled from the probability density

$$dP[U] = \frac{e^{-S_{\mathrm{G}}[U] - S_{\mathrm{eff}}[U]}}{\int \mathcal{D}[U] e^{-S_{\mathrm{G}}[U] - S_{\mathrm{eff}}[U]}}. \tag{C.2}$$

The central idea is to perform an importance sampling of the distribution eq. (C.2), such that regions of field space with high probability are highly populated with gauge configurations U_i. To achieve this, typically gauge configurations are generated following a Markov chain. This is defined as a sequence $\{U_k\}_{k=1}^{N_{\mathrm{cnfg}}}$ such that the k-th element is generated from the previous one, with k labeling the Monte Carlo (MC) time. This way, the Markov Chain is generated from the initial state U_1 and the transition probability $T(U_{k-1} \to U_k)$. Due to this gauge configurations in one same Markov Chain are highly correlated, issue which we deal with in Appendix D. The transition probabilities must obey the following conditions:

- Ergodicity: given a subset of states S from the Markov Chain, there are always at least two states $s \in S$ and $s' \notin S$ with $T(s \to s') > 0$. This is of particular importance in the context of Lattice QCD and Lattice Yang-Mills theories in order to ensure that the simulation algorithm is sampling correctly all topological sectors of the theory, which may not always be the case for different algorithms.

- Equilibrium: normalizing the transition probability as

$$\sum_s T(s \to s') = 1 \ \forall s, \tag{C.3}$$

then it must hold that

$$\sum_s P(s)T(s \to s') = P(s') \quad \forall s', \tag{C.4}$$

where $P(s)$ is the equilibrium distribution in eq. (C.2). This ensures that starting from a random configuration, after applying iteratively the transition probability, we asymptotically reach the target equilibrium distribution eq. (C.2).

Different choices for the transition probability $T(s \to s')$ satisfying the above conditions define the different sampling algorithms which we go on to review.

C.1 METROPOLIS ALGORITHM

The Metropolis algorithm [58] is one of the most popular choices for generating a Markov Chain of gauge field configurations for pure gauge theories, for which the target distribution is

$$dP[U] = \frac{e^{-S_G[U]}}{\int \mathcal{D}[U] e^{-S_G[U]}}. \tag{C.5}$$

The idea is to define an a priori selection probability $T_0(U_i \to U_j)$ to update a single gauge link. One such choice is to take a random element g of the SU(N) group close to the identity and update the gauge link $U_\mu(n)$ as $U_\mu(n)' = gU_\mu(n)$ such that the new gauge configuration U_j is close to the original one U_i. In order for the transition to be symmetric, group elements g and g^{-1} have to be selected with equal probability. After updating with this a priori transition probability, one supplements the updating process with an accept-reject step, such that the new proposed gauge link is accepted with probability

$$P_{\text{acc}}(i,j) = \min\left(1, e^{-\Delta S}\right), \quad \Delta S = S[U_j] - S[U_i]. \tag{C.6}$$

Then the total transition probability is given by

$$T(U_i \to U_j) = T_0(U_i \to U_j)P_{\text{acc}}(i,j) + \delta_{ij}\sum_k T_0(U_i \to U_j)(1 - P_{\text{acc}}(i,j)). \tag{C.7}$$

This T satisfies all the desired properties for a transition probability and asymptotically reaches the target distribution probability for pure gauge theories.

The drawback of this algorithm is that it only updates a single gauge link at each step and as such is highly inefficient, particularly for large volume simulations. Over the years new alternatives for pure gauge simulations have been proposed, such as the heat bath [22] and overrelaxation [1, 23] algorithms.

Having as target distribution that of pure gauge theory is equivalent as treating quarks in the sea as static sources (infinitely heavy). In order to simulate full QCD, one needs to have dynamical quarks in the sea, meaning having target distribution eq. (C.2), where S_{eff} introduces non-local dependencies in the gauge links due to the quark determinant. Therefore algorithms like Metropolis, which updates the gauge configurations link by link experience a significant computational cost that increases with the lattice volume squared, which makes the algorithm unpractical for dynamical simulations purposes. The Hybrid Monte Carlo (HMC) algorithm [30, 38] significantly improves efficiency by doing global updates of the gauge configurations.

The HMC uses the classical equations of motion to propose new gauge configurations. To this purpose, the field space is extended with the introduction of su(3)-valued conjugate momenta $\pi_\mu(x)$ of the link variables $U_\mu(x)$. The Hamiltonian of the system is

$$H[\pi, U] = \frac{1}{2} \sum_{x,\mu} \pi_\mu^a(x) \pi_\mu^a(x) + S_{\text{G}}[U] + S_{\text{eff}}[U]. \tag{C.8}$$

This way expectation values can be computed as

$$\langle O \rangle = \frac{\int \mathcal{D}[\pi, U] e^{-H[\pi,U]} O[U]}{\int \mathcal{D}[\pi, U] e^{-H[\pi,U]}}. \tag{C.9}$$

Now the classical equations of motion read

$$\dot{\pi}_\mu(x) = -F_\mu(x), \quad F_\mu(x) = \frac{\partial S[e^\omega U]}{\partial \omega}\Big|_{\omega=0}, \quad \omega \in su(N), \tag{C.10}$$

$$\dot{U}_\mu(x) = \pi_\mu(x) U_\mu(x), \tag{C.11}$$

where the dot notation "$\dot{a}$" means derivation w.r.t. MC time. This way, starting from an initial configuration at zero MC time, integrating the equations of motion provides with a global new gauge configuration to be used as proposal for the update of the gauge links. This new global proposal is subject to an accept-reject step like the one in the Metropolis algorithm with

$$P_{\text{acc}} = \min\left(1, e^{-\Delta H}\right), \quad \Delta H = H[\pi', U'] - H[\pi, U]. \tag{C.12}$$

We have presented the basic formulation of the HMC algorithm but further refinements and improvements, specially in terms of the integration of the classical equations of motion have taken place over the years [40, 65, 76].

This far we have not given details on how to compute the effective fermion action

$$S_{\text{eff}}[U] = -\sum_{i=1}^{N_f} \log \det(D_i). \tag{C.13}$$

This is a typically challenging task, since it involves dealing with Grassmann variables. A popular solution is to use pseudofermion fields $\Phi(x)$ [75], which are auxiliary fields that carry color and spinor indices c, α but that are complex instead of Grassmann numbers. Restricting to the mass-degenerate doublet of light quarks, where the effective action becomes

$$e^{-S_{\text{eff}}} = \det(D_l)\det(D_l) = \det(D_l^\dagger D_l), \tag{C.14}$$

in the pseudo-fermion representation this becomes

$$\det(D_l^\dagger D_l) = \frac{1}{\mathcal{Z}_\Phi} \int \mathcal{D}[\Phi] e^{-S_{\text{pf}}[U,\Phi]}, \tag{C.15}$$

with $\mathcal{Z}_\Phi$ the pseudo-fermion partition function, and the pseudo-fermion action given by

$$S_{\text{pf}}[U, \Phi] = \Phi^\dagger \left(D_l^\dagger D_l \right)^{-1} \Phi \tag{C.16}$$

Finally the integration measure for these auxiliary fields reads

$$\mathcal{D}[\Phi] = \Pi_{x,\alpha,c} d\Phi_{\alpha c}(x) d\Phi_{\alpha c}^*(x). \tag{C.17}$$

Now we have all ingredients needed for HMC sampling with dynamical fermions. First one samples randomly a set of conjugate momenta π_μ and pseudo-fermion fields Φ with Gaussian distribution $\propto \exp\left(-\frac{1}{2}\pi_\mu\pi_\mu - S_{\text{pf}}\right)$. Together with an initial gauge field configuration U_i, the classical equations of motion are integrated up to some later time. At this point one implements the accept-reject step and updates the gauge configuration to U_{i+1}.

This far we assumed two degenerate flavors of quarks to compute the effective fermion action. The inclusion of a strange quark, as in the case of the CLS ensembles we use in this work, complicates things since it does not belong to a mass-degenerate doublet, and thus one needs to compute $\det(D_s)$ and not $\det(D_l^\dagger D_l)$. When this happens the quark determinant is not ensured to be positive anymore due to explicit chiral symmetry breaking by the Wilson term in Wilson quarks. This is of particular relevance because if the strange quark determinant gets a negative value one cannot interpret the factor $e^{-S_G-S_{\text{eff}}}$ appearing in the path integral as a probability. In CLS ensembles this difficulty is tackled by the Rational Hybrid Monte Carlo algorithm [19, 44]. However, it was found that some configurations still suffered from a negative strange quark determinant. In this case we introduce a reweighting factor with minus sign to account for the effect. Reweighting is discussed in the next section.

C.3   REWEIGHTING

The idea of reweighting was first proposed [51] in order to deal with exceptional gauge configurations in the HMC algorithm. These are

gauge configurations with near to zero eigenvalues for the Dirac operator, which can appear due to the explicit chiral symmetry breaking induced by the Wilson term in the Wilson fermion action.

In the context of CLS ensembles, a small twisted mass term μ_0 is included in the light quark determinant as [53]

$$\det\left(Q^\dagger Q\right) \to \det\left(\left(Q^\dagger Q + \mu_0^2\right)^2 \left(Q^\dagger Q + 2\mu_0^2\right)^{-1}\right), \qquad \text{(C.18)}$$

with the Hermitian Dirac operator given by $Q = \gamma_5 D$. This provides an infrared cutoff to cancel low-mode eigenvalues. Using the Hasenbusch's mass factorization [40]

$$\det\left(\left(Q^\dagger Q + \mu_0^2\right)^2 \left(Q^\dagger Q + 2\mu_0^2\right)^{-1}\right) \qquad \text{(C.19)}$$

$$= \det\left(Q^\dagger Q + \mu_n^2\right) \det\left(\frac{Q^\dagger Q + \mu_0^2}{Q^\dagger Q + 2\mu_0^2}\right) \times \Pi_{i=1}^n \det\left(\frac{Q^\dagger Q + \mu_{i-1}^2}{Q^\dagger Q + \mu_i^2}\right), \qquad \text{(C.20)}$$

where the twisted mass factors are ordered as $\mu_0 < \mu_1 < ... < \mu_n$. We used γ_5-hermiticity of the Dirac operator D so that

$$Q^\dagger Q = \gamma_5 D^\dagger \gamma_5 D = D^\dagger D. \qquad \text{(C.21)}$$

The values of the twisted mass factors have to be properly chosen as large values might lead to large fluctuations and poor efficiency of the algorithm. After introducing such twisted masses, in order to account for their effect and recover the target desired distribution $dP[U]$ of QCD (in which this twisted mass is not present) a reweighting of expectation values over gauge configurations is needed

$$\langle O \rangle_{\text{rw}} = \frac{\langle OW \rangle}{\langle W \rangle}, \qquad \text{(C.22)}$$

where W is the reweighting factor and in this case reads

$$W = \det\left(Q^\dagger Q \left(Q^\dagger Q + 2\mu_0^2\right) \left(Q^\dagger Q + \mu_0^2\right)^{-2}\right). \qquad \text{(C.23)}$$

In addition to twisted mass reweighting, reweighting is also needed due to the use of the RHMC algorithm to simulate the strange quark determinant. This algorithm uses the rational approximation to the strange quark determinant [**RHMC**], which is expected to make it positive. However, as mentioned in the previous section, it was found that some configurations still got a negative sign for the strange quark determinant. This is solved by a reweighting factor of $W_s = -1$ for said configurations, which we list in Table C.1 for the ensembles of interest in this thesis.

id	cnfg
H105r001	3
H105r002	1
H105r005	254, 255, 256, 257, 259, 260, 261, 264, 265, 266, 269, 280, 282, 283, 284, 285, 286, 287, 288, 289, 291, 299, 301, 313, 314, 315, 316, 331, 332, 333, 334, 335, 336, 337, 338, 339, 340, 341, 342
J303r003	324, 325, 326

Table C.1: List of configurations with negative sign of the strange quark determinant for each affected ensemble in this study. A reweighting factor $W_s = -1$ is introduced in said configuration in order to account for the effect.

D

In this appendix we discuss how to perform the data analysis of correlation functions and the different lattice observables extracted from lattice simulations.

Lattice data is measured from Monte Carlo (MC) sampling, and estimates of expectation values of physical observables are extracted from means over the MC time. A crucial step is to assign a proper statistical and systematic uncertainties to these mean values, for which it is needed to take into account the autocorrelated nature of MC measurements. This autocorrelation arises form the fact that each gauge configuration is proposed from the previous one (Markov chain). Some popular methods to deal with these correlations are binning, bootstrap and the jack-knife methods.

A recent technique which we will use in this work was proposed by the ALPHA collaboration [66, 68, 78] and is known as Γ-method, which explicitly computes the autocorrelation function to estimate the statistical uncertainty.

In lattice simulations Typically one measures a primary observable p_i over several ensembles (defined by the simulation parameters like e.g. the inverse coupling β and κ parameter)

$$p_i^\alpha(k), k = 1, ..., N_\alpha, \tag{D.1}$$

where α labels the ensemble and k is the MC time running over the total number of gauge configurations N_α of the given ensemble. In our context, primary observable means a correlation function for some given euclidean time. An estimate for the true value P_i^α is given by the mean value

$$\bar{p}_i^\alpha = \frac{1}{N_\alpha} \sum_{k=1}^{N_\alpha} p_i^\alpha(k) \to_{N_\alpha \to \infty} P_i^\alpha. \tag{D.2}$$

This is an unbiased estimator. Fluctuations over the MC time can be computed as

$$\delta_i^\alpha(k) = p_i^\alpha(k) - \bar{p}_i^\alpha. \tag{D.3}$$

Due to the Central Limit theorem, we are ensured that $\bar{p}_i^\alpha$ behaves as a Gaussian distribution independently of the distribution of $p_i^\alpha(k)$, and so the statistical uncertainty associated to $\bar{p}_i^\alpha$ is simply given by the standard deviation σ_i^α,

$$P_i^\alpha \approx \bar{p}_i^\alpha \pm \sigma_i^\alpha. \tag{D.4}$$

This standard deviation can be computed from the autocorrelation Γ function

$$(\sigma_i^\alpha)^2 = \frac{1}{N_\alpha} \sum_{k=-\infty}^{\infty} \Gamma_{ii}^{\alpha\alpha}(k), \tag{D.5}$$

where the Γ function is defined as

$$\Gamma_{ij}^{\alpha\beta} = \frac{\delta_{\alpha\beta}}{N_\alpha - k} \sum_{k'=1}^{N_\alpha - k} \delta_i^\alpha(k+k')\delta_j^\alpha(k'). \tag{D.6}$$

From the primary observable p_i^α we can compute derived observables $F = f(p_i^\alpha)$, such as meson masses coming from pseudoscalar two point functions. As in the primary observable case, we can estimate this derived observable as

$$\bar{F} = f(\bar{p}_i^\alpha). \tag{D.7}$$

To compute the statistical uncertainty, we can expand f around the true value P_i^α

$$f(P_i^\alpha + \epsilon_i^\alpha) = f(P_i^\alpha) + \bar{f}_i^\alpha \epsilon_i^\alpha + \mathcal{O}((\epsilon_i^\alpha)^2), \tag{D.8}$$

with

$$\bar{f}_i^\alpha = \frac{\partial f(x)}{\partial x}\Big|_{x=P_i^\alpha}. \tag{D.9}$$

Now the autocorrelation function of the derived observable F for ensemble α can be defined as

$$\Gamma_F^\alpha(k) = \sum_{ij} \bar{f}_i^\alpha \bar{f}_j^\alpha \Gamma_{ij}^{\alpha\alpha}(k), \tag{D.10}$$

from which the standard deviation of F can be derived

$$\sigma_F^2 = \sum_\alpha \frac{\Gamma_F^\alpha(0)}{N_\alpha} 2\tau_{\text{int}}^\alpha(F), \tag{D.11}$$

where we assumed that several ensembles contribute to F, and hence the sum $\sum_\alpha$ over the subset of them which contribute. The integrated autocorrelation time $\tau_{\text{int}}^\alpha(F)$ is defined as

$$\tau_{\text{int}}^\alpha(F) = \frac{1}{2} + \sum_{k=1}^{\infty} \frac{\Gamma_F^\alpha(k)}{\Gamma_F^\alpha(k)}. \tag{D.12}$$

To estimate it, a truncation in MC time k is needed. The autocorrelation function admits the following expansion [52, 68]

$$\Gamma(k) \approx \sum_{n=0}^{\infty} e^{-k/\tau_n}. \tag{D.13}$$

The slowest mode $\tau_0 \equiv \tau_{\text{exp}}$ is called the exponential autocorrelation time and it gives the decay rate of $\Gamma(k)$. Truncating eq. (D.12) at MC

time $k = W_F^\alpha$ introduces a systematic uncertainty of $\mathcal{O}(\exp(-W_F^\alpha/\tau_{\exp}^\alpha))$. The Γ-method proposes as optimal window that which minimizes the sum of statistical (estimated in [56]) and systematic contributions

$$W_F^\alpha = \min_W \left(\sqrt{\frac{2(2W+1)}{N_\alpha}} + e^{-W/\tau_{\exp}^\alpha} \right). \tag{D.14}$$

In [78] it was proposed to set $\tau_{\exp} = S_\tau \tau_{\text{int}}$, with S_τ some value between 2 and 5. One can also vary W_F^α until saturation in τ_{int}^α is reached. Finally it was also proposed to add an exponential tail [78]

$$\tau_{\exp}^\alpha \frac{\Gamma_F^\alpha(W_F^\alpha+1)}{\Gamma_F^\alpha(0)}, \tag{D.15}$$

to eq. (D.12) to account for the systematic effect of truncating the sum over MC time. For this an estimate of $\tau_{\exp}^\alpha$ is needed for each ensemble. In the case of CLS ensembles an estimation is given in [15]

$$\tau_{\exp}^\alpha = 14(3)\frac{t_0}{a^2}. \tag{D.16}$$

In this thesis we use the Γ-method explained above as it is implemented by the ADerrors.jl julia package [67].

SOLVERS

For the computation of correlation functions of fermions in the lattice (e.g. a two-point function, see eq. (1.78)) the inversion of the Dirac operator is required. In particular it is needed to compute the inverse of $D(x,y)$ for all spatial positions $\vec{x}, \vec{y}$. This is referred to as inverting the all-to-all Dirac operator. This is computationally very expensive, and stochastic methods can be employed to reduce the computational cost. A set of stochastic noise sources η are introduced such that

$$\langle \eta_i(x) \rangle_\eta = 0, \quad \left\langle \eta_i^\dagger(x) \eta_j(y) \right\rangle_\eta = \delta_{x,y} \delta_{i,j}, \tag{E.1}$$

with $\langle . \rangle_\eta$ meaning average over the N_η samples of some noise distribution. Some common choices are Gaussian, Z_2 or $U(1)$. From these we define

$$\xi_i^q(x) = \sum_y D_q^{-1}(x,y) \eta_i(y), \quad \zeta_i^r(x) = \sum_y D_r^{-1}(x,y) \gamma_5 \Gamma_B^\dagger \eta_i(y), \tag{E.2}$$

with Γ_B some Gamma matrix. Now, two-point functions like the one in eq. (1.78) can be expressed as

$$\langle O_A^{rq} O_B^{qr} \rangle - \frac{a^6}{L^3} \sum_{\vec{y}} \left\langle \left\langle (\Gamma_A \gamma_5 \zeta_i^r(y))^\dagger \xi_i^q(y) \right\rangle_\eta \right\rangle \tag{E.3}$$

$$\approx -\frac{a^6}{L^3} \frac{1}{N_\eta} \sum_{i=1}^{N_\eta} \sum_{\vec{y}} \left\langle (\Gamma_A \gamma_5 \zeta_i^r(y))^\dagger \xi_i^q(y) \right\rangle, \tag{E.4}$$

without the need to compute the all-to-all inverted Dirac operator, therefore reducing significantly the computational effort.

We still need to solve the Dirac equation

$$D_q(x,y) \psi_r(y) = \delta_{x,y} \delta_{q,r} \equiv \eta_{x,y,q,r}, \tag{E.5}$$

in order to invert the Dirac operator D_q with flavor q. This is usually done by an iterative procedure. The basic idea is to start from an initial approximate solution ψ_0 and define the residue ρ (we suppress indices for simplicity)

$$\rho = D\psi_0 - \eta. \tag{E.6}$$

Then, one solves

$$D\psi_1 = \rho, \tag{E.7}$$

finding the new residue and iterates the process, with the final approximate solution given by

$$\psi = \psi_0 + \psi_1 + ... \tag{E.8}$$

The algorithm stops when some convergence criterion is met

$$|\rho| < \epsilon. \tag{E.9}$$

The difference between the true and approximate solutions is

$$|\psi - \psi_{\text{true}}| < \epsilon \kappa(D), \tag{E.10}$$

with $\kappa(D)$ the condition number of matrix D

$$\kappa(D) = |D||D^{-1}|. \tag{E.11}$$

The smaller the condition number of the Dirac operator, the less iterative steps one needs to perform in order to find the solution to the Dirac equation. Thus convergence can be improved by suitably transforming the system into one with a smaller $\kappa(D)$. This can be done by finding some similarity transformations easily invertible such that one can write

$$LDR\psi' = L\eta, \quad \psi = R^{-1}\psi'. \tag{E.12}$$

This is called preconditioning, and there are many different variations. Some of the most used are even-odd preconditioning [26] and distance preconditioning [27].

There are also more sophisticated algorithms to solve the Dirac equation based on conjugate gradient solvers and the Krylov subspace solvers, and we refer to [36] for a pedagogical introduction.

LEAST-SQUARES FITTING

We employ a least-squares method to fit our data to some fit function. This method is based on finding the minimum of the χ^2 function

$$\chi^2 = \sum_{i,j=1}^{N_{\text{dat}}} (y_i - f(x_i; \vec{p})) \, C_{ij}^{-1} \, (y_j - f(x_j; \vec{p})) \,, \tag{F.1}$$

where $\{x_i, y_i\}_{i=1,\dots,N_{\text{dat}}}$ are the data points we want to fit, x being the independent variable and y the abscissa. C^{-1} is the inverse of the covariance matrix of the y-data, and $f(x; \vec{p})$ is the fit function with fit parameters $\vec{p} = (p_1, \dots, p_{N_{\text{param}}})$. For a given fit function $f(x; \vec{p})$, the method finds the parameters values that minimize eq. (F.1) for given data points $\{x_i, y_i\}_{i=1,\dots,N_{\text{dat}}}$.

In our case we perform fits to extract the ground state signal of lattice observables, fitting e.g. an effective mass to a constant plus some exponential signals along the lattice time extent. In this case, euclidean time plays the role of the x. This means fitting $\sim 96 - 192$ points, which in practice makes it very difficult to compute an invertible covariance matrix. In this scenario it is common to use not the full covariance matrix in eq. (F.1) but only its diagonal part. This is referred to as uncorrelated fit, as opposed to a fully correlated fit, which uses the full covariance matrix. However, after minimizing the χ^2 using only the diagonal part of C, uncertainties are propagated taking into account all the correlations between the data.

In [14] a method to measure the quality of the fit for uncorrelated fits was defined, in terms of a p-value. It is also defined a method to compute the expected value of the minimum of χ^2, $\langle \chi^2 \rangle$. In the case of a fully correlated fit $\langle \chi^2 \rangle = $ dof.

We also perform fits for the chiral-continuum extrapolation of $\sqrt{8t_0} f_{\pi K}$ to set the scale. In this case, the y variable is $\sqrt{8t_0} f_{\pi K}$ while the x is ϕ_2, and thus the latter has its own uncertainty. In this situation, a generalized χ^2 function can be defined to include uncertainties in x as

$$\chi^2 = \sum_{i,j=1}^{2N_{\text{dat}}} (Y_i - F(X_i; \vec{p}, \vec{q})) \, \mathcal{C}_{ij}^{-1} \, (Y_j - F(X_j; \vec{p}, \vec{q})) \,, \tag{F.2}$$

$$Y = (x_1, \dots, x_{N_{\text{dat}}}, y_1, \dots, y_{N_{\text{dat}}}), \quad X = (x_1, \dots, x_{N_{\text{dat}}}, x_1, \dots, x_{N_{\text{dat}}}), \tag{F.3}$$

$$F(X_i; \vec{p}, \vec{q}) = \begin{cases} q_i & \text{if } 1 \leq i \leq N_{\text{dat}} \\ f(x_i; \vec{p}) & \text{if } N_{\text{dat}} + 1 \leq i \leq 2N_{\text{dat}} \end{cases}, \tag{F.4}$$

where $\mathcal{C}$ is now the covariance matrix of the generalized data vector Y. In this case we cannot invert the full covariance matrix $\mathcal{C}$ either, but we can use the χ^2 definition in eq. (F.1) (i.e. we neglect the correlation between ϕ_2 and $\sqrt{8t_0}f_{\pi K}$ in the definition of the χ^2) using the full covariance matrix of the $\sqrt{8t_0}f_{\pi K}$ data. Again, to propagate errors we take into account all the correlations between the data, and in particular between ϕ_2 and $\sqrt{8t_0}f_{\pi K}$. In this case we observe

$$\frac{\langle \chi^2 \rangle}{\text{dof}} \sim 0.98, \tag{F.5}$$

indicating an using the covariance matrix of $\sqrt{8t_0}f_{\pi K}$ captures most of the correlations.

For the scale setting we also perform the simultaneous fit of $\sqrt{t_0}f_\pi$ and $\sqrt{t_0}f_K$ to eqs. (4.23)-(4.24). In this case we can only take the diagonal of the full covariance matrix.

FINITE VOLUME EFFECTS

Simulating QCD in a finite box introduces finite volume effects which can be a source for systematic uncertainties. In Table B.1 we show the volume of each ensemble in terms of $m_\pi L$. It is conventional to consider finite volume effects under control if $m_\pi L \geq 4$.

ChPT provides us with formulae to account for these finite volume effects. In particular, to NLO the pion and kaon masses and decay constants receive the following corrections [20, 21]

$$X^{(\infty)} = X^{(L)} \frac{1}{1 + R_X}, \tag{G.1}$$

where $X^{(\infty)}$ is observable X at infinite volume and $X^{(L)}$ is said observable at a finite volume L^3, with $X = m_\pi, m_K, f_\pi, f_K$,

$$R_{m_\pi} = \frac{1}{4} \xi_\pi \tilde{g}_1(\lambda_\pi) - \frac{1}{12} \xi_\eta \tilde{g}_1(\lambda_\eta), \tag{G.2}$$

$$R_{m_K} = \frac{1}{6} \xi_\eta \tilde{g}_1(\lambda_\eta), \tag{G.3}$$

$$R_{f_K} = -\xi_\pi \tilde{g}_1(\lambda_\pi) - \frac{1}{2} \xi_K \tilde{g}_1(\lambda_K), \tag{G.4}$$

$$R_{f_\pi} = -\frac{3}{8} \xi_\pi \tilde{g}_1(\lambda_\pi) - \frac{3}{4} \xi_K \tilde{g}_1(\lambda_K) - \frac{3}{8} \xi_\eta \tilde{g}_1(\lambda_\eta), \tag{G.5}$$

$$\xi_{PS} = \frac{m_{PS}^2}{(4\pi f_\pi)^2}, \tag{G.6}$$

$$\lambda_{PS} = m_{PS} L, \tag{G.7}$$

$$\tilde{g}_1(x) = \sum_{n=1}^{\infty} \frac{4m(n)}{\sqrt{n}x} K_1(\sqrt{n}x), \tag{G.8}$$

$$m_\eta^2 = \frac{4}{3} m_K^2 - \frac{1}{3} m_\pi^2, \tag{G.9}$$

where $K_1(x)$ is a Bessel function of the second kind, and the multiplicities $m(n)$ [20] are listed in Table G.1. It is manifest that the lighter the pion mass and the smaller the volume, the stronger the volume corrections. We find these corrections to be less than half a standard deviation for the ensembles with the smallest volumes and lightest pion masses. We nonetheless apply the corrections to all the ensembles.

PCAC quark masses are short distance observables and as such do not receive any infinite volume correction.

n	1	2	3	4	5	6	7	8	9	10
$m(n)$	6	12	8	6	24	24	0	12	30	24

n	11	12	13	14	15	16	17	18	19	20
$m(n)$	24	8	24	48	0	6	48	36	24	24

Table G.1: Multiplicities $m(n)$ calculated in [20] for $n \leq 20$.

Wilson analysis	
$[SU(3)\chi PT]$	Eq. (4.15)
$[Tay]$	Eq. (4.21)
$[Tay4]$	Eq. (4.22)
$[SU(2)\chi PT]$	Eqs. (4.23)-(4.24)
$[a^2]$	Eq. (4.25)
$[a^2\alpha_S^\Gamma]$	Eq. (4.25)
$[a^2 + a^2\phi_2]$	Eq. (4.25)
$[-]$	No cut in data
$[\beta > 3.40]$	Remove $\beta = 3.40$ ensembles
$[\beta > 3.46]$	Remove $\beta = 3.40$ and $\beta = 3.46$ ensembles
$[m_\pi < 420\ MeV]$	Remove symmetric point ensembles
$[m_\pi < 350\ MeV]$	Remove $\phi_2 > 0.4$ ensembles
$[\beta > 3.40\ \&\ m_\pi < 420\ MeV]$	Remove symmetric point and $\beta = 3.40$ ensembles
$[m_\pi L > 4.1]$	Remove ensembles with volumes $m_\pi L \leq 4.1$

Table H.1: Correspondence between each fit model for the chiral-continuum extrapolation of $\sqrt{8t_0}f_{\pi K}$ and the labels used in Tables H.2-H.4 and Figs. 4.3-4.9. For the combined analysis, we are dealing with two independent cutoff effects, those of the Wilson results and those of the mixed action. In this case we will use two labels for these effects, the first referring to the lattice artifacts explored for the Wilson results, the second one for the mixed action results. If only one label is used it means the same lattice artifacts were explored for both regularizations.

Wilson analysis			
Model	p-value	W	$\sqrt{t_0}$ [fm]
$[\chi SU(3)][a^2][-]$	0.8096	0.19	0.1435(6)
$[\chi SU(3)][a^2][\beta > 3.40]$	0.598	0.0105	0.1434(9)
$[\chi SU(3)][a^2][\beta > 3.46]$	0.61	0.004	0.1427(10)
$[\chi SU(3)][a^2][m_\pi < 420\ MeV]$	0.4706	0.0022	0.1435(7)

$[\chi SU(3)][a^2][\beta > 3.40 \ \& \ m_\pi < 420 \ MeV]$	0.2848	0.0002	0.1427(11)
$[\chi SU(3)][a^2][m_\pi < 350 \ MeV]$	0.2308	0.0001	0.1434(8)
$[\chi SU(3)][a^2][m_\pi L > 4.1]$	0.7352	0.0218	0.1438(7)
$[\chi SU(3)][a^2 \alpha_s^{\hat{\Gamma}}][-]$	0.7902	0.181	0.1436(7)
$[\chi SU(3)][a^2 \alpha_s^{\hat{\Gamma}}][\beta > 3.40]$	0.5842	0.01	0.1434(9)
$[\chi SU(3)][a^2 \alpha_s^{\hat{\Gamma}}][\beta > 3.46]$	0.6222	0.004	0.1428(10)
$[\chi SU(3)][a^2 \alpha_s^{\hat{\Gamma}}][m_\pi < 420 \ MeV]$	0.4724	0.0021	0.1436(7)
$[\chi SU(3)][a^2 \alpha_s^{\hat{\Gamma}}][\beta > 3.40 \ \& \ m_\pi < 420 \ MeV]$	0.2762	0.0002	0.1427(11)
$[\chi SU(3)][a^2 \alpha_s^{\hat{\Gamma}}][m_\pi < 350 \ MeV]$	0.2196	0.0001	0.1435(8)
$[\chi SU(3)][a^2 \alpha_s^{\hat{\Gamma}}][m_\pi L > 4.1]$	0.724	0.0204	0.1439(7)
$[\chi SU(3)][a^2 + a^2 \phi_2][-]$	0.775	0.0914	0.1431(10)
$[\chi SU(3)][a^2 + a^2 \phi_2][\beta > 3.40]$	0.5378	0.005	0.1427(14)
$[\chi SU(3)][a^2 + a^2 \phi_2][\beta > 3.46]$	0.5004	0.0015	0.1425(15)
$[\chi SU(3)][a^2 + a^2 \phi_2][m_\pi < 420 \ MeV]$	0.4132	0.0009	0.1429(14)
$[\chi SU(3)][a^2 + a^2 \phi_2][m_\pi L > 4.1]$	0.6614	0.0084	0.1435(12)
$[Tay][a^2][-]$	0.7112	0.0954	0.1439(7)
$[Tay][a^2][\beta > 3.40]$	0.4926	0.0064	0.1438(9)
$[Tay][a^2][\beta > 3.46]$	0.5086	0.0025	0.1431(10)
$[Tay][a^2][m_\pi < 420 \ MeV]$	0.4012	0.0014	0.1440(7)
$[Tay][a^2][\beta > 3.40 \ \& \ m_\pi < 420 \ MeV]$	0.2236	0.0001	0.1431(11)
$[Tay][a^2][m_\pi < 350 \ MeV]$	0.1312	0.0001	0.1437(9)
$[Tay][a^2][m_\pi L > 4.1]$	0.7372	0.0225	0.1442(8)
$[Tay][a^2 \alpha_s^{\hat{\Gamma}}][-]$	0.6978	0.0903	0.1441(7)
$[Tay][a^2 \alpha_s^{\hat{\Gamma}}][\beta > 3.40]$	0.4786	0.0061	0.1439(9)
$[Tay][a^2 \alpha_s^{\hat{\Gamma}}][\beta > 3.46]$	0.5232	0.0026	0.1432(10)
$[Tay][a^2 \alpha_s^{\hat{\Gamma}}][m_\pi < 420 \ MeV]$	0.3774	0.0013	0.1441(7)
$[Tay][a^2 \alpha_s^{\hat{\Gamma}}][\beta > 3.40 \ \& \ m_\pi < 420 \ MeV]$	0.2098	0.0001	0.1432(11)
$[Tay][a^2 \alpha_s^{\hat{\Gamma}}][m_\pi < 350 \ MeV]$	0.1448	0.0001	0.1438(9)
$[Tay][a^2 \alpha_s^{\hat{\Gamma}}][m_\pi L > 4.1]$	0.7218	0.0213	0.1443(8)
$[Tay][a^2 + a^2 \phi_2][-]$	0.7028	0.0657	0.1433(10)
$[Tay][a^2 + a^2 \phi_2][\beta > 3.40]$	0.4792	0.0037	0.1428(14)
$[Tay][a^2 + a^2 \phi_2][\beta > 3.46]$	0.4376	0.0011	0.1425(16)
$[Tay][a^2 + a^2 \phi_2][m_\pi < 420 \ MeV]$	0.3518	0.0007	0.1430(14)
$[Tay][a^2 + a^2 \phi_2][m_\pi L > 4.1]$	0.7056	0.0102	0.1436(12)
$[Tay4][a^2][-]$	0.72	0.0657	0.1434(9)
$[Tay4][a^2][\beta > 3.40]$	0.494	0.0033	0.1433(11)
$[Tay4][a^2][\beta > 3.46]$	0.4686	0.0013	0.1427(11)
$[Tay4][a^2][m_\pi < 420 \ MeV]$	0.3522	0.0007	0.1434(10)

$[Tay4][a^2][\beta > 3.40 \ \& \ m_\pi < 420 \ MeV]$	0.1592	0.0001	0.1426(13)
$[Tay4][a^2][m_\pi < 350 \ MeV]$	0.5228	0.0002	0.1416(13)
$[Tay4][a^2][m_\pi L > 4.1]$	0.6524	0.0077	0.1442(11)
$[Tay4][a^2 + a^2\phi_2][-]$	0.6622	0.0279	0.1432(10)
$[Tay4][a^2 + a^2\phi_2][\beta > 3.40]$	0.4042	0.0015	0.1428(14)
$[Tay4][a^2 + a^2\phi_2][\beta > 3.46]$	0.3608	0.0005	0.1427(16)
$[Tay4][a^2 + a^2\phi_2][m_\pi < 420 \ MeV]$	0.2682	0.0003	0.1430(14)
$[Tay4][a^2 + a^2\phi_2][m_\pi L > 4.1]$	0.662	0.0054	0.1436(13)
$[\chi SU(2)][a^2][-]$	0.4746	0.7117	0.1426(8)
$[\chi SU(2)][a^2][\beta > 3.40]$	0.4762	0.0381	0.1421(10)
$[\chi SU(2)][a^2][\beta > 3.46]$	0.392	0.0035	0.1418(11)
$[\chi SU(2)][a^2][m_\pi < 420 \ MeV]$	0.3048	0.0013	0.1429(8)
$[\chi SU(2)][a^2][\beta > 3.40 \ \& \ m_\pi < 420 \ MeV]$	0.2296	0.0001	0.1420(13)
$[\chi SU(2)][a^2][m_\pi < 350 \ MeV]$	0.2934	0.0	0.1433(12)
$[\chi SU(2)][a^2][m_\pi L > 4.1]$	0.4718	0.0309	0.1427(8)
$[\chi SU(2)][a^2 + a^2\phi_2][-]$	0.4548	0.1941	0.1426(14)
$[\chi SU(2)][a^2 + a^2\phi_2][\beta > 3.40]$	0.4054	0.0106	0.1408(17)
$[\chi SU(2)][a^2 + a^2\phi_2][\beta > 3.46]$	0.3074	0.0007	0.1409(21)
$[\chi SU(2)][a^2 + a^2\phi_2][m_\pi < 420 \ MeV]$	0.2304	0.0004	0.1423(17)
$[\chi SU(2)][a^2 + a^2\phi_2][m_\pi L > 4.1]$	0.3882	0.0085	0.1423(16)

Table H.2: Model average results for the determination of $\sqrt{t_0}$ at the physical point using the Wilson results. In the first column we label the fit model and data cuts considered according to Table H.1. In the second and third columns we show the quality of fits as measured by the p-value [14] and the assigned weight to each model according to eq. (4.32), respectively. Finally, in the fourth column we show the results coming from each fit model. The SU(2)χPT models are separated by a horizontal line from the rest of the models to indicate that both sets of models are not averaged together, since they use different input data to extract the final result.

Mixed action analysis			
Model	p-value	W	$\sqrt{t_0}$ [fm]
$[\chi SU(3)][a^2][-]$	0.5996	0.1152	0.1445(9)
$[\chi SU(3)][a^2][\beta > 3.40]$	0.5264	0.014	0.1449(12)
$[\chi SU(3)][a^2][\beta > 3.46]$	0.4314	0.0034	0.1447(14)

$[\chi SU(3)][a^2][m_\pi < 420\ MeV]$	0.4596	0.0044	0.1442(8)
$[\chi SU(3)][a^2][\beta > 3.40\ \&\ m_\pi < 420\ MeV]$	0.23	0.0003	0.1448(15)
$[\chi SU(3)][a^2][m_\pi < 350\ MeV]$	0.221	0.0002	0.1445(10)
$[\chi SU(3)][a^2][m_\pi L > 4.1]$	0.6626	0.0333	0.1446(10)
$[\chi SU(3)][a^2\alpha_s^{\hat{\Gamma}}][-]$	0.5944	0.1148	0.1444(9)
$[\chi SU(3)][a^2\alpha_s^{\hat{\Gamma}}][\beta > 3.40]$	0.529	0.014	0.1449(13)
$[\chi SU(3)][a^2\alpha_s^{\hat{\Gamma}}][\beta > 3.46]$	0.4378	0.0034	0.1447(14)
$[\chi SU(3)][a^2\alpha_s^{\hat{\Gamma}}][m_\pi < 420\ MeV]$	0.4706	0.0043	0.1442(8)
$[\chi SU(3)][a^2\alpha_s^{\hat{\Gamma}}][\beta > 3.40\ \&\ m_\pi < 420\ MeV]$	0.2208	0.0003	0.1448(15)
$[\chi SU(3)][a^2\alpha_s^{\hat{\Gamma}}][m_\pi < 350\ MeV]$	0.2108	0.0002	0.1445(10)
$[\chi SU(3)][a^2\alpha_s^{\hat{\Gamma}}][m_\pi L > 4.1]$	0.6616	0.0331	0.1446(10)
$[\chi SU(3)][a^2 + a^2\phi_2][-]$	0.6816	0.1072	0.1436(9)
$[\chi SU(3)][a^2 + a^2\phi_2][\beta > 3.40]$	0.5126	0.0084	0.1437(16)
$[\chi SU(3)][a^2 + a^2\phi_2][\beta > 3.46]$	0.3434	0.0013	0.1443(19)
$[\chi SU(3)][a^2 + a^2\phi_2][m_\pi < 420\ MeV]$	0.3804	0.0016	0.1445(14)
$[\chi SU(3)][a^2 + a^2\phi_2][m_\pi L > 4.1]$	0.8118	0.0403	0.1429(13)
$[Tay][a^2][-]$	0.4358	0.0438	0.1449(6)
$[Tay][a^2][\beta > 3.40]$	0.3806	0.0062	0.1454(9)
$[Tay][a^2][\beta > 3.46]$	0.3112	0.0016	0.1451(12)
$[Tay][a^2][m_\pi < 420\ MeV]$	0.387	0.0027	0.1447(7)
$[Tay][a^2][\beta > 3.40\ \&\ m_\pi < 420\ MeV]$	0.1648	0.0002	0.1452(14)
$[Tay][a^2][m_\pi < 350\ MeV]$	0.1398	0.0001	0.1448(8)
$[Tay][a^2][m_\pi L > 4.1]$	0.6372	0.0301	0.1451(7)
$[Tay][a^2\alpha_s^{\hat{\Gamma}}][-]$	0.4434	0.0435	0.1449(7)
$[Tay][a^2\alpha_s^{\hat{\Gamma}}][\beta > 3.40]$	0.3908	0.0063	0.1453(10)
$[Tay][a^2\alpha_s^{\hat{\Gamma}}][\beta > 3.46]$	0.2984	0.0016	0.1451(12)
$[Tay][a^2\alpha_s^{\hat{\Gamma}}][m_\pi < 420\ MeV]$	0.3926	0.0028	0.1446(7)
$[Tay][a^2\alpha_s^{\hat{\Gamma}}][\beta > 3.40\ \&\ m_\pi < 420\ MeV]$	0.1636	0.0002	0.1451(14)
$[Tay][a^2\alpha_s^{\hat{\Gamma}}][m_\pi < 350\ MeV]$	0.1398	0.0001	0.1448(8)
$[Tay][a^2\alpha_s^{\hat{\Gamma}}][m_\pi L > 4.1]$	0.639	0.0302	0.1450(7)
$[Tay][a^2 + a^2\phi_2][-]$	0.5618	0.0644	0.1438(9)
$[Tay][a^2 + a^2\phi_2][\beta > 3.40]$	0.4	0.0045	0.1439(16)
$[Tay][a^2 + a^2\phi_2][\beta > 3.46]$	0.2384	0.0007	0.1445(19)
$[Tay][a^2 + a^2\phi_2][m_\pi < 420\ MeV]$	0.28	0.001	0.1447(13)
$[Tay][a^2 + a^2\phi_2][m_\pi L > 4.1]$	0.8902	0.0636	0.1431(12)
$[Tay4][a^2][-]$	0.6326	0.0881	0.1439(8)
$[Tay4][a^2][\beta > 3.40]$	0.5598	0.0098	0.1442(12)
$[Tay4][a^2][\beta > 3.46]$	0.419	0.0018	0.1443(13)

Model	p-value	W	$\sqrt{t_0}$ [fm]
$[Tay4][a^2][m_\pi < 420\ MeV]$	0.359	0.0014	0.1441(10)
$[Tay4][a^2][\beta > 3.40\ \&\ m_\pi < 420\ MeV]$	0.152	0.0001	0.1445(16)
$[Tay4][a^2][m_\pi < 350\ MeV]$	0.5838	0.0005	0.1426(13)
$[Tay4][a^2][m_\pi L > 4.1]$	0.5732	0.0117	0.1446(12)
$[Tay4][a^2 + a^2\phi_2][-]$	0.5974	0.0378	0.1436(9)
$[Tay4][a^2 + a^2\phi_2][\beta > 3.40]$	0.4564	0.0037	0.1441(16)
$[Tay4][a^2 + a^2\phi_2][\beta > 3.46]$	0.3304	0.0008	0.1451(19)
$[Tay4][a^2 + a^2\phi_2][m_\pi < 420\ MeV]$	0.3292	0.0008	0.1448(13)
$[Tay4][a^2 + a^2\phi_2][m_\pi L > 4.1]$	0.9286	0.0404	0.1435(13)
$[\chi SU(2)][a^2][-]$	0.1188	0.1172	0.1457(7)
$[\chi SU(2)][a^2][\beta > 3.40]$	0.338	0.4755	0.1448(10)
$[\chi SU(2)][a^2][\beta > 3.46]$	0.204	0.0147	0.1446(12)
$[\chi SU(2)][a^2][m_\pi < 420\ MeV]$	0.4502	0.1848	0.1463(7)
$[\chi SU(2)][a^2][\beta > 3.40\ \&\ m_\pi < 420\ MeV]$	0.2626	0.0026	0.1451(14)
$[\chi SU(2)][a^2][m_\pi < 350\ MeV]$	0.2686	0.0019	0.1469(9)
$[\chi SU(2)][a^2][m_\pi L > 4.1]$	0.1138	0.0138	0.1456(7)
$[\chi SU(2)][a^2 + a^2\phi_2][-]$	0.1224	0.0661	0.1467(12)
$[\chi SU(2)][a^2 + a^2\phi_2][\beta > 3.40]$	0.278	0.0775	0.1441(19)
$[\chi SU(2)][a^2 + a^2\phi_2][\beta > 3.46]$	0.1762	0.004	0.1435(23)
$[\chi SU(2)][a^2 + a^2\phi_2][m_\pi < 420\ MeV]$	0.3488	0.0328	0.1471(15)
$[\chi SU(2)][a^2 + a^2\phi_2][m_\pi L > 4.1]$	0.1202	0.0091	0.1455(16)

Table H.3: Model average results for the determination of $\sqrt{t_0}$ at the physical point using the mixed actions results. In the first column we label the fit model and data cuts considered according to Table H.1. In the second and third columns we show the quality of fits as measured by the p-value [14] and the assigned weight to each model according to eq. (4.32), respectively. Finally, in the fourth column we show the results coming from each fit model. The SU(2)χPT models are separated by a horizontal line from the rest of the models to indicate that both sets of models are not averaged together, since they use different input data to extract the final result.

Combined analysis			
Model	p-value	W	$\sqrt{t_0}$ [fm]
$[\chi SU(3)][a^2][-]$	0.6696	0.0745	0.1444(7)
$[\chi SU(3)][a^2][\beta > 3.40]$	0.4598	0.0004	0.1443(8)
$[\chi SU(3)][a^2][\beta > 3.46]$	0.6462	0.0001	0.1437(10)
$[\chi SU(3)][a^2][m_\pi < 420\ MeV]$	0.5134	0.0001	0.1440(6)

$[\chi SU(3)][a^2][\beta > 3.40 \ \& \ m_\pi < 420 \ MeV]$	0.4166	0.0	0.1435(10)
$[\chi SU(3)][a^2][m_\pi < 350 \ MeV]$	0.186	0.0	0.1443(8)
$[\chi SU(3)][a^2][m_\pi L > 4.1]$	0.588	0.0012	0.1445(7)
$[\chi SU(3)][a^2\alpha_s^{\hat{\Gamma}}][-]$	0.6518	0.067	0.1444(7)
$[\chi SU(3)][a^2\alpha_s^{\hat{\Gamma}}][\beta > 3.40]$	0.4156	0.0003	0.1444(8)
$[\chi SU(3)][a^2\alpha_s^{\hat{\Gamma}}][\beta > 3.46]$	0.6566	0.0001	0.1437(10)
$[\chi SU(3)][a^2\alpha_s^{\hat{\Gamma}}][m_\pi < 420 \ MeV]$	0.5216	0.0001	0.1441(6)
$[\chi SU(3)][a^2\alpha_s^{\hat{\Gamma}}][\beta > 3.40 \ \& \ m_\pi < 420 \ MeV]$	0.424	0.0	0.1436(10)
$[\chi SU(3)][a^2\alpha_s^{\hat{\Gamma}}][m_\pi < 350 \ MeV]$	0.1986	0.0	0.1443(8)
$[\chi SU(3)][a^2\alpha_s^{\hat{\Gamma}}][m_\pi L > 4.1]$	0.5576	0.0011	0.1446(7)
$[\chi SU(3)][a^2][a^2 + a^2\phi_2][-]$	0.8752	0.2702	0.1438(6)
$[\chi SU(3)][a^2][a^2 + a^2\phi_2][\beta > 3.40]$	0.732	0.0015	0.1436(8)
$[\chi SU(3)][a^2][a^2 + a^2\phi_2][\beta > 3.46]$	0.6452	0.0001	0.1434(9)
$[\chi SU(3)][a^2][a^2 + a^2\phi_2][m_\pi < 420 \ MeV]$	0.561	0.0	0.1437(6)
$[\chi SU(3)][a^2][a^2 + a^2\phi_2][m_\pi L > 4.1]$	0.882	0.0051	0.1437(7)
$[\chi SU(3)][a^2 + a^2\phi_2][a^2][[-]$	0.7474	0.0491	0.1446(8)
$[\chi SU(3)][a^2 + a^2\phi_2][a^2][\beta > 3.40]$	0.5802	0.0005	0.1447(10)
$[\chi SU(3)][a^2 + a^2\phi_2][a^2][\beta > 3.46]$	0.6382	0.0	0.1439(11)
$[\chi SU(3)][a^2 + a^2\phi_2][a^2][m_\pi < 420 \ MeV]$	0.5668	0.0	0.1443(7)
$[\chi SU(3)][a^2 + a^2\phi_2][a^2][m_\pi L > 4.1]$	0.7176	0.001	0.1448(9)
$[\chi SU(3)][a^2 + a^2\phi_2][-]$	0.841	0.0868	0.1435(8)
$[\chi SU(3)][a^2 + a^2\phi_2][\beta > 3.40]$	0.6804	0.0006	0.1431(12)
$[\chi SU(3)][a^2 + a^2\phi_2][\beta > 3.46]$	0.586	0.0	0.1433(14)
$[\chi SU(3)][a^2 + a^2\phi_2][m_\pi < 420 \ MeV]$	0.4938	0.0	0.1440(11)
$[\chi SU(3)][a^2 + a^2\phi_2][m_\pi L > 4.1]$	0.8696	0.0027	0.1432(10)
$[Tay][a^2][-]$	0.5308	0.0245	0.1448(5)
$[Tay][a^2][\beta > 3.40]$	0.3504	0.0002	0.1448(7)
$[Tay][a^2][\beta > 3.46]$	0.5384	0.0	0.1441(9)
$[Tay][a^2][m_\pi < 420 \ MeV]$	0.428	0.0	0.1445(6)
$[Tay][a^2][\beta > 3.40 \ \& \ m_\pi < 420 \ MeV]$	0.3152	0.0	0.1439(10)
$[Tay][a^2][m_\pi < 350 \ MeV]$	0.123	0.0	0.1446(7)
$[Tay][a^2][m_\pi L > 4.1]$	0.5706	0.001	0.1450(6)
$[Tay][a^2\alpha_s^{\hat{\Gamma}}][-]$	0.5276	0.0214	0.1449(5)
$[Tay][a^2\alpha_s^{\hat{\Gamma}}][\beta > 3.40]$	0.3196	0.0001	0.1448(7)
$[Tay][a^2\alpha_s^{\hat{\Gamma}}][\beta > 3.46]$	0.5636	0.0	0.1442(9)
$[Tay][a^2\alpha_s^{\hat{\Gamma}}][m_\pi < 420 \ MeV]$	0.447	0.0	0.1445(6)
$[Tay][a^2\alpha_s^{\hat{\Gamma}}][\beta > 3.40 \ \& \ m_\pi < 420 \ MeV]$	0.3422	0.0	0.1440(10)
$[Tay][a^2\alpha_s^{\hat{\Gamma}}][m_\pi < 350 \ MeV]$	0.1324	0.0	0.1446(7)

$[Tay][a^2\alpha_s^{\hat{\Gamma}}][m_\pi L > 4.1]$	0.5472	0.001	0.1450(6)
$[Tay][a^2][a^2 + a^2\phi_2][-]$	0.8248	0.128	0.1442(6)
$[Tay][a^2][a^2 + a^2\phi_2][\beta > 3.40]$	0.642	0.0007	0.1441(8)
$[Tay][a^2][a^2 + a^2\phi_2][\beta > 3.46]$	0.5634	0.0	0.1438(9)
$[Tay][a^2][a^2 + a^2\phi_2][m_\pi < 420\ MeV]$	0.4918	0.0	0.1441(6)
$[Tay][a^2][a^2 + a^2\phi_2][m_\pi L > 4.1]$	0.891	0.006	0.1442(7)
$[Tay][a^2 + a^2\phi_2][a^2][-]$	0.607	0.0165	0.1450(6)
$[Tay][a^2 + a^2\phi_2][a^2][\beta > 3.40]$	0.4518	0.0002	0.1451(8)
$[Tay][a^2 + a^2\phi_2][a^2][\beta > 3.46]$	0.5328	0.0	0.1443(9)
$[Tay][a^2 + a^2\phi_2][a^2][m_\pi < 420\ MeV]$	0.4726	0.0	0.1447(6)
$[Tay][a^2 + a^2\phi_2][a^2][m_\pi L > 4.1]$	0.6804	0.0007	0.1452(6)
$[Tay][a^2 + a^2\phi_2][-]$	0.8056	0.0588	0.1438(8)
$[Tay][a^2 + a^2\phi_2][\beta > 3.40]$	0.6164	0.0003	0.1433(12)
$[Tay][a^2 + a^2\phi_2][\beta > 3.46]$	0.4898	0.0	0.1434(14)
$[Tay][a^2 + a^2\phi_2][m_\pi < 420\ MeV]$	0.4262	0.0	0.1442(11)
$[Tay][a^2 + a^2\phi_2][m_\pi L > 4.1]$	0.899	0.0045	0.1433(10)
$[Tay4][a^2][-]$	0.6652	0.0417	0.1440(7)
$[Tay4][a^2][\beta > 3.40]$	0.4204	0.0002	0.1439(9)
$[Tay4][a^2][\beta > 3.46]$	0.5744	0.0	0.1435(10)
$[Tay4][a^2][m_\pi < 420\ MeV]$	0.424	0.0	0.1440(8)
$[Tay4][a^2][\beta > 3.40\ \&\ m_\pi < 420\ MeV]$	0.3326	0.0	0.1433(12)
$[Tay4][a^2][m_\pi < 350\ MeV]$	0.505	0.0	0.1422(11)
$[Tay4][a^2][m_\pi L > 4.1]$	0.5178	0.0003	0.1446(10)
$[Tay4][a^2][a^2 + a^2\phi_2][-]$	0.8262	0.0618	0.1437(7)
$[Tay4][a^2][a^2 + a^2\phi_2][\beta > 3.40]$	0.6694	0.0005	0.1435(10)
$[Tay4][a^2][a^2 + a^2\phi_2][\beta > 3.46]$	0.5694	0.0	0.1433(11)
$[Tay4][a^2][a^2 + a^2\phi_2][m_\pi < 420\ MeV]$	0.4626	0.0	0.1438(8)
$[Tay4][a^2][a^2 + a^2\phi_2][m_\pi L > 4.1]$	0.86	0.002	0.1442(10)
$[Tay4][a^2 + a^2\phi_2][a^2][-]$	0.7686	0.0389	0.1440(7)
$[Tay4][a^2 + a^2\phi_2][a^2][\beta > 3.40]$	0.6066	0.0003	0.1441(10)
$[Tay4][a^2 + a^2\phi_2][a^2][\beta > 3.46]$	0.584	0.0	0.1437(11)
$[Tay4][a^2 + a^2\phi_2][a^2][m_\pi < 420\ MeV]$	0.4796	0.0	0.1441(8)
$[Tay4][a^2 + a^2\phi_2][a^2][m_\pi L > 4.1]$	0.6686	0.0004	0.1446(10)
$[Tay4][a^2 + a^2\phi_2][-]$	0.7852	0.0243	0.1437(8)
$[Tay4][a^2 + a^2\phi_2][\beta > 3.40]$	0.593	0.0001	0.1433(12)
$[Tay4][a^2 + a^2\phi_2][\beta > 3.46]$	0.5018	0.0	0.1437(14)
$[Tay4][a^2 + a^2\phi_2][m_\pi < 420\ MeV]$	0.4076	0.0	0.1442(11)
$[Tay4][a^2 + a^2\phi_2][m_\pi L > 4.1]$	0.9244	0.0025	0.1435(11)

$[\chi SU(2)][a^2][-]$	0.0816	0.02	0.1442(5)
$[\chi SU(2)][a^2][\beta > 3.40]$	0.2132	0.0117	0.1436(8)
$[\chi SU(2)][a^2][\beta > 3.46]$	0.1248	0.0	0.1432(10)
$[\chi SU(2)][a^2][m_\pi < 420\ MeV]$	0.0944	0.0	0.1447(6)
$[\chi SU(2)][a^2][\beta > 3.40\ \&\ m_\pi < 420\ MeV]$	0.1104	0.0	0.1433(11)
$[\chi SU(2)][a^2][m_\pi < 350\ MeV]$	0.1252	0.0	0.1456(8)
$[\chi SU(2)][a^2][m_\pi L > 4.1]$	0.0922	0.0001	0.1442(6)
$[\chi SU(2)][a^2][a^2 + a^2\phi_2][-]$	0.1376	0.0664	0.1436(6)
$[\chi SU(2)][a^2][a^2 + a^2\phi_2][\beta > 3.40]$	0.4222	0.4019	0.1426(8)
$[\chi SU(2)][a^2][a^2 + a^2\phi_2][\beta > 3.46]$	0.2618	0.0005	0.1423(10)
$[\chi SU(2)][a^2][a^2 + a^2\phi_2][m_\pi < 420\ MeV]$	0.2236	0.0003	0.1438(7)
$[\chi SU(2)][a^2][a^2 + a^2\phi_2][m_\pi L > 4.1]$	0.233	0.0053	0.1432(7)
$[\chi SU(2)][a^2 + a^2\phi_2][a^2][[-]$	0.1694	0.4049	0.1450(6)
$[\chi SU(2)][a^2 + a^2\phi_2][a^2][\beta > 3.40]$	0.3204	0.063	0.1442(8)
$[\chi SU(2)][a^2 + a^2\phi_2][a^2][\beta > 3.46]$	0.2206	0.0002	0.1439(10)
$[\chi SU(2)][a^2 + a^2\phi_2][a^2][m_\pi < 420\ MeV]$	0.2566	0.0008	0.1456(6)
$[\chi SU(2)][a^2 + a^2\phi_2][a^2][m_\pi L > 4.1]$	0.1796	0.0022	0.1451(6)
$[\chi SU(2)][a^2 + a^2\phi_2][-]$	0.0816	0.011	0.1442(5)
$[\chi SU(2)][a^2 + a^2\phi_2][\beta > 3.40]$	0.2018	0.0113	0.1436(8)
$[\chi SU(2)][a^2 + a^2\phi_2][\beta > 3.46]$	0.1202	0.0	0.1432(10)
$[\chi SU(2)][a^2 + a^2\phi_2][m_\pi < 420\ MeV]$	0.096	0.0	0.1447(6)
$[\chi SU(2)][a^2 + a^2\phi_2][m_\pi L > 4.1]$	0.0832	0.0001	0.1442(6)

Table H.4: Model average results for the determination of $\sqrt{t_0}$ at the physical point using the combined analysis of both Wilson and mixed action results. In the first column we label the fit model and data cuts considered according to Table H.1. In the second and third columns we show the quality of fits as measured by the p-value [14] and the assigned weight to each model according to eq. (4.32), respectively. Finally, in the fourth column we show the results coming from each fit model. The SU(2)χPT models are separated by a horizontal line from the rest of the models to indicate that both sets of models are not averaged together, since they use different input data to extract the final result.

BIBLIOGRAPHY

[1] Stephen L. Adler. "An Overrelaxation Method for the Monte Carlo Evaluation of the Partition Function for Multiquadratic Actions." In: *Phys. Rev. D* 23 (1981), p. 2901. DOI: 10.1103/PhysRevD.23.2901.

[2] C. Allton et al. "Physical Results from 2+1 Flavor Domain Wall QCD and SU(2) Chiral Perturbation Theory." In: *Phys. Rev. D* 78 (2008), p. 114509. DOI: 10.1103/PhysRevD.78.114509. arXiv: 0804.0473 [hep-lat].

[3] S. Aoki et al. "Review of lattice results concerning low-energy particle physics." In: *Eur. Phys. J. C* 77.2 (2017), p. 112. DOI: 10.1140/epjc/s10052-016-4509-7. arXiv: 1607.00299 [hep-lat].

[4] Y. Aoki et al. "FLAG Review 2021." In: *Eur. Phys. J. C* 82.10 (2022), p. 869. DOI: 10.1140/epjc/s10052-022-10536-1. arXiv: 2111.09849 [hep-lat].

[5] Gunnar S. Bali, Sara Collins, Peter Georg, Daniel Jenkins, Piotr Korcyl, Andreas Schäfer, Enno E. Scholz, Jakob Simeth, Wolfgang Söldner, and Simon Weishäupl. "Scale setting and the light baryon spectrum in $N_f = 2 + 1$ QCD with Wilson fermions." In: *JHEP* 05 (2023), p. 035. DOI: 10.1007/JHEP05(2023)035. arXiv: 2211.03744 [hep-lat].

[6] Oliver Bar and Maarten Golterman. "Chiral perturbation theory for gradient flow observables." In: *Phys. Rev. D* 89.3 (2014). [Erratum: Phys.Rev.D 89, 099905 (2014)], p. 034505. DOI: 10.1103/PhysRevD.89.034505. arXiv: 1312.4999 [hep-lat].

[7] A. Bazavov et al. "Gradient flow and scale setting on MILC HISQ ensembles." In: *Phys. Rev. D* 93.9 (2016), p. 094510. DOI: 10.1103/PhysRevD.93.094510. arXiv: 1503.02769 [hep-lat].

[8] Claude W. Bernard, Tom Burch, Kostas Orginos, Doug Toussaint, Thomas A. DeGrand, Carleton E. DeTar, Steven A. Gottlieb, Urs M. Heller, James E. Hetrick, and Bob Sugar. "The Static quark potential in three flavor QCD." In: *Phys. Rev. D* 62 (2000), p. 034503. DOI: 10.1103/PhysRevD.62.034503. arXiv: hep-lat/0002028.

[9] W. Bietenholz et al. "Flavour blindness and patterns of flavour symmetry breaking in lattice simulations of up, down and strange quarks." In: *Phys. Rev. D* 84 (2011), p. 054509. DOI: 10.1103/PhysRevD.84.054509. arXiv: 1102.5300 [hep-lat].

[10] V. G. Bornyakov et al. "Determining the scale in Lattice QCD." In: Dec. 2015. arXiv: 1512.05745 [hep-lat].

[11]   Szabolcs Borsányi, Stephan Dürr, Zoltán Fodor, Christian Hoel-
       bling, Sándor D. Katz, Stefan Krieg, Thorsten Kurth, Laurent
       Lellouch, Thomas Lippert, and Craig McNeile. "High-precision
       scale setting in lattice QCD." In: *JHEP* 09 (2012), p. 010. DOI:
       `10.1007/JHEP09(2012)010`. arXiv: `1203.4469 [hep-lat]`.

[12]   Nathan Joseph Brown. "Lattice Scales from Gradient Flow and
       Chiral Analysis on the MILC Collaboration's HISQ Ensembles."
       PhD thesis. Washington U., St. Louis, Washington U., St. Louis,
       2018. DOI: `10.7936/K7S181ZQ`.

[13]   Mattia Bruno, Tomasz Korzec, and Stefan Schaefer. "Setting the
       scale for the CLS $2 + 1$ flavor ensembles." In: *Phys. Rev. D* 95.7
       (2017), p. 074504. DOI: `10.1103/PhysRevD.95.074504`. arXiv:
       `1608.08900 [hep-lat]`.

[14]   Mattia Bruno and Rainer Sommer. "On fits to correlated and
       auto-correlated data." In: *Comput. Phys. Commun.* 285 (2023),
       p. 108643. DOI: `10.1016/j.cpc.2022.108643`. arXiv: `2209.14188
       [hep-lat]`.

[15]   Mattia Bruno et al. "Simulation of QCD with $N_f = 2 + 1$ flavors
       of non-perturbatively improved Wilson fermions." In: *JHEP* 02
       (2015), p. 043. DOI: `10.1007/JHEP02(2015)043`. arXiv: `1411.3982
       [hep-lat]`.

[16]   John Bulava, Michele Della Morte, Jochen Heitger, and Christian
       Wittemeier. "Non-perturbative improvement of the axial current
       in N_f=3 lattice QCD with Wilson fermions and tree-level im-
       proved gauge action." In: *Nucl. Phys. B* 896 (2015), pp. 555–568.
       DOI: `10.1016/j.nuclphysb.2015.05.003`. arXiv: `1502.04999
       [hep-lat]`.

[17]   Andrea Bussone, Alessandro Conigli, Julien Frison, Gregorio
       Herdoíza, Carlos Pena, David Preti, Alejandro Sáez, and Javier
       Ugarrio. "Hadronic physics from a Wilson fermion mixed-action
       approach: Charm quark mass and $D_{(s)}$ meson decay constants."
       In: (Sept. 2023). arXiv: `2309.14154 [hep-lat]`.

[18]   Isabel Campos, Patrick Fritzsch, Carlos Pena, David Preti, Al-
       berto Ramos, and Anastassios Vladikas. "Non-perturbative quark
       mass renormalisation and running in $N_f = 3$ QCD." In: *Eur.
       Phys. J. C* 78.5 (2018), p. 387. DOI: `10.1140/epjc/s10052-018-
       5870-5`. arXiv: `1802.05243 [hep-lat]`.

[19]   M. A. Clark and A. D. Kennedy. "Accelerating dynamical fermion
       computations using the rational hybrid Monte Carlo (RHMC)
       algorithm with multiple pseudofermion fields." In: *Phys. Rev.
       Lett.* 98 (2007), p. 051601. DOI: `10.1103/PhysRevLett.98.051601`.
       arXiv: `hep-lat/0608015`.

[20] Gilberto Colangelo and Stephan Durr. "The Pion mass in finite volume." In: *Eur. Phys. J. C* 33 (2004), pp. 543–553. DOI: 10.1140/epjc/s2004-01593-y. arXiv: hep-lat/0311023.

[21] Gilberto Colangelo, Stephan Durr, and Christoph Haefeli. "Finite volume effects for meson masses and decay constants." In: *Nucl. Phys. B* 721 (2005), pp. 136–174. DOI: 10.1016/j.nuclphysb.2005.05.015. arXiv: hep-lat/0503014.

[22] M. Creutz. "Monte Carlo Study of Quantized SU(2) Gauge Theory." In: *Phys. Rev. D* 21 (1980), pp. 2308–2315. DOI: 10.1103/PhysRevD.21.2308.

[23] Michael Creutz. "Overrelaxation and Monte Carlo Simulation." In: *Phys. Rev. D* 36 (1987), p. 515. DOI: 10.1103/PhysRevD.36.515.

[24] Mattia Dalla Brida, Roman Höllwieser, Francesco Knechtli, Tomasz Korzec, Alessandro Nada, Alberto Ramos, Stefan Sint, and Rainer Sommer. "Determination of $\alpha_s(m_Z)$ by the non-perturbative decoupling method." In: *Eur. Phys. J. C* 82.12 (2022), p. 1092. DOI: 10.1140/epjc/s10052-022-10998-3. arXiv: 2209.14204 [hep-lat].

[25] Mattia Dalla Brida, Tomasz Korzec, Stefan Sint, and Pol Vilaseca. "High precision renormalization of the flavour non-singlet Noether currents in lattice QCD with Wilson quarks." In: *Eur. Phys. J. C* 79.1 (2019), p. 23. DOI: 10.1140/epjc/s10052-018-6514-5. arXiv: 1808.09236 [hep-lat].

[26] Thomas A. DeGrand. "A conditioning technique for matrix inversion for Wilson fermions." In: *Computer Physics Communications* 52.1 (1988), pp. 161–164. ISSN: 0010-4655. DOI: https://doi.org/10.1016/0010-4655(88)90180-4. URL: https://www.sciencedirect.com/science/article/pii/0010465588901804.

[27] G. M. de Divitiis, R. Petronzio, and N. Tantalo. "Distance preconditioning for lattice Dirac operators." In: *Phys. Lett. B* 692 (2010), pp. 157–160. DOI: 10.1016/j.physletb.2010.07.031. arXiv: 1006.4028 [hep-lat].

[28] Giulia Maria de Divitiis, Maurizio Firrotta, Jochen Heitger, Carl Christian Köster, and Anastassios Vladikas. "Non-perturbative determination of improvement b-coefficients in $N_f = 3$." In: *EPJ Web Conf.* 175 (2018). Ed. by M. Della Morte, P. Fritzsch, E. Gámiz Sánchez, and C. Pena Ruano, p. 10008. DOI: 10.1051/epjconf/201817510008. arXiv: 1710.07020 [hep-lat].

[29] R. J. Dowdall et al. "The Upsilon spectrum and the determination of the lattice spacing from lattice QCD including charm quarks in the sea." In: *Phys. Rev. D* 85 (2012), p. 054509. DOI: 10.1103/PhysRevD.85.054509. arXiv: 1110.6887 [hep-lat].

[30]   S. Duane, A. D. Kennedy, B. J. Pendleton, and D. Roweth. "Hybrid Monte Carlo." In: *Phys. Lett. B* 195 (1987), pp. 216–222. DOI: 10.1016/0370-2693(87)91197-X.

[31]   R. Frezzotti and G. C. Rossi. "Chirally improving Wilson fermions. 1. O(a) improvement." In: *JHEP* 08 (2004), p. 007. DOI: 10.1088/1126-6708/2004/08/007. arXiv: hep-lat/0306014.

[32]   Roberto Frezzotti, Pietro Antonio Grassi, Stefan Sint, and Peter Weisz. "A Local formulation of lattice QCD without unphysical fermion zero modes." In: *Nucl. Phys. B Proc. Suppl.* 83 (2000). Ed. by M. Campostrini, S. Caracciolo, L. Cosmai, A. Di Giacomo, P. Rossi, and F. Rapuano, pp. 941–946. DOI: 10.1016/S0920-5632(00)91852-8. arXiv: hep-lat/9909003.

[33]   Roberto Frezzotti, Pietro Antonio Grassi, Stefan Sint, and Peter Weisz. "Lattice QCD with a chirally twisted mass term." In: *JHEP* 08 (2001), p. 058. DOI: 10.1088/1126-6708/2001/08/058. arXiv: hep-lat/0101001.

[34]   Roberto Frezzotti, Stefan Sint, and Peter Weisz. "O(a) improved twisted mass lattice QCD." In: *JHEP* 07 (2001), p. 048. DOI: 10.1088/1126-6708/2001/07/048. arXiv: hep-lat/0104014.

[35]   Julien Frison. "Bayesian Inference for Contemporary Lattice Quantum Field Theory." In: *40th International Symposium on Lattice Field Theory*. Dec. 2023. arXiv: 2401.00577 [hep-lat].

[36]   Christof Gattringer and Christian B. Lang. *Quantum chromodynamics on the lattice*. Vol. 788. Springer, 2010. DOI: 10.1007/978-3-642-01850-3.

[37]   Paul H. Ginsparg and Kenneth G. Wilson. "A Remnant of Chiral Symmetry on the Lattice." In: *Phys. Rev. D* 25 (1982), p. 2649. DOI: 10.1103/PhysRevD.25.2649.

[38]   Steven A. Gottlieb, W. Liu, D. Toussaint, R. L. Renken, and R. L. Sugar. "Hybrid Molecular Dynamics Algorithms for the Numerical Simulation of Quantum Chromodynamics." In: *Phys. Rev. D* 35 (1987), pp. 2531–2542. DOI: 10.1103/PhysRevD.35.2531.

[39]   A. Gray, I. Allison, C. T. H. Davies, Emel Dalgic, G. P. Lepage, J. Shigemitsu, and M. Wingate. "The Upsilon spectrum and m(b) from full lattice QCD." In: *Phys. Rev. D* 72 (2005), p. 094507. DOI: 10.1103/PhysRevD.72.094507. arXiv: hep-lat/0507013.

[40]   Martin Hasenbusch. "Speeding up the hybrid Monte Carlo algorithm for dynamical fermions." In: *Phys. Lett. B* 519 (2001), pp. 177–182. DOI: 10.1016/S0370-2693(01)01102-9. arXiv: hep-lat/0107019.

[41] Roman Höllwieser, Francesco Knechtli, and Tomasz Korzec. "Scale setting for $N_f = 3 + 1$ QCD." In: *Eur. Phys. J. C* 80.4 (2020), p. 349. DOI: 10.1140/epjc/s10052-020-7889-7. arXiv: 2002.02866 [hep-lat].

[42] Nikolai Husung. "Logarithmic corrections to O(a) and O(a^2) effects in lattice QCD with Wilson or Ginsparg–Wilson quarks." In: *Eur. Phys. J. C* 83.2 (2023). [Erratum: Eur.Phys.J.C 83, 144 (2023)], p. 142. DOI: 10.1140/epjc/s10052-023-11258-8. arXiv: 2206.03536 [hep-lat].

[43] Alan C. Irving, James C. Sexton, Eamonn Cahill, Joyce Garden, Balint Joo, Stephen M. Pickles, and Zbigniew Sroczynski. "Tuning actions and observables in lattice QCD." In: *Phys. Rev. D* 58 (1998), p. 114504. DOI: 10.1103/PhysRevD.58.114504. arXiv: hep-lat/9807015.

[44] A. D. Kennedy, Ivan Horvath, and Stefan Sint. "A New exact method for dynamical fermion computations with nonlocal actions." In: *Nucl. Phys. B Proc. Suppl.* 73 (1999). Ed. by Thomas A. DeGrand, Carleton E. DeTar, R. Sugar, and D. Toussaint, pp. 834–836. DOI: 10.1016/S0920-5632(99)85217-7. arXiv: hep-lat/9809092.

[45] Bartosz Kostrzewa et al. "Gradient-flow scale setting with $N_f = 2 + 1 + 1$ Wilson-clover twisted-mass fermions." In: *PoS* LATTICE2021 (2022), p. 131. DOI: 10.22323/1.396.0131. arXiv: 2111.14710 [hep-lat].

[46] G. Peter Lepage. "The Analysis of Algorithms for Lattice Field Theory." In: *Theoretical Advanced Study Institute in Elementary Particle Physics*. June 1989.

[47] M. Luscher and P. Weisz. "Computation of the Action for On-Shell Improved Lattice Gauge Theories at Weak Coupling." In: *Phys. Lett. B* 158 (1985), pp. 250–254. DOI: 10.1016/0370-2693(85)90966-9.

[48] M. Luscher and P. Weisz. "On-shell improved lattice gauge theories." In: *Commun. Math. Phys.* 98.3 (1985). [Erratum: Commun.Math.Phys. 98, 433 (1985)], p. 433. DOI: 10.1007/BF01205792.

[49] Martin Luscher. "Computational Strategies in Lattice QCD." In: *Les Houches Summer School: Session 93: Modern perspectives in lattice QCD: Quantum field theory and high performance computing*. Feb. 2010, pp. 331–399. arXiv: 1002.4232 [hep-lat].

[50] Martin Luscher. "Topology, the Wilson flow and the HMC algorithm." In: *PoS* LATTICE2010 (2010). Ed. by Giancarlo Rossi, p. 015. DOI: 10.22323/1.105.0015. arXiv: 1009.5877 [hep-lat].

[51] Martin Luscher and Filippo Palombi. "Fluctuations and reweighting of the quark determinant on large lattices." In: *PoS* LATTICE2008 (2008). Ed. by Christopher Aubin, Saul Cohen, Chris Dawson, Jozef Dudek, Robert Edwards, Balint Joo, Huey-Wen Lin, Kostas Orginos, David Richards, and Hank Thacker, p. 049. DOI: 10.22323/1.066.0049. arXiv: 0810.0946 [hep-lat].

[52] Martin Luscher and Stefan Schaefer. "Lattice QCD without topology barriers." In: *JHEP* 07 (2011), p. 036. DOI: 10.1007/JHEP07(2011)036. arXiv: 1105.4749 [hep-lat].

[53] Martin Luscher and Stefan Schaefer. "Lattice QCD with open boundary conditions and twisted-mass reweighting." In: *Comput. Phys. Commun.* 184 (2013), pp. 519–528. DOI: 10.1016/j.cpc.2012.10.003. arXiv: 1206.2809 [hep-lat].

[54] Martin Luscher, Stefan Sint, Rainer Sommer, and Peter Weisz. "Chiral symmetry and O(a) improvement in lattice QCD." In: *Nucl. Phys. B* 478 (1996), pp. 365–400. DOI: 10.1016/0550-3213(96)00378-1. arXiv: hep-lat/9605038.

[55] Martin Lüscher. "Properties and uses of the Wilson flow in lattice QCD." In: (2010). DOI: 10.1007/JHEP08(2010)071. eprint: arXiv:1006.4518.

[56] Neal Madras and Alan D. Sokal. "The Pivot algorithm: a highly efficient Monte Carlo method for selfavoiding walk." In: *J. Statist. Phys.* 50 (1988), pp. 109–186. DOI: 10.1007/BF01022990.

[57] Robert D. Mawhinney. "Lattice QCD with zero, two and four quark flavors." In: *RHIC Summer Study 96: Brookhaven Theory Workshop on Relativistic Heavy Ions.* Nov. 1996. arXiv: hep-lat/9705030.

[58] N. Metropolis, A. W. Rosenbluth, M. N. Rosenbluth, A. H. Teller, and E. Teller. "Equation of state calculations by fast computing machines." In: *J. Chem. Phys.* 21 (1953), pp. 1087–1092. DOI: 10.1063/1.1699114.

[59] Daniel Mohler, Stefan Schaefer, and Jakob Simeth. "CLS 2+1 flavor simulations at physical light- and strange-quark masses." In: *EPJ Web Conf.* 175 (2018). Ed. by M. Della Morte, P. Fritzsch, E. Gámiz Sánchez, and C. Pena Ruano, p. 02010. DOI: 10.1051/epjconf/201817502010. arXiv: 1712.04884 [hep-lat].

[60] Silvia Necco and Rainer Sommer. "The N(f) = 0 heavy quark potential from short to intermediate distances." In: *Nucl. Phys. B* 622 (2002), pp. 328–346. DOI: 10.1016/S0550-3213(01)00582-X. arXiv: hep-lat/0108008.

[61] Ethan T. Neil and Jacob W. Sitison. "Model averaging approaches to data subset selection." In: *Phys. Rev. E* 108.4 (2023), p. 045308. DOI: 10.1103/PhysRevE.108.045308. arXiv: 2305.19417 [stat.ME].

[62] Ethan T. Neil and Jacob W. Sitison. "Improved information criteria for Bayesian model averaging in lattice field theory." In: *Phys. Rev. D* 109.1 (2024), p. 014510. DOI: `10.1103/PhysRevD.109.014510`. arXiv: `2208.14983 [stat.ME]`.

[63] Holger Bech Nielsen and M. Ninomiya. "Absence of Neutrinos on a Lattice. 1. Proof by Homotopy Theory." In: *Nucl. Phys. B* 185 (1981). Ed. by J. Julve and M. Ramón-Medrano. [Erratum: Nucl.Phys.B 195, 541 (1982)], p. 20. DOI: `10.1016/0550-3213(82)90011-6`.

[64] Holger Bech Nielsen and M. Ninomiya. "No Go Theorem for Regularizing Chiral Fermions." In: *Phys. Lett. B* 105 (1981), pp. 219–223. DOI: `10.1016/0370-2693(81)91026-1`.

[65] I.P. Omelyan, I.M. Mryglod, and R. Folk. "Symplectic analytically integrable decomposition algorithms: classification, derivation, and application to molecular dynamics, quantum and celestial mechanics simulations." In: *Computer Physics Communications* 151.3 (2003), pp. 272–314. ISSN: 0010-4655. DOI: `https://doi.org/10.1016/S0010-4655(02)00754-3`. URL: `https://www.sciencedirect.com/science/article/pii/S0010465502007543`.

[66] Alberto Ramos. "Automatic differentiation for error analysis of Monte Carlo data." In: *Comput. Phys. Commun.* 238 (2019), pp. 19–35. DOI: `10.1016/j.cpc.2018.12.020`. arXiv: `1809.01289 [hep-lat]`.

[67] Alberto Ramos. "Automatic differentiation for error analysis." In: *PoS* TOOLS2020 (2021), p. 045. DOI: `10.22323/1.392.0045`. arXiv: `2012.11183 [hep-lat]`.

[68] Stefan Schaefer, Rainer Sommer, and Francesco Virotta. "Critical slowing down and error analysis in lattice QCD simulations." In: *Nucl. Phys. B* 845 (2011), pp. 93–119. DOI: `10.1016/j.nuclphysb.2010.11.020`. arXiv: `1009.5228 [hep-lat]`.

[69] B. Sheikholeslami and R. Wohlert. "Improved Continuum Limit Lattice Action for QCD with Wilson Fermions." In: *Nucl. Phys. B* 259 (1985), p. 572. DOI: `10.1016/0550-3213(85)90002-1`.

[70] Andrea Shindler. "Twisted mass lattice QCD." In: *Phys. Rept.* 461 (2008), pp. 37–110. DOI: `10.1016/j.physrep.2008.03.001`. arXiv: `0707.4093 [hep-lat]`.

[71] R. Sommer. "A New way to set the energy scale in lattice gauge theories and its applications to the static force and α_s in SU(2) Yang-Mills theory." In: *Nucl. Phys. B* 411 (1994), pp. 839–854. DOI: `10.1016/0550-3213(94)90473-1`. arXiv: `hep-lat/9310022`.

[72] Rainer Sommer. "Scale setting in lattice QCD." In: *PoS* LATTICE2013 (2014), p. 015. DOI: `10.22323/1.187.0015`. arXiv: `1401.3270 [hep-lat]`.

[73] Ben Straßberger. "Towards Higher Precision Lattice QCD Results: Improved Scale Setting and Domain Decomposition Solvers." PhD thesis. Humboldt U., Berlin, 2023. DOI: 10.18452/26517.

[74] Yusuke Taniguchi and Akira Ukawa. "Perturbative calculation of improvement coefficients to O(g**2a) for bilinear quark operators in lattice QCD." In: *Phys. Rev. D* 58 (1998), p. 114503. DOI: 10.1103/PhysRevD.58.114503. arXiv: hep-lat/9806015.

[75] D. H. Weingarten and D. N. Petcher. "Monte Carlo Integration for Lattice Gauge Theories with Fermions." In: *Phys. Lett. B* 99 (1981), pp. 333–338. DOI: 10.1016/0370-2693(81)90112-X.

[76] D. H. Weingarten and J. C. Sexton. "Hamiltonian evolution for the hybrid Monte Carlo algorithm." In: *Nucl. Phys. B Proc. Suppl.* 26 (1992), pp. 613–616. DOI: 10.1016/0920-5632(92)90349-W.

[77] Kenneth G. Wilson. "Confinement of Quarks." In: *Phys. Rev. D* 10 (1974). Ed. by J. C. Taylor, pp. 2445–2459. DOI: 10.1103/PhysRevD.10.2445.

[78] Ulli Wolff. "Monte Carlo errors with less errors." In: *Comput. Phys. Commun.* 156 (2004). [Erratum: Comput.Phys.Commun. 176, 383 (2007)], pp. 143–153. DOI: 10.1016/S0010-4655(03)00467-3. arXiv: hep-lat/0306017.

[79] P. A. Zyla et al. "Review of Particle Physics." In: *PTEP* 2020.8 (2020), p. 083C01. DOI: 10.1093/ptep/ptaa104.